NTNU

Norwegian University of
Science and Technology

CFD Simulations of Multiphase Flows with Particles

Timur Bikmukhametov

EPT-M-2016-13

MASTER THESIS

for

Student
Timur Bikmukhametov

Spring 2016

CFD simulations of multiphase flows with particles

CFD simuleringer av flerfasestrøm med partikler

Background and objective

Multiphase subsea pipelines can include flow of sand an oil/gas mixtures. Another particle-liquid
flow problem is deep sea mining, where particles are lifted from the sea bed by a pumped two
phase flow in long vertical pipes. Different flow scenarios related to deep sea mining have been
investigated in a specialization project, using the 1D OLGA simulator. This included a
comparison with available data on liquid flushing of a particle plug in a bend.
The simulations revealed limitations of 1D models. A master thesis work will follow up on
testing of how CFD simulators will perform on similar flow cases. The cases can cover both
particle-liquid flows and particle-gas-liquid flows.

The following tasks are to be considered:

1 Identify flow cases for simulations: hypothetical and/or experimental
2 Evaluate computational options in a CFD simulator in relation to the cases and in relation to
1D simulations
3 Document the work in a report including recommendations for the use of CFD on this class of
flow problem

-- ” --

Within 14 days of receiving the written text on the master thesis, the candidate shall submit a research plan for his project to the department.

When the thesis is evaluated, emphasis is put on processing of the results, and that they are presented in tabular and/or graphic form in a clear manner, and that they are analyzed carefully.

The thesis should be formulated as a research report with summary both in English and Norwegian, conclusion, literature references, table of contents etc. During the preparation of the text, the candidate should make an effort to produce a well-structured and easily readable report. In order to ease the evaluation of the thesis, it is important that the cross-references are correct. In the making of the report, strong emphasis should be placed on both a thorough discussion of the results and an orderly presentation.

The candidate is requested to initiate and keep close contact with his/her academic supervisor(s) throughout the working period. The candidate must follow the rules and regulations of NTNU as well as passive directions given by the Department of Energy and Process Engineering.
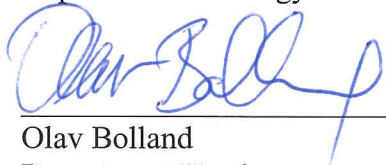
Risk assessment of the candidate's work shall be carried out according to the department's procedures. The risk assessment must be documented and included as part of the final report. Events related to the candidate's work adversely affecting the health, safety or security, must be documented and included as part of the final report. If the documentation on risk assessment represents a large number of pages, the full version is to be submitted electronically to the supervisor and an excerpt is included in the report.

Pursuant to "Regulations concerning the supplementary provisions to the technology study program/Master of Science" at NTNU §20, the Department reserves the permission to utilize all the results and data for teaching and research purposes as well as in future publications.

The final report is to be submitted digitally in DAIM. An executive summary of the thesis including title, student's name, supervisor's name, year, department name, and NTNU's logo and name, shall be submitted to the department as a separate pdf file. Based on an agreement with the supervisor, the final report and other material and documents may be given to the supervisor in digital format.

☐ Work to be done in lab (Water power lab, Fluids engineering lab, Thermal engineering lab)
☐ Field work

Department of Energy and Process Engineering, 13. January 2016

Olav Bolland
Department Head

Reidar Kristoffersen
Academic Supervisor

Research Advisor: Ole Jorgen Nydal

Abstract

This Master's thesis describes two CFD studies – particle plug propagation in bent pipes and critical velocity determination in dilute slurry flows. The objective of this study is to extend an understanding of these phenomena and to test the capabilities of the CFD software ANSYS Fluent in modelling of particle flows. In addition, contribution to 1D modelling of particle flows is considered as another important goal of this project. The particle plug propagation is simulated by Eulerian Granular model while the critical velocity determination is simulated using Discrete Phase Model (DPM).

The obtained results regarding the propagating particle plug show that Eulerian Granular model in ANSYS Fluent is capable to reproduce the particle plug movement in pipes, specifically the dispersion and transition zones are well captured and show a good qualitative fit with the experimental measurements. The detailed model selection study is conducted which could be potentially used in similar research works. In addition, a slip relation for 1D particle modelling is proposed which is capable to reproduce the particle dispersion zone at the plug front in an accurate way.

DPM model in ANSYS Fluent demonstrated a reasonably good performance in predicting critical velocity in slurry flows, but the value of the velocity is underestimated. Also, it is obtained that the critical velocity is independent on the particle volume fraction which is not the same as in the experimental observations. The obtained results need more investigations with regards to mesh dependency and missing physics in the default DPM model.

Further work might address to predicting the value of the particle volume fraction in the dispersion and transition zones of the particle plug using different specularity coefficients. It could useful to obtain a grid independent solution in terms of the value of the first layer thickness. The proposed slip relation for 1D modelling might be further improved and generalized if all the parameters are described by a single variable, for example, average particle fraction. As for the critical velocity modelling, the better predictions might be obtained if important factors such as particle-particle interaction and Shields parameter are included in the simulations.

Acknowledgement

Table of Contents

List of Figures

x

List of Tables

Nomenclature

a – speed of sound, m/s

A – pipe cross-sectional area, m^2

A – constant in the slip relation

B – constant in the slip relation

C – distribution slip coefficient

$C_{1\varepsilon}$ – constant in k-ε model

$C_{2\varepsilon}$ – constant in k-ε model

C_D – drag coefficient

$C_{fr,ls}$ – coefficient of friction between lth and sth solid phase particles

C_{TD} – turbulent dispersion coefficient

C_μ – constant in k-ε model

C_{vm} – the virtual mass factor

C_v – sand volume fraction

d – pipe diameter, m

d_h – hydraulic diameter, m

d_{ij} – deformation tensor, Pa

d_p – particle diameter, m

d_l – diameter of the particles in the solid phase "l", m

D – constant in the slip relation

D_p – dispersion scalar of particles

D_q – dispersion scalar of qth phase

D_{tq} – turbulent dispersion scalar

e_{ls} – coefficient of restitution

e_{ss} – coefficient of restitution

f – drag function

$\vec{F}$ – additional force term, N

$\vec{F}_{lift,q}$ – lift force, N

$\vec{F}_{q}$ – external body force, N

$\vec{F}_{td,q}$ – turbulent dispersion force, N

$\vec{F}_{vm,q}$ – virtual mass force, N

$\vec{F}_{wl,q}$ – wall lubrication force, N

$\vec{g}$ – gravity acceleration, m/s^2

$g_{o,ls}$ – radial distribution coefficient

$g_{o,ss}$ – radial distribution coefficient

G_{b} – generation of turbulent kinetic energy due to buoyancy effect, kg/m.s^3

G_{k} – generation of turbulent kinetic energy due to mean velocity gradients, kg/m.s^3

h_{q} – specific enthalpy of the qth phase, m^2/s^2

h_{pq} – specific interphase enthalpy, m^2/s^2

I – turbulent intensity, %

$\overline{\overline{I}}$ - first invariant of stress tensor

I_{2D} – the second invariant of the deviatoric stress tensor

k – turbulent kinetic energy, m^2/s^2

$K_{ls} = K_{sl}$ – momentum exchange coefficients

K_{pq} – interphase exchange coefficient

K_{qp} – interphase momentum exchange coefficient

L_{e} – entrance length, m

$\dot{m}_{pq}$ – mass transfer from the pth to qth phase, kg/s

$\dot{m}_{qp}$ – mass transfer from phase qth to pth phase, kg/s

$\dot{m}_{ls}$ – mass transfer from the lth to sth phase, kg/s

$\dot{m}_{sl}$ – mass transfer from the sth to lth phase, kg/s

n – total number of phases

p – pressure, Pa

P_{fr} – frictional pressure, Pa

p_s – the sth solids pressure

Re – Reynolds number

Re_s – Reynolds number of solids

$\vec{q}_q$ – heat flux, J/m^2

Q_{pq} – intensity of heat exchange between the pth and qth phases, J/s

S_{ij} – rate-of-strain, 1/s

S_k – the source term

S_q – source term

S_ω – source term

T – integration time, s

u – the velocity which is perpendicular to the gravity, m/s

$\vec{u}$ – local fluid phase velocity, m/s

$u_i{}'$ – fluctuation velocity value, m/s

$\vec{u}_p$ – particle velocity, m/s

U_i – mean velocity value, m/s

U_p – average particle velocity, m/s

U_{sp} – superficial particle velocity, m/s

U_{sw} – superficial water velocity, m/s

U_w – water velocity, m/s

$\vec{\upsilon}_l$ – liquid velocity, m/s

$\vec{\upsilon}_{ls}$ – interphase velocity, m/s

$\vec{\upsilon}_p$ – pth phase velocity, m/s

$\vec{\upsilon}_{pq}$ – interphase velocity, m/s

$\vec{\upsilon}_q$ – velocity of qth phase, m/s

$\vec{\upsilon}_{qp}$ – interphase velocity, m/s

$\upsilon_{r,s}$ – terminal velocity

$\vec{\upsilon}_s$ – solids velocity, m/s

$\vec{\upsilon}_{sl}$ – interphase velocity, m/s

V_q – volume of qth phase

y^+_w – dimensionless length scale at the wall

Y_M – contribution of the fluctuating dilatation in compressible turbulence to the dissipation rate, kg/m.s^3

Greek symbols

α_l – liquid volume fraction

α_p – particle fraction

α_q – qth phase volume fraction

α_s – solid volume fraction

$\alpha_{s,MAX}$ – maximum local particle fraction

$\alpha_{s,min}$ – minimum local particle fraction

δ_{ij} – Kronecker delta

ε – turbulent dissipation rate, m^2/s^3

ε_s – solids fraction

ε_s^* – packing limit of solids

ϕ – angle of internal friction

λ_q – bulk viscosity of the qth phase, kg/m.s

λ_s – bulk viscosity, kg/m.s

μ – dynamic viscosity of the fluid, kg/m.s

μ_q – shear viscosity of the qth phase, kg/m.s

$\mu_{s,fr}$ – frictional viscosity, kg/m.s

$\mu_{s,kin}$ – granular viscosity, kg/m.s

μ_t – turbulent viscosity, kg/m.s

μ_{tq} – turbulent viscosity of the qth phase, kg/m.s

v – kinematic viscosity, m^2/s

ρ – continuum phase density, kg/m^3

ρ_p – particle density, kg/m^3

ρ_q – density of the qth phase, kg/m^3

ρ_{rq} – phase reference density for the qth phase, kg/m^3

ρ_s – density of solids, kg/m^3

σ_k – constant in k-ε model

σ_{pq} – Prandtl number

σ_ε – constant in k-ε model

τ_r – particle relaxation time, s

$\overset{=}{\tau}_q$ – the qth phase stress tensor, Pa

τ_s – solids relaxation time, s

ω – specific dissipation, 1/s

Θ_s – granular temperature, m^2/s

Abbreviations

2D – two-dimensional

3D – three-dimensional

CFD – Computational Fluid Dynamics

DPM – Discrete Phase Model

EWT – Enhanced Wall Treatment

MTC – Minimum Transport Condition

OLGA – OiL and Gas multiphase flow simulation tool

QUICK – Quadratic Upstream Interpolation for Convective Kinematics

RANS – Reynolds Averaged Navier-Stokes

UDF – User-Defined Function

Chapter 1
Introduction

1.1 Problem description

Transportation of solid particles in liquid flows has a wide range of applications in chemical, mining and food industries and play an important role in process operations. In opposite, in oil and gas production, solid particles in a liquid flow might cause problems such as erosion of pipes, wells and process equipment. In order to predict the slurry flow behavior, engineers need to know many parameters of the flows such as particle fraction, particle and flow velocities, line pressure drop, etc. These parameters define the operating conditions, operating equipment and equipment location along the process, for example, pump characteristics and placement along the pipelines.

The solid-liquid flows are defined as multiphase flows since more than one phase are present in the flow (Hewitt, 2010). The physics behind the multiphase flows is often much more complicated than for single phase flows and the reason for this is interaction between phases which makes the flow behavior hard to analyze.

Even though behavior of a single solid particle in a liquid flow is a well-understood phenomenon, the solid-liquid flows with higher particle concentration are continuously being investigated. The problem with high concentrated particle flows is that there is a big influence of particle-particle interaction on the flow structure, so that the flow behavior becomes hard to predict and model. In addition, if the flow is turbulent, there is an influence of turbulence on the particle motion, so that the flow becomes even more difficult to model and control.

Similarly to gas-liquid flows, solid-liquid flows have different flow regimes. These regimes depend on the water velocity and particle properties such as diameter, density and concentration. There are four major types of solid-liquid flow regimes which can be seen in the Figure 1.1.
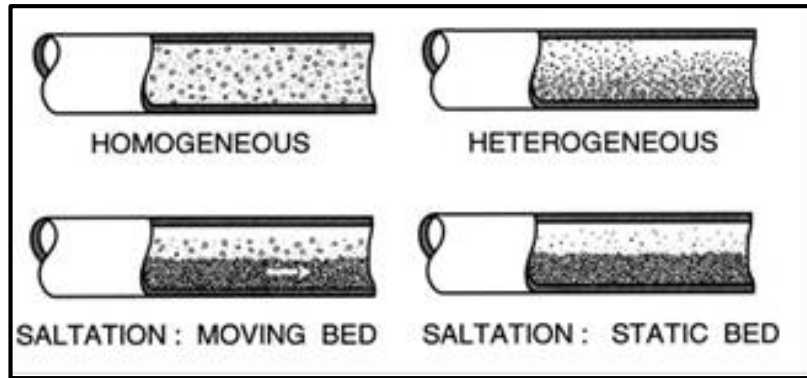
Figure 1.1 Typical slurry flow regimes in horizontal and inclined pipes (Brennen, 2005).

In the homogeneous regime, the flow is uniformly distributed in the carrier liquid and all the particles are suspended in a high velocity flow. In the heterogeneous flow, the particles with higher density tend to locate at the lower part of the pipe. As the flow velocity decreases, moving bed regime occurs, so that most of the particles are located at the pipe bottom. However, the shear force caused by the flow is able to move these deposited bed. If the flow velocity is further decreased, the deposited particles become stationary and static bed regime occurs. (Polanský, 2014)

If look closer at these regimes, the transition between the heterogeneous flow and the moving/static bed can be described in more details. At some point, the moving bed might be represented by moving or scouring particle dunes depending on the flow velocity. The transition can be seen in the Figure 1.2.
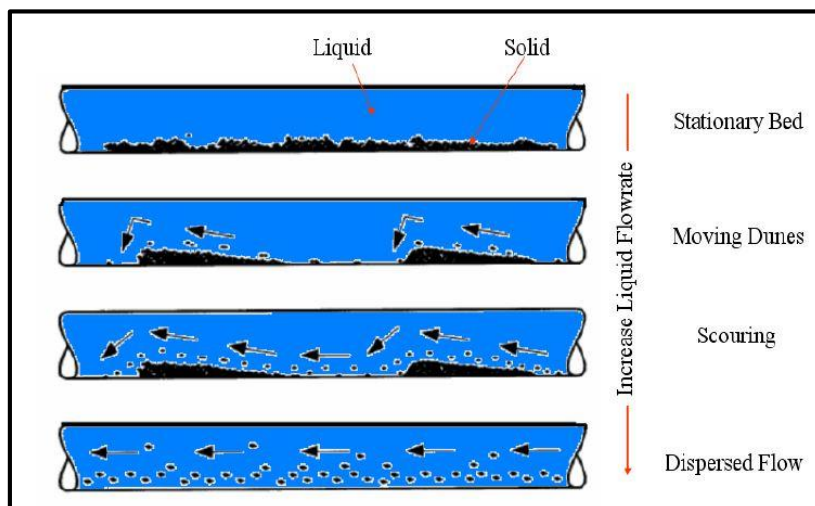
Figure 1.2 Liquid-solid particles flow regimes in horizontal pipelines (Yan, 2010)

In addition to these regimes, different dynamic situations might occur in the flow, for example, plug initiation inside the pipe. Different reasons might cause such plug initiation. One of them

is different velocities of particles with different diameters and densities – lighter and/or smaller particles move faster than larger and heavier ones, as such they create particle waves inside the pipe. These waves can merge which causes extreme particle concentrations and pipe blocking. (Talmon & van Rhee, 2011)

Another dynamic situation associated with plug initiation is stop-start operations. When the flow is stopped or has a very low velocity, in low points of the pipelines or risers particles start accumulating since they are usually denser than water. This situation might lead to pipe blocking and can cause serious operational consequences. Therefore, it is important to understand how the particle plug will propagate when the flow velocity increases again. This multiphase flow problem is studied in details in this thesis work.

In 2012, experiments of particles accumulation and particle plug propagation during stop-start operations were carried out at the Norwegian University of Science and Technology at Energy and Process Department by Mohammad Mehdi Shabani as a part of the PhD research work (Shabani, 2012). The experiments have been conducted using a rig which consists of a bent pipe with a diameter of 0.032 m. The angle between the tubes and the horizontal plane is 12.5 degrees. The experiments were conducted within several stages (Shabani, 2012):

- initiation of the plug in the bend;
- start pumping the water flow in the upstream pipe by a hydraulic pump;
- flushing the plug out of the bend by the water flow;
- taking measurements of particle volume fraction along the downstream pipe section.

An initiated plug can be seen in the Figure 1.3. The detailed schematic setup of the experimental rig with the marked measurement points can be found in the Appendix A.

The particles have the following properties:

- diameter varies from 200 to 1000 micrometers;
- median diameter d_{50}=350 micrometers;
- density ρ=1070 kg/m^3;
- packing limit (max. particle concentration): 0.63-0.66.

Many experiments with different plug lengths and mixture velocities were conducted. In this section, the case with 2 m plug length and the mixture velocity of 0.66 m/s is shown.
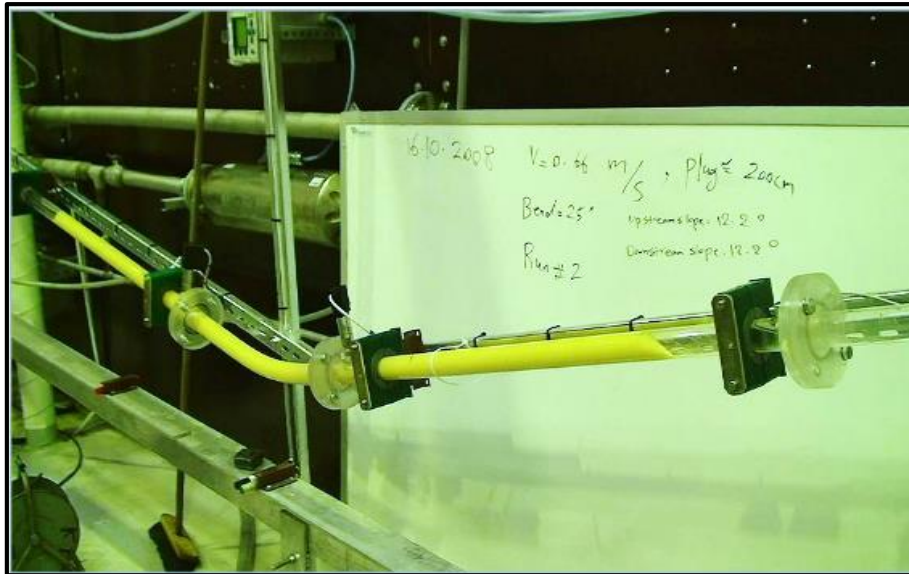
Figure 1.3 Photo of the experimental setup with an initiated plug (Shabani, 2012)

In the Figures 1.4 and 1.5, the visual observations of the front, main body and the tail of the propagating particle plug are presented. In the Figure 1.4, the zone of particle dispersion at the front of the plug is clearly observed. The dispersed particles tend to propagate slightly below the pipe center axis since the particle density is slightly higher the water density. The same behavior can be observed at the tail.
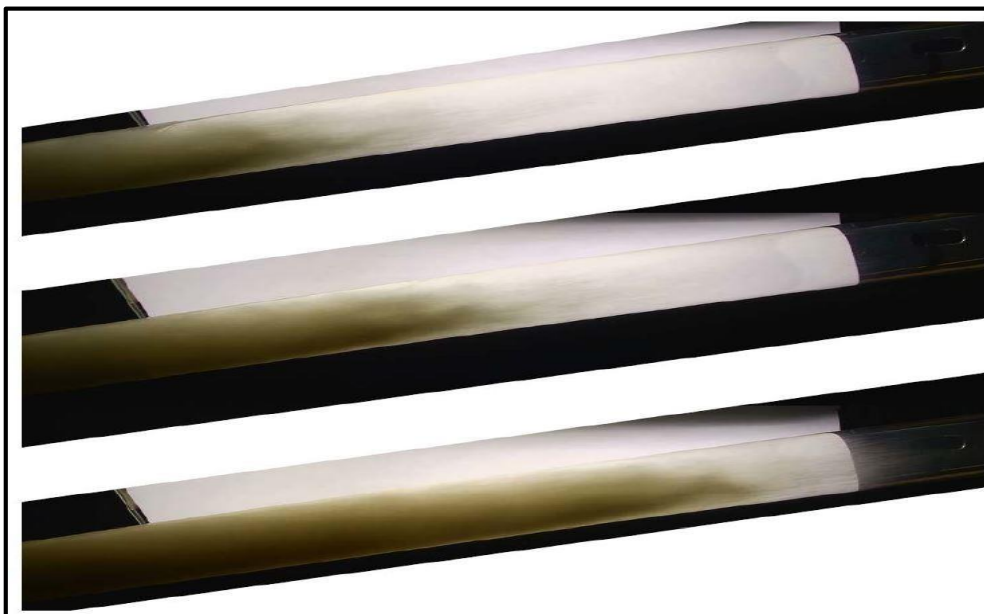
Figure 1.4 Front propagation of the particle plug (Shabani, 2012)

Figure 1.5 Main body and tail propagation of the particle plug (Shabani, 2012)

The visual observations are confirmed by measurements of particle volume fractions versus time. The measurements were taken at three consecutive locations along the downstream rig section. In the Figure 1.6, it is possible to see the dispersed front pointed out by the black dashed lines. It was also measured that particle velocity at the front is higher than the particle velocity in the rest of the plug body, as such the front region becomes dispersed (Shabani, 2012).
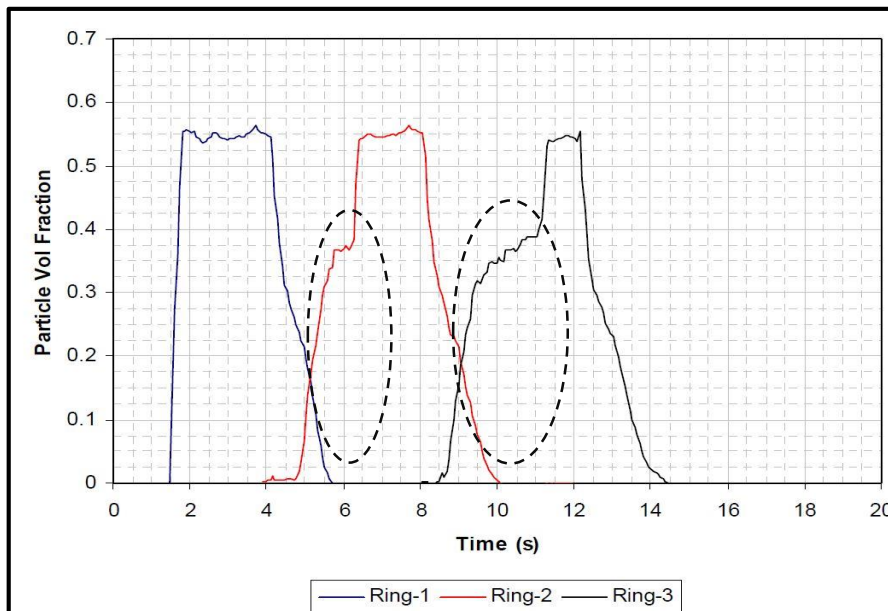
Figure 1.6 Particle volume fraction measurements by three conductance rings along the downstream pipe section (Shabani, 2012)

In Autumn 2015, as a part of the Specialization Project by the author of this Master's thesis, the case of particle plug propagation in a bent pipe was studied in terms of its modelling in OLGA and compared with the experimental results presented above. In the Figure 1.7, the comparison of the experimental and OLGA results is shown.
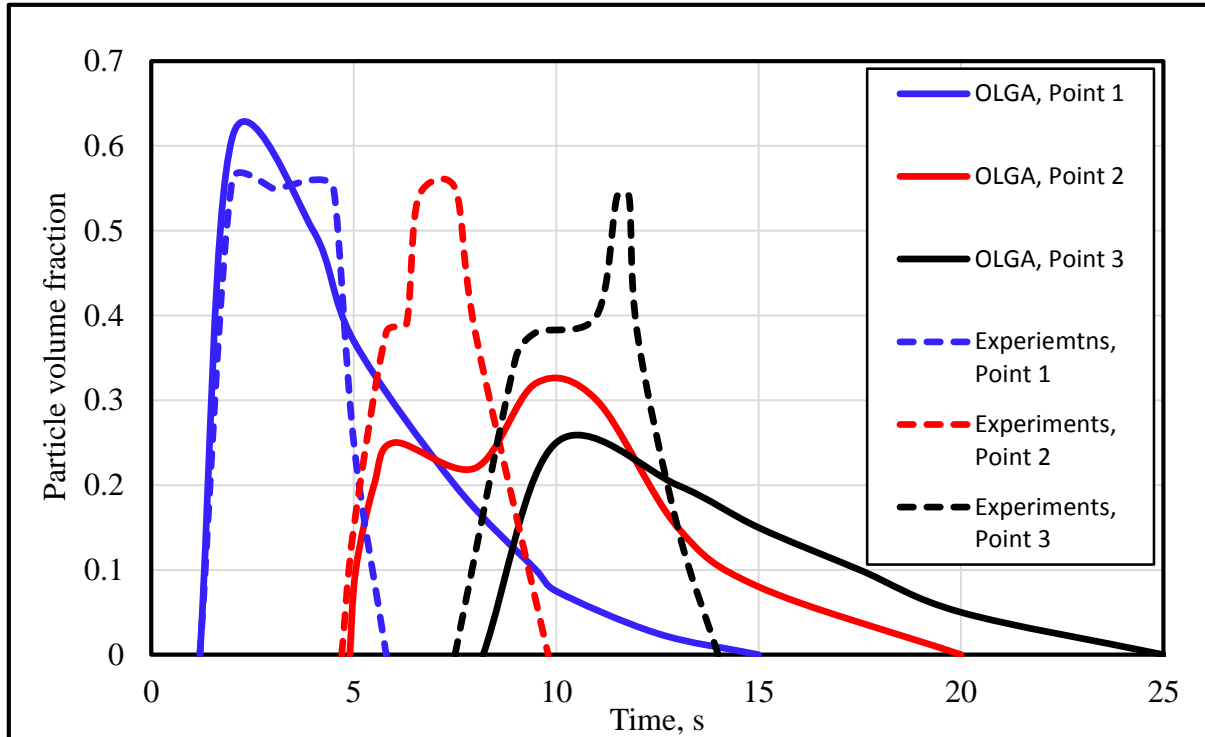
Figure 1.7 Experimental and simulated particle volume fractions, ADVANCED model

As it can be seen from the figure, there are big differences between the OLGA and experimental results. The reason for having such differences is the fact that OLGA divides the particle plug in two layers: bed and suspension. In opposite, the experiments show that all the particles are suspended in the flow. This fact gives significant deviation between the simulation and the experimental results (Bikmukhametov, 2015).

The simulations presented in the Figure 1.7 have been conducted in the ADVANCED Particle Flow Option model in OLGA which means that the program considers the bed deposition effect. When it has been revealed that the deposition effect hinders to reproduce the experimental results, the ADVANCED model was switched to the SIMPLE model which assumes that all the particles are suspended in the flow. The Figure 1.8 shows the results obtained by the SIMPLE model.

The figure shows that by using the SIMPLE model in OLGA, it is possible to reproduce the plug behavior in a more accurate way than by using the ADVANCED model. However, OLGA

does not predict any dispersion zone at the front of the plug. The length of the plug keeps almost constant along the propagation line. The small changes in the plug length is explained by the fact that there is a small slip effect between the particles and water flow which is implemented in the model. However, the implemented slip effect is not able to predict the particle dispersion in an appropriate manner. The difference in the peak concentrations is explained by the fact that the conductance rings used in the experiments might give wrong measurements of the particle volume fractions for high values (Shabani, 2012). As such, the deviation in the peak values between the OLGA and experimental results should not mislead the reader.
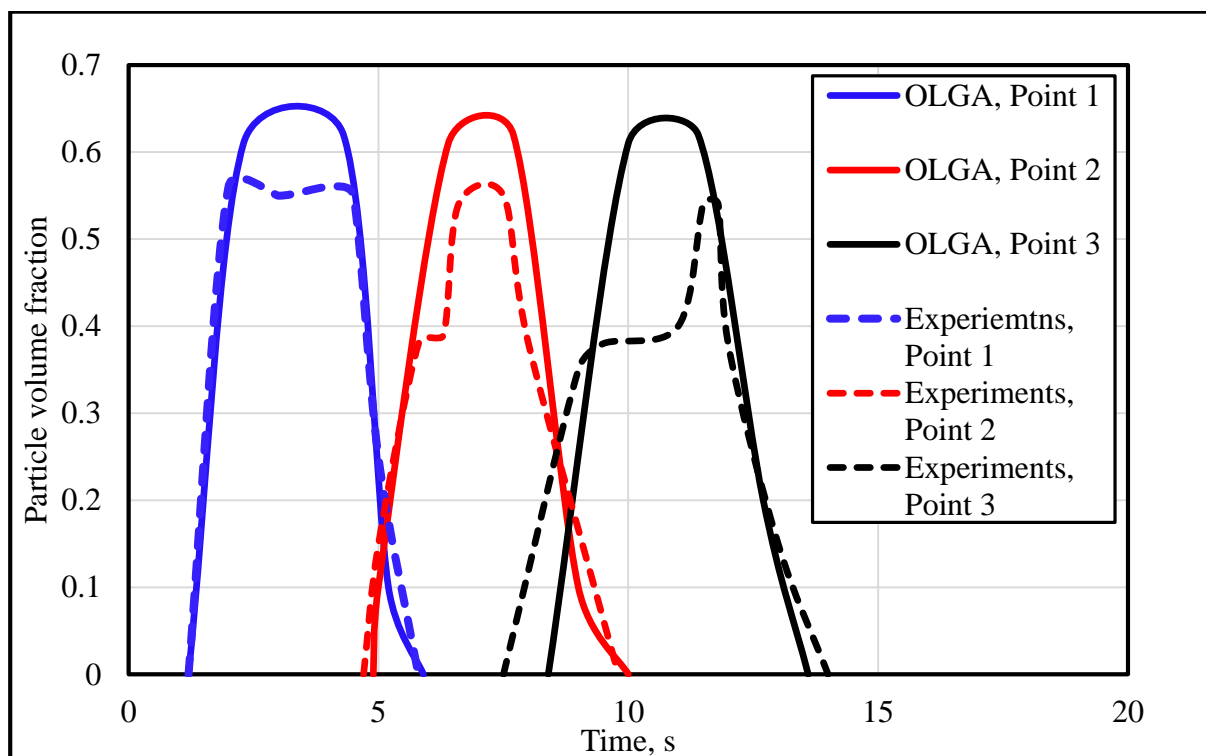
Figure 1.8 Experimental and simulated particle volume fractions, SIMPLE model

As it can be seen, even a well-developed multiphase flow simulator was not able to predict the particle plug behavior accurately. Understanding of the particle plug behavior is important in order to control particle transportation, especially in extreme cases such as a stop-start case. For this purpose, ANSYS Fluent is used in this Master's thesis in order to model particle plug behavior and check capabilities of this CFD tool for modelling such type of flows. It is also suggested that the data from the CFD simulations might be used in order to improve the OLGA code.

Another situation which has a significant importance in operation of hydraulic particle transportation is bed deposition in dilute sand-water flows. Small concentrations of sand is common in oil and gas production lines. From the operational point of view, it is important to understand at which velocity sand particles start forming sand dunes and a static bed, i.e. critical velocity of the flow. Such a velocity is also often called minimum transport condition (MTC). Several studies have been attempted to create a numerical model which predicts MTC condition such as **Danielson, 2007, Salama, 2000** and **Turian et al., 1987**.

Yan, 2010 conducted his PhD work at Cranfield University regaring the minimum transport condition in multiphase pipelines and in the literature the results are published in the journal paper by **Al-lababidi et al., 2012**. In order to investigate the critical sand velocity in the flow, an experimental rig was constructed which allows to create different flow regimes and clearly observe sand transport phenomenon. The figure with the schematic rig setup and relevant parameters can be found in the Appendix A.

In the experiments, the minimum transport condition was investigated, i.e. the minimum water velocity at which the accumulation of a sliding particle layer at the pipe bottom is prevented (Al-lababidi et al., 2012). Five different concentrations are tested within ten different velocities for each concentration. For each combination of concentration and velocity, visual observations are perfromed. In the Figure 1.9, these observations for each case are summarized. In the black rectangles, the critical velocity conditions are emphasized.

Water Velocity (m/s)	Sand Volume fraction				
	1.61×10^{-5}	5.38×10^{-5}	1.08×10^{-4}	2.15×10^{-4}	5.38×10^{-4}
1	most sand transport in the liquid core	most sand transport in the liquid core	most sand transport in the liquid core	sand streaks observed on the pipe bottom	sand streaks observed on the pipe bottom
0.9	most sand transport in the liquid core	most sand transport in the liquid core	few sand streaks observed on the pipe bottom	more sand streaks observed on the pipe bottom	more sand streaks observed on the pipe bottom
0.8	few sand streaks observed on the pipe bottom	few sand streaks observed on the pipe bottom	more sand streaks observed on the pipe bottom	more sand streaks observed on the pipe bottom	more sand streaks observed on the pipe bottom
0.7	more sand streaks observed on the pipe bottom	more sand streaks observed on the pipe bottom	sand concentration was higher in streaks	sand concentration was highest in streaks	sand concentration was highest in streaks
0.6	sand concentration was higher in streaks	sand concentration was higher in streaks	sand concentration was highest in streaks	sliding sand layer observed on the pipe bottom	sliding sand layer observed on the pipe bottom
0.5	sand concentration was highest in streaks	sand concentration was highest in streaks	sliding sand layer observed on the pipe bottom	sliding sand layer observed on the pipe bottom	sliding sand layer observed on the pipe bottom
0.4	scouring sand dunes formation	scouring sand dunes formation	scouring sand dunes formation	scouring sand dunes formation	scouring sand dunes formation
0.3	slowing moving sand dunes	slowing moving sand dunes	slowing moving sand dunes	slowing moving sand dunes	slowing moving sand dunes
0.2	few sand particles moving on the top of the dunes	few sand particles moving on the top of the dunes	few sand particles moving on the top of the dunes	few sand particles moving on the top of the dunes	few sand particles moving on the top of the dunes
0.1	few sand particles moving on the top of the dunes	few sand particles moving on the top of the	few sand particles moving on the top of the dunes	few sand particles moving on the top of the dunes	few sand particles moving on the top of the dunes

Figure 1.9 Experimental observations of MTC (Al-lababidi et al., 2012)

In order to understand the visual observations used in the table in a more clear way, one may take a look at the Figure 1.10 and Figure 1.11.

The Figure 1.10 shows the streaks which are observed at the pipe bottom. The Figure 1.11 represents the sand dunes which are observed at the pipe bottom. The change between these two observations is counted as the minimum transport condition of sand in the water flow. Through the analysis of the experimental observations, it was concluded that the critical velocity depends on the particle volume fraction in the flow. With an increase of the particle fraction, the increase of the critical velocity value follows (Al-lababidi et al., 2012).
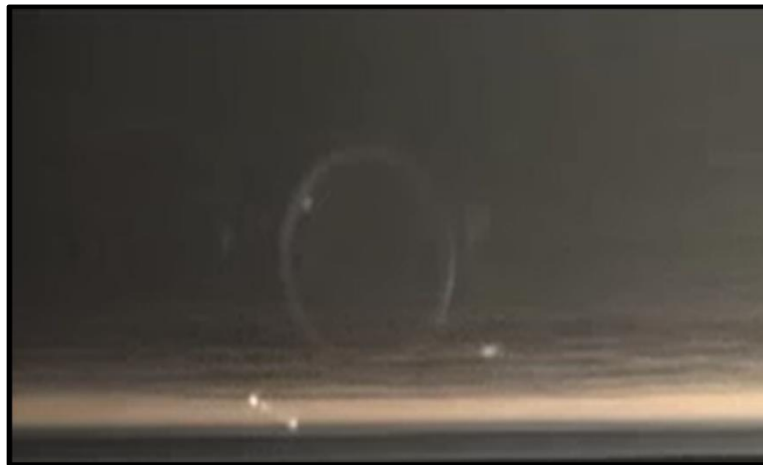
Figure 1.10 Sand streaks at the pipe bottom. Side view.
(C_v=5.38·10^{-5}. Vw=0.5 m/s. Yan, 2010)

Figure 1.11 Sand dunes at the pipe bottom. Side view.
(C_v=5.38·10^{-5}. Vw=0.4 m/s. Yan, 2010)

Based on these experimental results, OLGA simulations were conducted by Sporleder, Lutro and Xu in 2014. In OLGA, there are three different bed conditions in slurry flows: static bed, moving bed and entrainment. For the critical velocity measurements (or MTC condition), the change from the entrainment to the moving bed is taken.

In the Figure 1.12, comparison of the simulation and experimental results is shown. In the figure it is possible to see that OLGA predicts the MTC condition to be constant for all the sand volume fractions. As such, the critical velocity is independent on the sand fraction which is not the same as in the experiments. On the other hand, such independency is observed in several other research works. Also, it can be noticed that there is a strong correspondance between the experimental results by **Al-lababidi et al., 2012** and model of **Turian et al., 1987**.
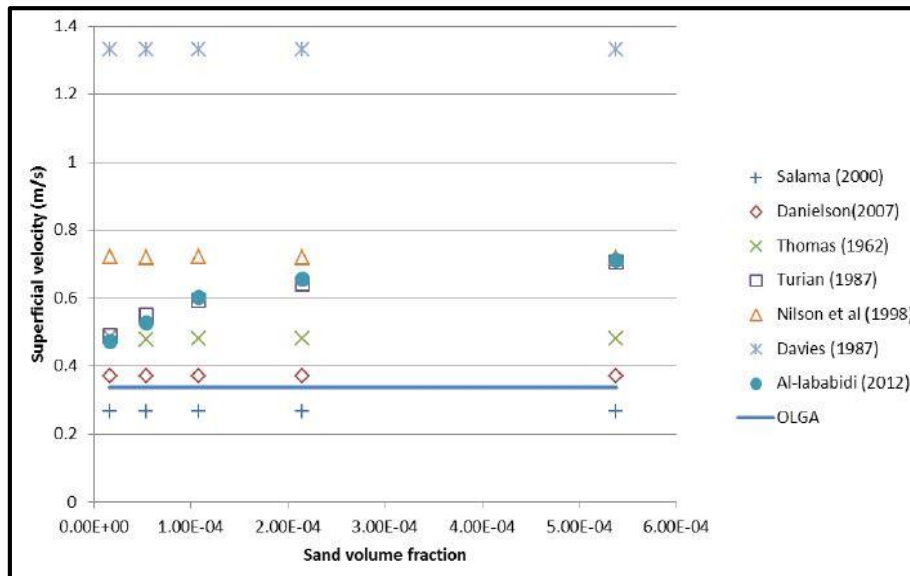
Figure 1.12 Results comparison of the MTC condition in water-sand flows
(Sporleder et al., 2014)

The sand volume concentration in oil and gas production lines can vary significantly from one field to another. For each situation, it is quite costly to conduct such experiments, but the critical velocity parameter is important to identify in order to avoid unpleasant situations such as sand accumulation and pipe blocking. As such, a modeling tool can be a useful asset in predicting the MTC condition for any variation of the flow velocity and concentration. In this thesis, capabilities of the CFD tool ANSYS Fluent are tested for the evaluation of the MTC conditions in dilute slurry flows.

1.2 Motivation for the present work

This section outlines the motivation for conducting this Master's thesis. First, consider the motivation for the particle plug propagation case. As shown, even a well-developed 1D dynamic multiphase simulator such as OLGA is not able to predict the dispersion effect of the propagating particle plug in an appropriate manner. As such, it is decided to model this

phenomenon in a commercial CFD package ANSYS Fluent. CFD techniques have much more capabilities to predict flows behavior at different conditions than OLGA. However, it is not obvious that ANSYS Fluent would model this phenomenon in an accurate manner, since during the literature review none CFD simulation cases of such flows are found which will be mentioned in Chapter 2. As such, the first motivation and goal of the project is to test the ANSYS Fluent capabilities to model particle plug propagation and the dispersion effect in 2D and 3D modes.

CFD simulation can be a very time consuming operation. Sometimes it is difficult to understand which model or correlation is suitable for a particular simulation case, as such the research might take a lot of effort without producing any result. Since many parameters are required to be selected in the CFD simulation of particle flows at high concentration using Eulerian Granular model, another motivation point is to conduct a detailed discussion of all the possible models for modelling of the particle plug flows and select the most appropriate model setup.

In addition, it is decided to try to contribute to 1D modelling of particle flows using data from the CFD simulations. Potentially, a slip relation could be obtained from CFD results and used in the future development of 1D codes for dense particle flows.

As for the minimum transport condition case, it can be seen that most of the research works show independency of the critical velocity on the particle volume fraction. As such, the motivation for this work is test the ANSYS Fluent capability in predicting the critical velocity conditions, more specifically, its dependency on the particle volume fraction. In addition, it is interesting to see if ANSYS Fluent is able to predict dunes formation at the pipe bottom, as it was observed in the experiments. If ANSYS Fluent is capable to reproduce the MTC conditions in the similar way as the experiments do, such a tool might be extensively used in the analysis of the multiphase flows in oil and gas production lines to avoid sand deposition.

Last but not least, general recommendations for using ANSYS Fluent in slurry flows modelling from dilute to packed conditions are considered as a goal and motivation of this research work.

Chapter 2
Literature review

2.1 Introduction

As one of the most important parts of the research work, the literature review has to be carried out carefully. It completes the overall overview of the problem, helps to understand the phenomena better and to use the best practices in the research field as well as helps to avoid mistakes previously done by other researchers.

During the continuous literature review, it is found that it is very hard and almost impossible to find any CFD study of the plug propagation case. The same situation is for the critical velocity study. Despite this fact, other similar research works are found and carefully studied which helps in the simulations performed in this thesis.

In addition, a huge part of the literature review is done for understanding of different models, theories and correlations which are used in ANSYS Fluent. Before selecting every single parameter, a lot of work is done to understand the meaning of the parameter, its applicability, different models for its implementation and its influence on the overall results. Moreover, for some parameters, the ANSYS Fluent User's Guide does not provide enough details, as such it is required to read original articles and papers to get full understanding of the models. However, this part of the literature review is not presented in this chapter while it is discussed along the entire thesis report, mainly in the sections of model selections as well as in Chapter 3 which describes the applied theory.

2.2 Particle plug propagation

One of the most similar cases with the particle plug in a pipe which has been studied using ANSYS Fluent is pneumatic conveying of dense phase in pipelines carried out by **Don McGlinchey et al., 2012.** In this work, pneumatic particle transport in pipes is considered, i.e. particle transport by an air flow. The particles are transported at packed conditions from the

beginning of the simulation. The plug length is 0.5 m with a particle diameter of 25 µm and density of 2500 kg/m^3. Different pipe geometries are investigated such as a straight pipe and pipes with different forms of expansions. The initial pipe diameter is 0.1 m. For turbulence modelling, the standard k-ε model is selected. The main objective of the research is understanding of particle behavior in sudden pipe expansion zones and checking an existence of a recirculation flow in these zones.

Based on this research many question appeared to be asked. The authors did not consider many important simulations features. For example, only standard wall function was considered for boundary layer resolution and other options were not discussed at all. In addition, only one set of parameters was discussed, for example, models for the drag law, frictional viscosity, etc. Moreover, only first order upwind discretization was presented and the results were not compared with experiments. As such, the results are very unreliable.

Despite the weaknesses of this research work, many important features are understood. First, it is necessary to consider and discuss carefully as many options as possible in order to make the results more reliable. As such, it gave a big motivation for this research to consider all the possible models for different parameters as well as all possibilities for wall boundary layer resolution. Secondly, the second order discretization is mandatory to consider since the figures with the simulation results clearly show numerical diffusion which should be taken into account. Finally, the research work shows that it is at least possible to simulate the particle plug propagation at high particle concentration in pipes. As such, a lot of motivation and understanding of important parameters have been obtained though the review of this paper.

Kushal 2014 conducted a CFD modelling research of slurry flows in ANSYS Fluent using Eulerian model. The objective of the research was investigation of particle distribution in slurry pipe flows and the corresponding pressure drop. The particle concentration by weight was investigated from 30 to 60% which correspond to a noticeable pipe volume loading, so that a considerably high concentrated flows were investigated. Standard wall functions along with standard k-ε model was used for turbulence modelling. The first order upwind discretization schemes were used for all the parameters. The particles with a diameter of 33 µm were tested over a wide range of flow velocities. Syamlal models for drag and granular viscosity were successfully used. Fluent software was capable to model solid-liquid flow and the measurements of pressure drop, particle velocities and flow regime predictions were successfully modelled and validated with experimental data.

The weakness of the work is the fact that the second order discretization is not tested, which could potentially change the particle distribution and make it to be even a better fit with the experimental data. However, the work provides many details which are very useful for the development of the present research work.

Ekambara et.al., 2009 conducted a CFD research of slurry flows in pipes in ANSYS CFX. The simulations were carried out in a 3D horizontal pipe. The objective of the investigation was testing of the influence of particle volume concertation, size and velocities on the particle concentration profiles and pressure losses. The volume concentrations were tested up to 45% with a particle diameter up to 500μm. The standard k-ε model was applied to simulate the turbulence effect. Gidaspow models were used for the drag and granular viscosity models. A very important conclusion from the research is the fact that turbulent dispersion force significantly influences the particle concentration profiles and it is mandatory to include it when the concentration profile is of interest in a CFD simulation. As a result of the research work, it was shown that the ANSYS CFX is capable to predict particle concentration profiles as well as pressure drop which excellently fit the experimental data.

A similar research work was conducted by **Lahiri et al., 2010.** However, ANSYS Fluent software was used for CFD simulations instead of ANSYS CFX. Moreover, the particle volume fraction of 50% was tested and the results were validated with experimental data. As in most of such researches, the standard k-ε model with mixture properties was used for turbulent modelling. Different drag models such as Syamlal, Gidaspow and Wen and Yu were tested in a wide range of particle velocities and concentrations. The simulations were run with double precision. Generally, CFD results showed a good agreement with the experimental data for concentration profiles and the results could be potentially applied for models development of slurry flows in large pipeline systems. However, in the results, the information about the difference in using different drag models is not presented, as such it is not clear why the researcher decided to use three models without further evaluation. If such information would have been presented in a more clear way, the results would be much more valuable for this particular thesis because it would significantly shorten the model selection process.

Nabil et al., 2013 conducted experiments as well as ANSYS Fluent simulations of slurry flows. In contrary with the above mentioned researches, higher particle sizes were used in the simulation such as 0.2, 0.7 and 1.4 mm. Up to 30% particle volume concentration was tested with a particle density of 2650 kg/m^3. Eulerian Granular model was used in the CFD study. As

often, the standard k-ε model with mixture properties was used for turbulence modelling. An important conclusion which is different from other researches was the fact that it is also possible to predict the particle flow regimes such as moving bed. Moreover, it was also confirmed that for relatively big particles, the particle concentration profiles had a good agreement with the experimental data. However, only the first order discretization schemes were used in the CFD study, as such, the results have some uncertainty with respect to accuracy. Also, the first wall cell size is not discussed which might be a very important parameter for Eulerian Granular model simulations.

Chen et al., 2009 applied Eulerian Granular model for CFD simulations of coal-water slurry flows in horizontal pipelines. For turbulence modelling, RNG k-ε model was applied. The tested particle diameters followed bimodal distribution with diameter values of 65 and 345 μm. The Lun et al. models for radial distribution function and solids pressure were applied in this CFD study. Second order upwind discretization was used, as such high accuracy of the simulation results was obtained which makes the obtained results more valuable. The results were validated with experiments conducted by the author as well as with other research works. The conclusions of the paper state that the Eulerian model is capable to predict the main features of dense slurry flows at many different operating conditions. In addition, it was concluded that particle-particle interaction plays an important role in the particle concentration profile and the restitution coefficient was found to be in the range of 0.7-0.95.

The research work of high concentrated solid-liquid flows by **Smoldyrev A. and Safonov Y. 1979** show that there is radial particle migration from walls to the pipe core, as such the particle concentration in the pipe center axis is higher than at the walls. Based on their observations, **Neil, 1988** provided a formula to calculate the thickness of the depleted particle boundary layer. However, in his formula, the viscosity of the boundary layer is assumed to be equal to water viscosity, which is wrong for high concentrated flows. Since in such flows the viscosity at the boundary layer is much higher, the estimation of the depleted boundary layer might differ significantly from the Neil's calculations. This conclusion was made by **Paterson, 1991.** The discussion of the boundary layer depletion is important and it is expected to see a similar particle behavior in the present research and has to be discussed in the simulation results part.

2.3 MTC condition study

One similar research work on dilute sand-water flows has been carried out by **Tebowei et al., 2015**. The goal of the research work was to test the capabilities of CFD techniques in predicting sand transport flow regimes at dilute concentrations. A horizontral and V-shape pipes have been studied by using Eulerian Granular model. The Gidaspow drag model has been applied toghether with Lun et al. models for bulk viscosity and radial distribution. Unfortunately, the RANS modelling and solver settings are not discussed. The study led to the conclusion that influence of the particle size and concentration on the sand transport characteristices are well compared with the experimental data. However, for the V-shape pipe, an improved CFD model should be developed due to the fact that the curvature of the pipe might induce a secondary field which has a strong influence on the sand tranport conditions.

This part of the literature review is also intended to consider some research works which used DPM model in ANSYS Fluent for the simulation of slurry flows. The most common situation for using DPM model in particle transport is pneumatic conveying transport of solids. **Quek et al., 2005** applied DPM model in CFD simultaions of dilute gas-solids flow in pipe bends. RNG k-ε model was used for turbulence modelling. The Rosin-Rammler distribution diameter function was applied to take into account the difference in the particle size. Solid volume fraction was $2.4 \cdot 10^{-4}$ which is similar to the volume fractions used in this thesis work. Two-way coupling was applied. The results state that the DPM model is able to capture the basic physics of dilute gas-particle flows and the results were validated with the experimental data.

Mezhericher et al., 2011 studied conveying transport of solids using a default and modified DPM models as well as DEM model in ANSYS Fluent. The modified model contained several additional features (User-Defined Functions) in comparison with the default model, for example, particle-particle interaction. Second order upwind discretization was used for all the parameters. The standard k-ε model was applied for turbulence modelling. The volume fraction varied significantly in the tested cases. As a result of the research work, the DPM model produced satisfactory results for the case with the solids volume fraction less than 10%, however, the modified DPM model showed more reliable and precise results with regards to suspended clouds formations. The DEM model produced over a wide range of the particle volume fractions. Based on the example of this work, it can be concluded that even though the default DPM model produces satisfactory results for dilute slurry flows, some improvement of the model using user-defined functions can be made which increases reliability of the results.

2.4 Summary

Particle plug propagation

Based on the literature review, several conclusions are made. First, it is very rear to find a CFD simulations of solid-liquid flows at packing limit conditions. To be more precise, similar researches were conducted only in pneumatic particle transport where the primary phase is air, while the information about particle transport at packing conditions by a liquid flow is absent. Very often packing conditions can be met in fluidized bed systems and a lot of CFD researches have been done in that area, but it does not have a direct relevance for the present research study.

Secondly, many CFD studies using ANSYS Fluent and CFX were conducted regarding the slurry flows transportation using Eulerian model over a wide range of particle volume concentrations and velocities. The highest particle concentrations in those studies are around 50%. Even though the conditions in the current research is not the same, the tested particle concentrations are also high and Fluent and CFX software showed good capabilities to predict the main parameter of such flows.

In addition, it is observed that in all the researches, k-ε model with mixture properties was applied for turbulence modelling. This model showed good abilities to model a turbulent flow behavior in slurry flows. Between the three different types of models, the standard type of k-ε model is mostly used.

Last but not least, many questions appeared during the literature review which helped to make a more extensive research plan for the present thesis work. For example, the grid cell size as well as the boundary layer resolutions are not well discussed in the reviewed research works. One should not have any doubts that these parameters are extremely important to be tested and discussed in turbulent slurry flows, especially for high concentrated flows. It might have a significant impact on the particle concentration profiles, particle velocities, pressure drop, etc. Moreover, in most research works, only the first order discretization schemes are applied for all the parameters. It can be definitely used for slurry flow applications, however, it should be first confirmed that there is not any difference between the first and the second order discretization in terms of the obtained results, or this difference can be neglected. Also, not much attention is paid to the model selection process. By the model selection process, it is meant that it is necessary to provide the reasons why a particular model is chosen for a particular parameter, for example, the drag relation or the bulk viscosity model.

<u>MTC condition study</u>

There is not much applicable material in the literature regarding modelling dilute sand-water flows using the DPM model. As such, some similar gas-solid flows are reviewed. It can be said that the DPM model generally produces satisfactory results, however, sometimes, some improvements of the model are required. Moreover, based on the reviewed research works, it is again difficult to understand which parameters have been used for modelling, for example, any information regarding the tracking options and turbulent dispersion of the DPM model is absent. As such, the weak discussion of the selection process of model parameters will be tried to be avoided in this thesis work.

Generally, based on the advantages and disadvantages of the considered material, all the important features of CFD simulations of slurry flows using Eulerian Granular and DPM models are understood. All the best practices are applied in the CFD study of the particle plug propagation and MTC condition cases, while the weak and unreliable approaches are tried to be avoided or fixed.

Chapter 3
CFD Multiphase Modelling

3.1 Introduction

Computational Fluid Dynamics (CFD) is an engineering tool which is used to predict fluid flow behavior by numerical simulations. Capability of CFD modelling is continuously growing as people apply this powerful tool for different types of flows. In this Master's thesis, multiphase particle flows are studied. In this chapter, CFD approaches for multiphase particle flows modelling used in ANSYS Fluent are described in details.

3.2 CFD multiphase modelling

There are many types of flows which can be resolved by CFD. However, since this particular report considers simulation of multiphase flow problems, approaches for multiphase flow CFD modelling in ANSYS Fluent are discussed. Basically, there are two approaches for multiphase flow modelling: Euler-Euler and Euler-Lagrange. The Euler-Euler approach has three sub-models as shown in the Figure 3.1.
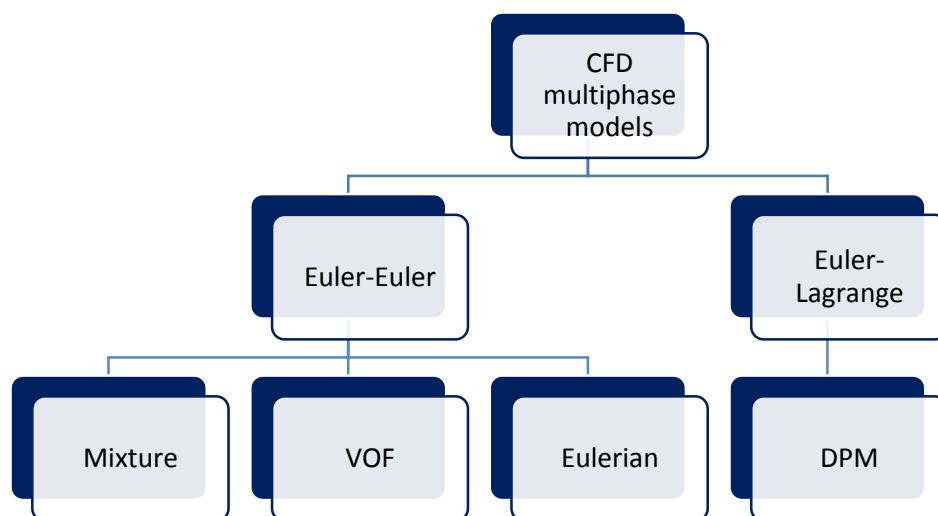
Figure 3.1 Multiphase modelling approaches in ANSYS Fluent

Since the Eulerian Granular and DPM models are used in this research work, it is discussed in details. The description of the rest models can be found in the **ANSYS Fluent User's Guide, 2015**.

3.2.1 Euler-Lagrange approach. DPM model.

In the Euler-Lagrange method, the fluid is considered as continuum in which Navier-Stokes equations are solved while the discrete phase is solved by tracking the particles, droplets or bubbles (ANSYS Fluent User's Guide, 2015). There is an exchange of momentum, mass and energy between the continuum and discrete phases. Particle-particle interaction can be included or neglected in the simulation. If it is neglected, the approach becomes much simpler which shortens the computational time.

This method requires the discrete phase to have a low volume fraction, while the mass loading can be high. Each particle is tracked separately, so that during post-processing, one is able to see the motion of a particular particle in space and time.

Prediction of the particle trajectory becomes possible by integrating the force balance on each individual particle which is considered in a Lagrangian reference frame (ANSYS Fluent User's Guide, 2015). The force balance can be written as follows:

$$\frac{d\vec{u}_p}{dt} = \frac{\vec{u} - \vec{u}_p}{\tau_r} + \frac{\vec{g} \cdot (\rho_p - \rho)}{\rho_p} + \vec{F} \tag{1}$$

where:

$\vec{u}$ – local fluid phase velocity;

$\vec{u}_p$ – particle velocity;

ρ_p – particle density;

ρ – continuum phase density;

$\vec{F}$ – additional force term;

$\dfrac{\vec{u} - \vec{u}_p}{\tau_r}$ – drag force per unit particle mass.

The particle relaxation time τ_r is written in the form:

$$\tau_r = \frac{\rho_p \cdot d_p^2}{18\mu} \frac{24}{C_d \cdot \mathrm{Re}}$$

(2)

where:

C_d – drag coefficient;

d_p – particle diameter;

μ – dynamic viscosity of the fluid.

The Reynolds number in this case is computed as follows:

$$\mathrm{Re} \equiv \frac{\rho d_p \left| \vec{u} - \vec{u}_p \right|}{\mu}$$

(3)

The force $\vec{F}$ in the equation (1) might include several forces which can be selected by a user. The first option is the virtual mass force which describes acceleration of the fluid around the particle. The force can be expressed as follows (ANSYS Fluent User's Guide, 2015):

$$\vec{F} = C_{vm} \frac{\rho}{\rho_p} \left(\vec{u}_p \nabla \vec{u} - \frac{d\vec{u}_p}{dt} \right)$$

(4)

where C_{vm} – the virtual mass factor.

In addition, the force due to the pressure gradient can be included. The force expression has the following form (ANSYS Fluent User's Guide, 2015):

$$\vec{F} = \frac{\rho}{\rho_p} \vec{u}_p \nabla \vec{u}$$

(5)

For this thesis work it is also important to mention the Shaffman lift force which describes the lift effect due to shear. The force has the following form (ANSYS Fluent User's Guide, 2015):

$$\vec{F} = \frac{2Kv^{1/2}\rho d_{ij}}{\rho_p d_p \left(d_{lk}d_{kl}\right)^{1/4}} \left(\vec{u} - \vec{u}_p\right)$$
(6)

where:

K=2.594;

d_{ij} – deformation tensor;

v – kinematic viscosity.

<u>Turbulent dispersion</u>

The influence of the turbulence on the particle dispersion can be taken into account by using stochastic tracking or particle cloud model.

When stochastic tracking is used, the turbulent dispersion is predicted by integrating trajectory equations of particles and taking into account the instantaneous fluid velocity. The number of representative particles can be defined by a user as "number of tries" parameter. In such a way, randomness of the turbulence is included in the particle dispersion effect (ANSYS Fluent User's Guide, 2015).

The particle cloud tracking model uses statistical methods for predicting the influence of the turbulence on the particle dispersion. The particle concentration about the mean trajectory is described by a probability density function. The mean trajectory is calculated using the ensemble-averaged equations of particle motions which represent the cloud (ANSYS Fluent User's Guide, 2015).

The more detailed description of the turbulent dispersion models can be found in the **ANSYS Fluent User's Guide, 2015**.

<u>Phase coupling</u>

When a particle trajectory is computed, the mass, momentum and heat is received and lost by a particle stream and these parameters can be included in the subsequent calcuations of the continious phase. During the simulation, the continious phase always affects the disrete phase (one-way coupling), but it is also possible to include an impact of the discrete phase on the continious phase (two-way coupling). The two-way coupling is achieved by solving the motion equations of the discrete and continious phases in an alternate manner until the solutions in

both phases stop changing (ANSYS Fluent User's Guide, 2015). A typical interphase exchange from the particle to the continuum is shown in the Figure 3.2.
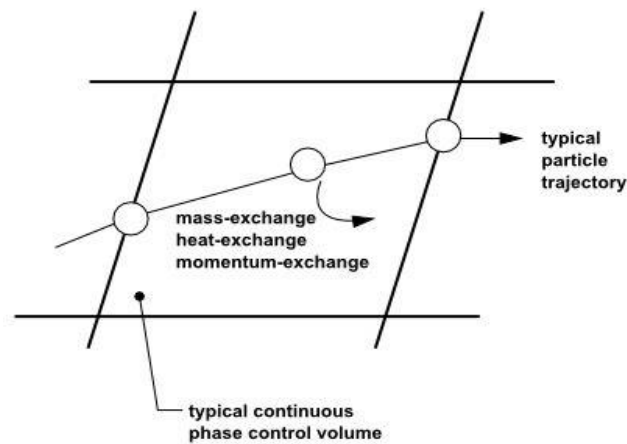
Figure 3.2 Transfer of mass, momentum and heat between the discrete and continuum phases (ANSYS Fluent User's Guide, 2015)

Particle tracking

There are two approaches of particle tracking in ANSYS Fluent: steady and unsteady. If steady tracking is used, a released particle is tracked until it reaches the final destination according to boundary conditions or until a specified number of particle time steps have been reached. As such, the particle typically crosses many domain cells and interacts with the continuous phase and if the simulation is coupled, changes the DPM sources in each cell. These sources affect the continuous phase solution for a specified number of iterations or time steps depending if the flow is steady or unsteady (ANSYS Fluent User's Guide, 2015).

If unsteady tracking is used, a particle is advanced by a defined number of particle time steps. The particle is not required to reach its final destination, before the flow solution is updated (ANSYS Fluent User's Guide, 2015).

3.2.2 Euler-Euler approach. Eulerian model

In Euler-Euler method, the phases of the flow are assumed to be interpenetrating continua. Due to the fact that it is not possible for a fluid volume to be occupied by another phase, the concept of phase volume fraction takes place. It means that these volume fractions are functions of space and time which sum is equal to unity (ANSYS Fluent User's Guide, 2015).

For each phase, conservation equations are applied which are closed by empirical laws. If the granular flow is considered, kinetic theory is also applied.

Eulerian model

The model solves momentum and continuity equations for each phase. Pressure in the domain is shared by all phases. The number of phases is limited by only the memory requirements, computational time and convergence behavior.

The Eulerian model in ANSYS Fluent does not separate fluid-fluid and fluid-solid multiphase flows. A fluid-solid (granular) flow is a flow which involves one phase as a granular phase which is treated as a continuum one (ANSYS Fluent User's Guide, 2015).

Please note, that the Eulerain model contains a lot of different models and correlations for many different parameters. However, not all of them are applicable for the particle plug propagation case considered in this thesis work and, therefore, are not discussed. The most applicable equations and models are described below.

Volume fraction equation

Volume fraction α_q expresses the relative space occupied by each phase. The volume of the phase is defined as:

$$V_q = \int_V \alpha_q dV \tag{7}$$

$$\sum_{q=1}^{n} \alpha_q = 1 \tag{8}$$

where:

V_q – volume of qth phase;

α_q – qth phase volume fraction;

n – number of phases.

The volume fraction equations (7) and (8) can be solved by implicit or explicit time discretization.

Continuity equation

The continuity equation is written in the form:

$$\frac{1}{\rho_{rq}} \left(\frac{\partial}{\partial t} \left(\alpha_q \rho_q \right) + \nabla \cdot \left(\alpha_q \rho_q \vec{\upsilon}_q \right) \right) = \sum_{p=1}^{n} \left(\dot{m}_{pq} - \dot{m}_{qp} \right) \tag{9}$$

where:

ρ_q – density of the qth phase;

ρ_{rq} – phase reference density for the qth phase;

$\vec{\upsilon}_q$ – velocity of the qth phase

$\dot{m}_{pq}$ and $\dot{m}_{qp}$ – mass transfer from the pth to qth phase and vice versa.

Together with the condition of the equation (7), solution for the continuity equation for the secondary phase gives the primary volume fraction. This approach is common to fluid-fluid and granular flows (ANSYS Fluent User's Guide, 2015).

Fluid-Fluid momentum equation

Fluid-Fluid momentum equation has the following form:

$$\frac{\partial}{\partial t}\left(\alpha_q \rho_q \vec{\upsilon}_q\right) + \nabla \cdot \left(\alpha_q \rho_q \vec{\upsilon}_q \vec{\upsilon}_q\right) = -\alpha_q \nabla p + \nabla \cdot \overline{\overline{\tau}}_q + \alpha_q \rho_q \vec{g} +$$
$$+ \sum_{p=1}^{n}\left(K_{qp}\left(\vec{\upsilon}_p - \vec{\upsilon}_q\right) + \dot{m}_{pq}\vec{\upsilon}_{pq} - \dot{m}_{qp}\vec{\upsilon}_{qp}\right) + \left(\vec{F}_q + \vec{F}_{lift,q} + \vec{F}_{wl,q} + \vec{F}_{vm,q} + \vec{F}_{td,q}\right)$$

(10)

where:

$\overline{\overline{\tau}}_q$ – the qth phase stress tensor;

$\vec{F}_q$ – external body force;

$\vec{F}_{lift,q}$ – lift force;

$\vec{F}_{wl,q}$ – wall lubrication force;

$\vec{F}_{vm,q}$ – virtual mass force;

$\vec{F}_{td,q}$ – turbulent dispersion force;

$\vec{g}$ – gravity acceleration;

$\vec{\upsilon}_{pq}$ and $\vec{\upsilon}_{qp}$ – interphase velocities;

K_{qp} – interphase momentum exchange coefficient;

$\vec{\upsilon}_p$ and $\vec{\upsilon}_q$ – phase velocities;

n – total number of phases.

The qth phase stress tensor has the following form:

$$\bar{\bar{\tau}}_q = \alpha_q \mu_q \left(\nabla \vec{\upsilon}_q + \nabla \vec{\upsilon}_q^T \right) + \alpha_q \left(\lambda_q - \frac{2}{3} \mu_q \right) \nabla \cdot \vec{\upsilon}_q \bar{\bar{I}} \tag{11}$$

where:

μ_q – shear viscosity of the qth phase;

λ_q – bulk viscosity of the qth phase;

$\bar{\bar{I}}$ – stress tensor invariant.

Fluid-Solid momentum equation

$$\frac{\partial}{\partial t} \left(\alpha_s \rho_s \vec{\upsilon}_s \right) + \nabla \cdot \left(\alpha_s \rho_s \vec{\upsilon}_s \vec{\upsilon}_s \right) = -\alpha_s \nabla p - \nabla p_s + \nabla \cdot \bar{\bar{\tau}}_s + \alpha_s \rho_s \vec{g} +$$
$$+ \sum_{p=1}^{n} \left(K_{ls} \left(\vec{\upsilon}_l - \vec{\upsilon}_s \right) + \dot{m}_{ls} \vec{\upsilon}_{ls} - \dot{m}_{sl} \vec{\upsilon}_{sl} \right) + \left(\vec{F}_s + \vec{F}_{lift,s} + \vec{F}_{wl,s} + \vec{F}_{vm,s} + \vec{F}_{td,s} \right) \tag{12}$$

where:

p_s – the sth phase solids pressure;

$K_{ls} = K_{sl}$ – momentum exchange coefficient between fluid or solid phase "l" and solid phase "s";

$\dot{m}_{ls}$ and $\dot{m}_{sl}$ – interphase mass transfer;

n – total number of phases.

The force terms are analogical with ones in the equation (8), but "s" notation corresponds to solids.

Conservation of energy

In order to describe energy conservation in multiphase flows in Eulerian model, an individual enthalpy equation is written for each phase:

$$\frac{\partial}{\partial t}\left(\alpha_q \rho_q h_q\right) + \nabla \cdot \left(\alpha_q \rho_q h_q \vec{\upsilon}_q\right) = \alpha_q \frac{\partial p_q}{\partial t} + \bar{\bar{\tau}}_q : \nabla \vec{\upsilon}_q - \nabla \cdot \vec{q}_q + S_q + \sum_{p=1}^{n}\left(Q_{pq} + \dot{m}_{pq} h_{pq} - \dot{m}_{qp} h_{qp}\right) \quad (13)$$

where:

h_q – specific enthalpy of the qth phase;

$\vec{q}_q$ – heat flux;

S_q – source term;

Q_{pq} – intensity of heat exchange between the pth and qth phases;

h_{pq} – specific interphase enthalpy.

Models and correlations for granular flow

Since for this thesis the granular model is selected for modelling, only models which are suitable for modelling of fluid-solid as well as solid-solid interaction are described while fluid-fluid interaction is disregarded.

As it can be seen from the governing equations above, there are many terms which influence the flow behavior and have to be modelled appropriately. There are many correlations for each of the terms and it is not always an easy task to select the appropriate one. Sometimes, only port-processing of the results can help to understand which model has to be used for a particular flow problem. The phase interaction parameters such as drag, lift, turbulent dispersion and interfacial area are discussed below.

Drag force

The drag force functions in ANSYS Fluent are modeled using the solid-liquid exchange coefficient K$_{sl}$. Generally, this coefficient is written in the form:

$$K_{sl} = \frac{\alpha_s \rho_s f}{\tau_s} \quad (14)$$

where:

α_s – solids volume fraction;

ρ_s – solids density;

f – drag function which is computed differently in each model.

Particulate relaxation time τ_s is computed as:

$$\tau_s = \frac{\rho_s d_s^2}{18\mu_l} \tag{15}$$

where:

d_s – diameter of particles of the phase "s";

μ_l – dynamic viscosity of the phase "l".

The parameter f includes drag coefficient C_D which is calculated based on the relative Reynolds number. There are several approaches for calculating the parameter f.

Syamlal-O'Brien model

The first approach is Syamlal-O'Brien model. In this model, the parameter f and C_D are computed as follows (ANSYS Fluent User's Guide, 2015):

$$f = \frac{C_D \operatorname{Re}_s \alpha_l}{24 v_{r,s}^2} \tag{16}$$

$$C_D = \left(0.63 + \frac{4.8}{\sqrt{\operatorname{Re}_s / v_{r,s}}}\right)^2 \tag{17}$$

The relative Reynolds number has the following formula:

$$\operatorname{Re}_s = \frac{\rho_l d_s \left|\overrightarrow{v_s} - \overrightarrow{v_l}\right|}{\mu_l} \tag{18}$$

where "l" is defined for liquid and "s" is defined for solid phase particles.

An important parameter here is $v_{r,s}$ – the terminal velocity for the solids phase which is calculated as follows:

$$v_{r,s} = 0.5\left(\alpha_l^{4.14} - 0.06\operatorname{Re}_s + \sqrt{\left(0.06\operatorname{Re}_s\right)^2 + 0.12\operatorname{Re}_s\left(1.6\alpha_l^{1.28} - \alpha_l^{4.14}\right) + \alpha_l^{8.28}}\right) \tag{19}$$

Based on the formulas above, the fluid-solid exchange coefficient is calculated as (ANSYS Fluent User's Guide, 2015):

$$K_{sl} = \frac{\alpha_s \alpha_l \rho_l}{4 \upsilon_{r,s}^2 d_s} C_D \left(\frac{\text{Re}_s}{\upsilon_{r,s}} \right) \left| \vec{\upsilon}_s - \vec{\upsilon}_l \right| \qquad (20)$$

Wen and Yu model

In this model the fluid-solid exchange coefficient is written as follows:

$$K_{sl} = \frac{3 \alpha_s \alpha_l \rho_l}{4 d_s} C_D \left| \vec{\upsilon}_s - \vec{\upsilon}_l \right| \alpha_l^{-2.65} \qquad (21)$$

$$C_D = \frac{24}{\alpha_l \text{Re}_s} \left[1 + 0.15 \left(\alpha_l \text{Re}_s \right)^{0.687} \right] \qquad (22)$$

The Reynolds number is calculated as in the previous model. This model is recommended for dilute systems (ANSYS Fluent User's Guide, 2015).

Gidaspow model

For the flow with high solid volume fractions, the Gidaspow model computes the fluid-solid exchange coefficient as follows (ANSYS Fluent User's Guide, 2015):

$$K_{sl} = 150 \frac{\alpha_s \left(1 - \alpha_l \right) \mu_l}{\alpha_l d_s^2} + 1.75 \frac{\rho_l \alpha_s \left| \vec{\upsilon}_s - \vec{\upsilon}_l \right|}{d_s} \qquad (23)$$

Solid-Solid exchange coefficient

In order to take into account the particle-particle interaction, the solid-solid exchange coefficient is introduced as follows:

$$K_{sl} = \frac{3 \left(1 + e_{ls} \right) \left(\frac{\pi}{2} + C_{fr,\text{ls}} \frac{\pi^2}{8} \right) \alpha_s \rho_s \alpha_l \rho_l \left(d_l + d_s \right)^2 g_{0,ls} \left| \vec{\upsilon}_s - \vec{\upsilon}_l \right|}{2 \pi \left(\rho_l d_l^3 + \rho_s d_s^3 \right)} \qquad (24)$$

where:

e_{ls} − coefficient of restitution;

$C_{fr,\text{ls}}$ − coefficient of friction between l[th] and s[th] solid phase particles;

$g_{o,ls}$ − radial distribution coefficient;

d_l – diameter of the particles in the solid phase "l". If the flow has only one solid phase, it is equal to zero.

Lift force

As it is stated in the ANSYS Fluent User's Manual, the lift force can be neglected if the flow has high particle concentration. In this report, the Eulerian model simulates the flow with particles at packing limit, so that the influence of the lift force is negligible. As such, the detailed description of the force is not provided.

Turbulent dispersion force

The turbulent dispersion force takes into account the turbulent momentum exchange between the interphases.

There are several models of the turbulent dispersion force in ANSYS Fluent:

- Lopez de Bernardo;
- Simonin;
- Burns et al..

The model of Lopez de Bernardo is derived for turbulent bubbly flows and not appropriate for modelling of solids transportation, as such it is not described in details.

Simonin derived the model of the turbulent dispersion force based on turbulence theory of Tchen. The Simonin model is applicable for dilute particle flows which have low inertia (Yam, 2012). Since in the plug the particles are at packing limit, the model is not suitable for this type of flows, as such, it is not described in details.

The last model is Burns et.al. This model is develop based on Favre averaging of the drag. The dispersion scalar is estimated by using the turbulent viscosity of the continuous phase:

$$D_q = D_p = D_{tq} = \frac{\mu_{tq}}{\rho_q} \tag{25}$$

where:

D_q, D_p and D_{tq} – dispersion scalars;

μ_{tq} – turbulent viscosity of the qth (continuous) phase;

ρ_q – density the qth (continuous) phase.

The turbulent dispersion force is computed as (Burns et al., 2004):

$$\vec{F}_{td,q} = -F_{td,p} = C_{TD} K_{pq} \frac{\vec{D}_q}{\sigma_{pq}} \left(\frac{\nabla \alpha_p}{\alpha_p} - \frac{\nabla \alpha_q}{\alpha_q} \right) \tag{26}$$

where:

$\vec{F}_{td,q}$ – turbulent dispersion force;

C_{TD} – turbulent dispersion coefficient;

K_{pq} – interphase exchange coefficient;

σ_{pq} – Prandtl number;

α_p and α_q – volume fractions of the particle and continuous phases respectively.

According to the **Burns et al., 2004**, the model is a general framework for modelling of turbulent dispersion in Eulerian multiphase flows. It is tested against a wide range of multiphase flows including liquid-solid flows.

Interfacial area

There are two possibilities to compute the interfacial are (ANSYS Fluent User's Guide, 2015):

- ia-symmetric – takes into account the primary and secondary phase volume fractions in order to estimate the interfacial area;
- ia-particle –takes into account the secondary phase only when estimates the interfacial area.

Phase properties models

The phase properties models is a crucial part of the granular flow modelling. If an inappropriate model is selected for a particular parameter, the simulation might not converge and give unrealistic results. The granular flow includes the following properties:

- Diameter;
- Granular viscosity;
- Granular bulk viscosity;
- Frictional viscosity;

- Granular temperature;

- Solids pressure;

- Radial distribution;

- Elasticity modulus;

- Packing limit.

For most of the parameters there are several alternative models. The models for properties of the granular flow in ANSYS Fluent are based on several research works. They are:

1) Syamlal, Rogers, & O'Brien, 1993;

2) Lun, Savage, Jeffrey, & Chepurniy, 1984;

3) Ahmadi & Ma, 1990;

4) Gidaspow, Bezburuah, & Ding, 1992;

5) Schaeffer, 1987;

6) Johnson & Jackson, 1987.

Below there is description of the properties models.

Granular viscosity

The Syamlal-O'Brien model defines the granular (or kinetic) viscosity as follows (Syamlal et al., 1993):

$$\mu_{s,kin} = \frac{\alpha_s d_s \rho_s \sqrt{\Theta_s \pi}}{6(3 - e_{ss})} \left[1 + \frac{2}{5}(1 + e_{ss})(3e_{ss} - 1)\alpha_s g_{0,ss} \right] \tag{27}$$

where:

α_s – particle fraction;

d_s – particle diameter;

ρ_s – particle density;

$\mu_{s,kin}$ – granular viscosity;

e_{ss} – coefficient of restitution;

$g_{o,\text{ss}}$ – radial distribution coefficient;

Θ_s – granular temperature.

In the Gidaspow formulation, the same parameter is defined as (Gidaspow et al., 1992):

$$\mu_{s,kin} = \frac{10 d_s \rho_s \sqrt{\Theta_s \pi}}{96 \alpha_s (1+e_{ss}) g_{0,ss}} \left[1 + \frac{4}{5} (1+e_{ss}) \alpha_s g_{0,ss} \right]^2 \alpha_s \qquad (28)$$

It is advisable to use the kinetic viscosities models linking to the drag functions of the respective authors (ANSYS Fluent User's Guide, 2015).

Bulk viscosity

For the bulk viscosity, it is possible to specify a constant number, UDF, or use Lun et al. model which defines the bulk viscosity as (Lun et al., 1984):

$$\lambda_s = \frac{4}{3} \alpha_s^2 \rho_s d_s g_{0,ss} (1+e_{ss}) \left(\frac{\Theta_s}{\pi} \right)^{1/2} \qquad (29)$$

where λ_s – bulk viscosity.

Frictional viscosity

For the frictional viscosity, it is possible to specify a constant value, UDF or use one of the two models:

- Schaeffer;
- Johnson and Jackson.

The Schaeffer model uses the expression (Schaeffer, 1987):

$$\mu_{s,fr} = \frac{p_s \sin \phi}{2 \sqrt{I_{2D}}} \qquad (30)$$

where:

$\mu_{s,fr}$ – frictional viscosity;

p_s – solids pressure;

ϕ – angle of internal friction;

I_{2D} – second invariant of the deviatoric stress tensor.

In the Johnson model, the frictional viscosity is formulated as (Johnson & Jackson, 1987):

$$\mu_{fr} = P_{fr} \sin \phi \qquad (31)$$

$$P_{fr} = 0.05 \alpha_s \frac{\left(\alpha_s - \alpha_{s,min} \right)^2}{\left(\alpha_{s,max} - \alpha_s \right)^5} \qquad (32)$$

where:

P_{fr} – frictional pressure;

$\alpha_{s,MAX}$ – maximum local particle fraction;

$\alpha_{s,\min}$ – minimum local particle fraction.

Frictional pressure

For the frictional pressure, the Johnson model can be used which is described above. As an alternative, the Syamlal et al. model can be used. The form is as follows (Syamlal et al., 1993):

$$\mu_{fr} = \frac{P_{fr} \cdot \sin\phi}{2\sqrt{I_{2D}}} \tag{33}$$

$$P_{fr} = 10^{25} \left(\varepsilon_s^* - \varepsilon_s \right)^{10} \tag{34}$$

where:

ε_s^* – packing limit of solids;

ε_s – solids fraction.

Solids pressure

There are three available models which can be used to define the solids pressure in ANSYS Fluent. The first one is the model of Lun et al., which is written in the following form (Lun et al., 1984):

$$P_s = \alpha_s \rho_s \Theta_s + 2\rho_s(1 + e_{ss})\alpha_s^2 g_{0,ss} \Theta_s \tag{35}$$

where P_s – solids pressure.

The Syamlal model has almost the same form, however, neglects the first term (Syamlal et al., 1993):

$$P_s = 2\rho_s(1 + e_{ss})\alpha_s^2 g_{0,ss} \Theta_s \tag{36}$$

If compare these two models, they can differ by orders of magnitude because the first term in the Lun et al. model has the main impact on the total value of solids pressure.

The last model is a model of D.Ma and G. Ahmadi which is written in the following form (Ahmadi & Ma, 1990):

$$P_s = \alpha_s \rho_s \Theta_s \left[\left(1 + 4\alpha_s g_{0,ss}\right) + \frac{1}{2}\left[\left(1 + e_{ss}\right)\left(1 - e_{ss} + 2\mu_{fr}\right)\right] \right] \tag{37}$$

Radial distribution

The last modeling parameter is a radial distribution function. This parameter is important since it is included in many other ones. There are four possible models to select:

- Syamlal (Syamlal et al., 1993)

$$g_{0,ss} = \frac{1}{1-\alpha_s} + \frac{3\alpha_s}{2(1-\alpha_s)^2} \qquad (38)$$

- Lun et.al. (Lun et al., 1984)

$$g_{0,ss} = \left[1 - \left(\frac{\alpha_s}{\alpha_{s,MAX}} \right)^{1/3} \right]^{-1} \qquad (39)$$

- Arastoopour (Arastoopour & Ibdir, 2005)

$$g_{0,ss} = \frac{1}{1 - \dfrac{\alpha_s}{\alpha_{s,MAX}}} \qquad (40)$$

- Ma-Ahmadi (Ahmadi & Ma, 1990)

$$g_{0,ss} = \frac{1 + 2.5\alpha_s + 4.59\alpha_s^2 + 4.52\alpha_s^3}{\left(1 - \left(\dfrac{\alpha_s}{\alpha_{s,MAX}} \right)^3 \right)^{0.678}} \qquad (41)$$

3.3 RANS modelling

Any fluid flow motion can be described by the Navier-Stokes equations. Despite the fact that the equation was derived in 1800's, there is no general exact analytical solution up to now. This is a 3-dimentsional non-linear partial differential equation which has the following general form (Andersson, 2015):

$$\rho \frac{\partial \vec{u}}{\partial t} + \rho (\vec{u} \cdot \nabla \vec{u}) = -\nabla p + \mu \cdot \nabla^2 \vec{u} + \rho \cdot \vec{f} \qquad (42)$$

where:

$\rho \dfrac{\partial \vec{u}}{\partial t}$ – rate of change of momentum;

$\rho (\vec{u} \cdot \nabla \vec{u})$ – net convective rate of momentum;

$-\nabla p$ – pressure force;

$\mu \cdot \nabla^2 \vec{u}$ – viscous force;

$\rho \cdot \vec{f}$ – body force.

Since this equation is not generally solved yet, people have to find another way to apply the equation for resolving the fluid flow behavior. One of the most common and widely used approaches is modelling this equation by using time averaging. In this method, flow variables are decomposed on the mean and fluctuation values, for example:

$$\tilde{u}_i = U_i + u_i'$$
(43)

where:

U_i – mean value;

u_i' – fluctuation value.

$$U_i = \frac{1}{T} \int_{t_0}^{t_0+T} \tilde{u} dt$$
(44)

The integration time T is called "time window".

This decomposition is named after Osborne Reynolds who applied it for the Navier-Stokes equation in 1895 (Reynolds, 1895). The time averaged values of the fluid flow parameters are often sufficient to understand the general behavior of the flow. By means of time averaged decomposition, the Navier-Stokes equation becomes:

$$\frac{\partial U_i}{\partial t} + U_j \frac{\partial U_i}{\partial x_j} = \frac{1}{\rho} \frac{\partial}{\partial x_j} \left(-P \cdot \delta_{ij} + 2\mu S_{ij} - \rho \overline{u_i' u_j'} \right)$$
(45)

Here velocity, pressure and strain rate have mean values and written with capital letters. One may notice that this is almost the same equation as the original Navier-Stokes except the very last term $-\rho \overline{u_i u_j}$ which is called Reynolds stress term which is necessary to be modelled in order to use the RANS equation for a particular flow problem. This becomes possible with a help of Boussinesq's eddy viscosity hypothesis which Boussinesq postulated in 1877. This hypothesis can be written as (Andersson, 2015):

$$\tau_{ij} = 2\mu_t S_{ij} - \frac{2}{3} \rho k \delta_{ij}$$
(46)

As it can be seen, the hypothesis states about the proportional relation of Reynolds stress tensor τ_{ij} and mean strain rate tensor S_{ij}. The second term on the right hand side is required in order to be consistent with turbulent kinetic energy definition for incompressible flow modelling.

In an open general form the hypothesis is written as follows (Andersson, 2015):

$$-\rho\overline{u_i u_j} = 2\mu_t\left(\frac{\partial U_i}{\partial x_j} + \frac{\partial U_j}{\partial x_i} - \frac{2}{3}\frac{\partial U_k}{\partial x_k}\delta_{ij}\right) - \frac{2}{3}\rho k\delta_{ij} \tag{47}$$

When the Boussinesq eddy viscosity hypothesis is applied for modelling, the next task appears – getting the value of the turbulent viscosity. If this value is obtained, all the parameters are known, so that it is possible to model the Reynolds stresses and the RANS equations.

In ANSYS Fluent, modelling of the turbulent viscosity is done by several different models. These models are shown in the Figure 3.3. In details, only k-ε and k-ω models are described since they are mostly relevant for all the CFD simulations of this thesis.
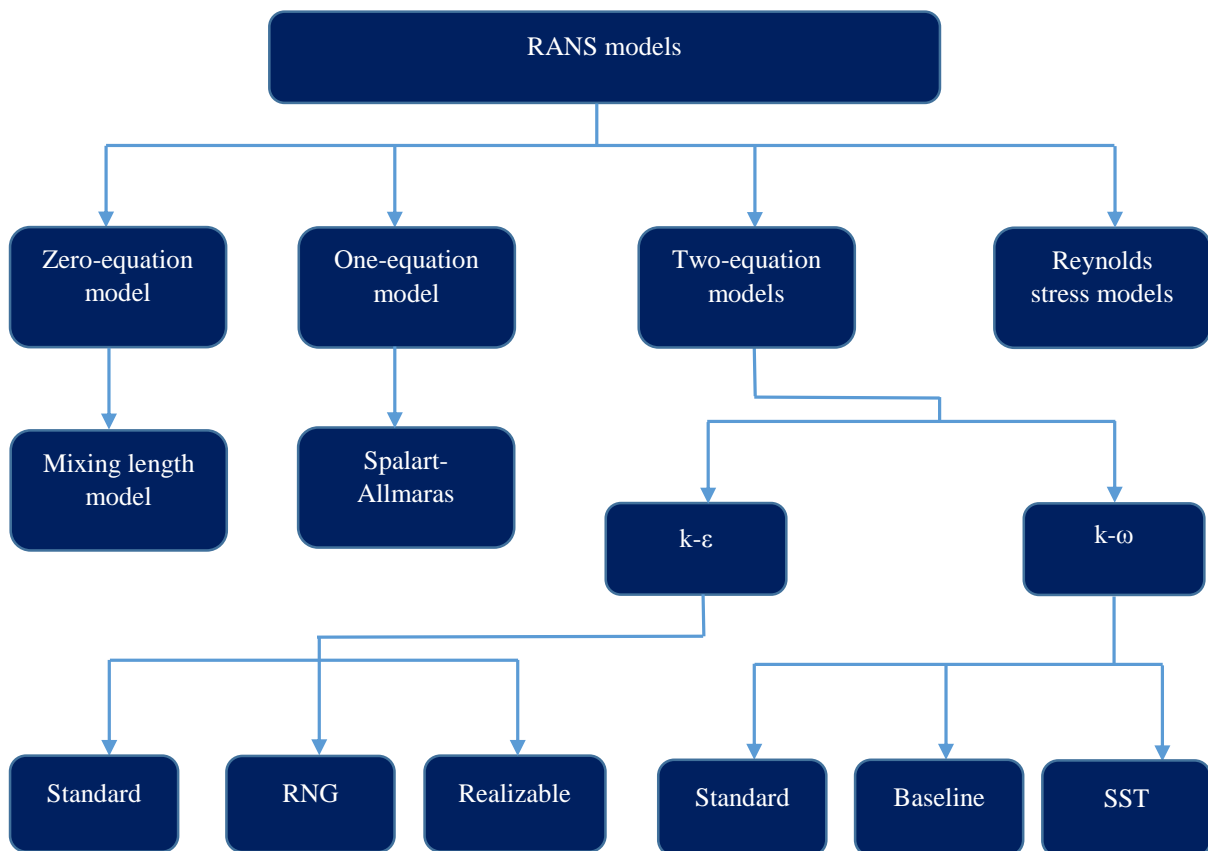
Figure 3.3 Schematic overview of the RANS models in ANSYS Fluent

k-ε models

The k-ε model is a two-equation type model. The two-equation models give a possibility to determine a turbulent length and time scales by solving two transport equations. The standard k-ε model is based on transport equations for k – turbulent kinetic energy and ε – turbulent dissipation rate. The derivation of the model is based on the assumption that the flow is fully turbulent. In addition, the model neglects the effect of molecular viscosity. Therefore, the standard k-ε model is usable for fully turbulent flows. This model is the most commonly used model in the industry and has a wide range of applications.

The equation for turbulent kinetic energy can be written in a general form as follows (ANSYS Fluent User's Guide, 2015):

$$\frac{\partial}{\partial t}(\rho k) + \frac{\partial}{\partial x_i}(\rho k u_i) = \frac{\partial}{\partial x_j}\left[\left(\mu + \frac{\mu_t}{\sigma_k}\right)\frac{\partial k}{\partial x_j}\right] + G_k + G_b - \rho\varepsilon - Y_M + S_k \tag{48}$$

where:

k – turbulent kinetic energy;

ε – turbulent dissipation rate;

S_k – source term which can be defined by the user;

$\frac{\partial}{\partial t}(\rho k)$ – the rate of change of turbulent kinetic energy;

$\frac{\partial}{\partial x_i}(\rho k u_i)$ – transport of turbulent kinetic energy by convection;

$\frac{\partial}{\partial x_j}\left[\left(\mu + \frac{\mu_t}{\sigma_k}\right)\frac{\partial k}{\partial x_j}\right]$ – diffusive transport of turbulent kinetic energy;

G_k is generation of turbulent kinetic energy due to mean velocity gradients which is expressed as:

$$G_k = 2\mu_t S_{ij} S_{ij} \tag{49}$$

The term G_b represents the generation of turbulent kinetic energy due to buoyancy effect. This effect is included in the equation if nonzero gravity field and temperature gradient

simultaneously exist in the flow. The term is expressed as (ANSYS Fluent User's Guide, 2015):

$$G_b = -\frac{1}{\rho}\left(\frac{\partial \rho}{\partial T}\right)_p \frac{\partial T}{\partial x_i} \tag{50}$$

The term Y_M is contribution of the fluctuating dilatation in compressible turbulence to the dissipation rate. This term is usually neglected in incompressible flows. It is calculated as follows (ANSYS Fluent User's Guide, 2015):

$$Y_M = 2\rho\varepsilon \frac{k}{a^2} \tag{51}$$

where a is the speed of sound.

The equation for turbulent dissipation rate is written as follows (ANSYS Fluent User's Guide, 2015):

$$\frac{\partial}{\partial t}(\rho\varepsilon) + \frac{\partial}{\partial x_i}(\rho\varepsilon u_i) = \frac{\partial}{\partial x_j}\left[\left(\mu + \frac{\mu_t}{\varepsilon}\right)\frac{\partial \varepsilon}{\partial x_j}\right] + C_{1\varepsilon}\frac{\varepsilon}{k}(G_k + C_{3\varepsilon}G_b) - C_{2\varepsilon}\rho\frac{\varepsilon^2}{k} + S_\varepsilon \tag{52}$$

where:

$\frac{\partial}{\partial t}(\rho\varepsilon)$ – the rate of change of turbulent dissipation rate;

$\frac{\partial}{\partial x_i}(\rho\varepsilon u_i)$ – transport of turbulent dissipation rate by convection;

$\frac{\partial}{\partial x_j}\left[\left(\mu + \frac{\mu_t}{\varepsilon}\right)\frac{\partial \varepsilon}{\partial x_j}\right]$ – diffusive transport of turbulent dissipation rate;

S_ε – source term which can be defined by the user.

The extent to which the dissipation rate is affected by the buoyancy effect is expressed by the constant $C_{3\varepsilon}$ which is calculated according to the relation:

$$C_{3\varepsilon} = \tanh\left|\frac{\upsilon}{u}\right| \tag{53}$$

where:

υ – velocity which is parallel to the gravity;

u – the velocity which is perpendicular to the gravity.

The rest constants have specific values:

$C_{1\varepsilon} = 1.44, C_{2\varepsilon} = 1.92, C_{\mu} = 0.09, \sigma_k = 1.0, \sigma_\varepsilon = 1.3$.

Based on the values of turbulent kinetic energy and turbulent dissipation rate, the turbulent viscosity μ_t is calculated as follows:

$$\mu_t = \rho C_\mu \frac{k^2}{\varepsilon} \tag{54}$$

The model described above is the standard k-ε model. There are two most commonly used modifications: RNG and Realizable models.

The RNG model includes some refinements (ANSYS Fluent User's Guide, 2015):

- The model has an additional term in the equation for turbulent dissipation rate which predicts rapidly strained flows more accurately.
- Flows with a swirl effect on turbulence is predicted in a more accurate manner.
- The model has an analytical formula for Pr_t - turbulent Prandtl number while the standard model has a constant value.
- Accounts low-Reynolds numbers effects.

Another modification is Realizable k-ε model. This model has an improved equation for turbulent dissipation rate and uses variable value C_μ instead of constant as in the standard model. In comparison with the standard model, it has a better performance for (ANSYS Fluent User's Guide, 2015):

- planar and round jets;
- boundary layers which have strong adverse separation or pressure gradients;
- streamline curvature;
- rotation or circulation flows.

Nowadays, the Realizable model is the most commonly used in ANSYS Fluent since it has all the features of the standard model and has important additional refinements.

k-ω models

The k-ω is another two-equation model. In the model, ω represents an inverse time scale which is associated with turbulence. The first equation for turbulent kinetic energy is written as follows (ANSYS Fluent User's Guide, 2015):

$$\frac{\partial}{\partial t}(\rho k) + \frac{\partial}{\partial x_i}(\rho k u_i) = \frac{\partial}{\partial x_j}\left[\left(\mu + \frac{\mu_t}{\sigma_k}\right)\frac{\partial k}{\partial x_j}\right] + G_k - Y_K + S_k \qquad (55)$$

The meaning of the terms are exactly the same as in the k-ε model, so that it is not discussed here.

The equation for ω is written in the form (ANSYS Fluent User's Guide, 2015):

$$\frac{\partial}{\partial t}(\rho \omega) + \frac{\partial}{\partial x_i}(\rho \omega u_i) = \frac{\partial}{\partial x_j}\left[\left(\mu + \frac{\mu_t}{\sigma_\omega}\right)\frac{\partial \omega}{\partial x_j}\right] + G_\omega - Y_\omega + S_\omega \qquad (56)$$

where:

ω – specific dissipation;

G_ω – generation of ω;

Y_ω – dissipation of ω due to turbulence;

S_ω – source term.

The turbulent viscosity is calculated based on the obtained values for k and ω:

$$\mu_t = \frac{\rho k}{\omega} \qquad (57)$$

Chapter 4
CFD analysis of the particle plug

4.1 Introduction

In order to simulate the propagating particle plug using Eulerain Granular model, it is necessary to conduct a detailed study of many parameters. Since along the entire simulation the particle volume fraction is mostly higher than 0.5, the friction interaction between the particles is important (ANSYS Fluent User's Guide, 2015). Moreover, it is important to select an appropriate grid, RANS model, wall function and interaction forces models. Variation of each of the parameters might have a big influence on the overall result. During the literature review, it is noticed that the parameters are often selected without any discussions, so that it is not always possible to understand the reasons behind the choices. As such, in this chapter the model selection is discussed in details to avoid random model choices. In such a way, the reader can understand the logic of the discussion as well as the work can be potentially used in similar models in the future. After that, the detailed analysis of the obtained results is provided with validation with the experimental data.

4.2 Approach

As a first step of the evaluation of the particle plug propagation, it is decided to perform 2D simulations in much smaller scale of the rig and plug than the one used in the experiments. Using these simulations, it should be possible to understand which models and parameters are appropriate to include in subsequent simulations with a larger scale plug. In this way, a lot of computational time is saved and many different options can be tested and compared. Most of the model selection work is done at this evaluation step.

The next step is increasing the 2D model up to the scale which is supposed to be tested for the final 3D simulation. In such a way, it is possible to see if changes in the plug behavior occur

when plug size increases. If so, it is possible to come back to the small scale simulations and find potential errors. All the flow features are investigated at this step as well as the data extraction for 1D code development is conducted.

The last step in the study is performing the 3D simulation which shows all the capabilities of ANSYS Fluent in modelling of such a flow. It completes the pictures of the entire study and gives a possibility to make overall conclusions about the success of the research.

To summarize, a simple diagram with the approach used in the plug propagation study is shown in the Figure 4.1.

2D simulation
- Small scale plug of 15 cm
- Selection of appropriate models and parameters

2D simulation with increased scale
- Plug length of 53 cm
- Comparison of plug behavior with small scale simulation
- Decision for an appropriate model setup for the 3D case
- Detailed investigation of the model
- Development of the 1D model based on the CFD results

3D simulation
- Plug length of 53 cm
- Analysis of plug behavior and comparison with 2D results
- Conclusions

Figure 4.1 Schematic approach applied for the CFD study of the particle plug propagation

4.3 Assumptions and uncertainties

Before considering the CFD simulations, it is necessary to mention the assumptions and uncertainties which might have an influence on the results. These assumptions and uncertainties present in all the simulations of the all the research phases, as such it is logical to mention them in this part of the report.

Assumptions:

- all the particles have the same diameter;

- the particles do not dissolve and react with water;

- no heat transfer is included;

- the hydraulic pump is simulated by the velocity boundary conditions;

- pipe walls have zero hydraulic roughness.

Uncertainties:

1. Constant particle diameter.

In opposite, the experiments include the particles with a range of diameters. This fact will influence the deviation between the experimental and simulation results.

2. Dimensions of the plug and pipe.

There is a possibility that the initiated plugs and rig dimensions might be slightly different from the experimental ones due to inaccuracy of the experimental measurements as well as design modelling process.

3. Fluid properties.

The fluid properties used in the simulation might be slightly different from the experimental ones. The fluid properties offered by default ANSYS Fluent settings are used in the simulation.

4. Experimental measurements of high particle volume fractions.

In the experiments, the measurements of the particle volume fraction higher than 0.3-0.4 are qualitative since the conductance rings are not capable to measure high volume fraction in an accurate way. This fact might have an impact on the difference between the experimental and simulation results.

4.4 Phase 1. 2D simulations of the small scale plug

4.4.1 Geometry

Geometry for all the simulations is created in ANSYS Design Modeler. This tool is good enough to create simple pipe geometries. The geometry for the 2D simulations of the 15 cm plug is shown in the Figure 4.2.

The entire pipe is divided by 3 bodies: Upstream, Plug region (bend) and Downstream. This is made in order to easily use Patch method in order to initiate the particle plug where it is needed.
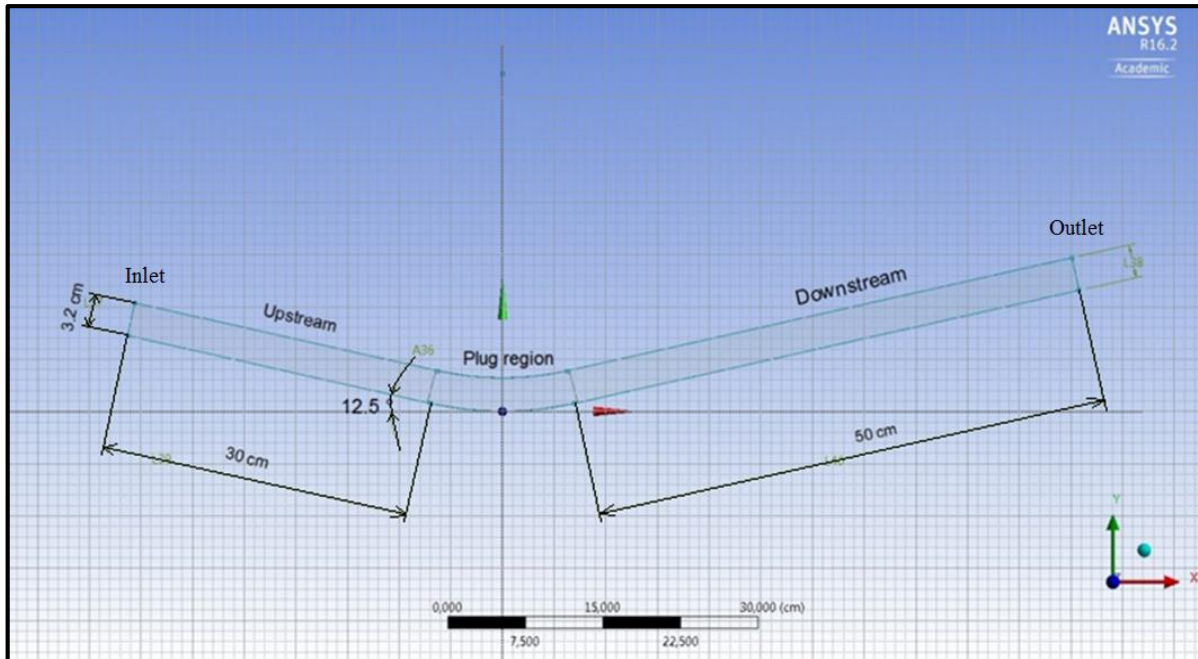
Figure 4.2 Pipe geometry for 2D simulations of the 15 cm plug

4.4.2 Preliminary model selection approach

In order to discuss the model selection process in details, it is first necessary to mention which parameters are required to be selected and which options are available. Below there is a list of the most important parameters to be selected and possible alternatives:

I.   RANS models

- k-ε – Standard, RNG, Realizable
- k-ω – Standard, Baseline, SST
- Turbulence properties – mixture, dispersed or per phase

II.   Properties and phase interaction

  1) Granular viscosity model

- Syamlal-O'Brien
- Gidaspow

  2)   Frictional viscosity

- Schaeffer
- Johnson

  3)   Frictional pressure

- Syamlal
- Johnson

4) Solids pressure

- Lun
- Syamlal-O'Brien
- Ma-Ahmadi

5) Radial distribution

- Lun
- Syamlal-O'Brien
- Ma-Ahmadi
- Arastoopour

6) Drag model

- Syamlal-O'Brien
- Gidaspow
- Wen and Yu

7) Turbulent dispersion

- Simonin
- Burns

8) Interfacial area

- ia-symmetric
- ia-particle

III. Specularity coefficient

IV. The value of y^+_w linking to the suitable wall function

- Standard wall function
- Scalable wall function
- Enhanced Wall Treatment

As it is possible to see, there are a lot of possible combinations for the simulation setup. One should take into account that many options are already excluded at this stage in order to shorten the model selection process and only the most relevant options are presented above.

Since many parameters are required to be selected as well as there are several options for most of the parameters, it is impossible to test all the model combinations. It would take a numerous amount of time while the time to complete this research work is limited. Instead, a systematic approach has to be used in order to complete the study within a reasonable time frame. This approach is presented schematically in the Figure 4.3.

1) Select a preliminary model based on the literature review, ANSYS User's Guide, best practicies and logical conclusions

2) Test the preliminary model in different grids and options for wall treatment

3) Select the best wall treatment option and grid and test alternative models

4) Select the most representable models and use 2nd order discretization scheme to evaluate the importance of the discretization accuracy

5) Conclude the most suitable options for all the parameters to use for the cases with larger scale plugs

Figure 4.3 Schematic approach for the 2D model evaluation

4.4.3 Preliminary model selection

I. RANS models.

For a simple pipe with small curvature, both k-ε and k-ω models are suitable. However, in order to obtain accurate results with k-ω model, y^+_w has to be less than 5 (ANSYS Fluent User's Guide, 2015). For the flow velocity of 0.66 m/s, y^+_w=5 gives a first layer thickness of around 0.00002 m which is less than the particle diameter. At the same time, in order to perform a successful simulation using Eulerian Granular model, one has to have the first cell height higher than at least one particle diameter, preferably, the value should contain several particle diameters (ANSYS Fluent Support, 2016). Therefore, it is concluded that k-ω model is not a correct choice for this study.

Moreover, during the literature review it is found out that in most research studies which apply Eulerian Granular model for slurry flow modelling, k-ε model is selected for turbulence modelling (Ekambaraet al., 2009; Nabil et al., 2013; Kushal, 2014; Lahiri & Ghanta, 2010).

As such, based on these two reasons, it is decided to use k-ε model turbulence modelling. Among three different options of k-ε model, Realizable model is selected. It is not expected to have big differences between these three models in this case because the geometry is relatively simple and the Realizable model would not give a strong advantage in comparisson with the Standard model. However, the usage of the Realizable model is recommended by the Fluent Course material (ANSYS Fluent Lectures, Turbulence Modelling, 2015), as such this model is selected for evaluation.

Mixture model is selected for turbulent properties modelling. This model is recommended in several situations and one of them is a case when the fluid density ratio is around unity. Since the particle density in the experiments has a value of 1070 kg/m^3 and water is used as the continuum phase, this model is selected to be with the best fit.

Dispersed model is rejected since it is usually applicable for dispersed dilute secondary phase while the case under consideration includes secondary phase at packing limit conditions.

Properties modelling for each phase is not a good choice either because it is usually used when there is strong turbulent transfer between the phases which is not evident in the case under consideration. Moreover, it would cost additional computational time without giving any strong advantages.

II.   Properties and phase interaction.

Properties

1) Granular viscosity model

Both models are appropriate for modelling particle plug propagation. Using preliminary calculations, it is observed that both models have the same order of magnitude values within the entire range of volume fractions. Therefore, both models are tested. However, as the first trial, Syamlal-O'Brien model is selected.

2) Frictional viscosity

During the preliminary tests of both options, it is revealed that the model of Johnson gives very unstable behavior of the solution with a tendency to disconvergence. This result is unexpected, because the Johnson model is widely used in the literature. However, in the plug propagation

case, the Johnson frictional viscosity model causes the convergence problems which are not possible to fix until the model is switched to another one.

In opposite, the Schaeffer model significantly improves convergence and gives qualitatively good predictions with any other models for the rest parameters. As such, the Schaeffer model is selected to be with the best fit.

3) Frictional pressure

For the frictional pressure, the same situation occurred as for the frictional viscosity – Johnson model causes convergence problem. As such, Syamlal model is selected which provides a stable solution.

4) Solids pressure and 5) Radial distribution

These two parameters are based on same research works of three different authors. As such, it is recommended to use the same approach (model) for both parameters. As such, three possibilities are available.

As the first approach, Syamlal formulas for both parameters are selected. Afterwards, other two options are tested and compared with the preliminary model.

Phase interaction

6) Drag model

Wen and Yu model is not selected to be tested because despite the fact that it can be used for particle flows, the secondary fraction has to be dilute (ANSYS Fluent User's Guide, 2015). Since the plug propagates with particle fraction about the packing limit, this model is not suitable.

The other two models are suitable for the case under consideration. These models are recommended to be used together with the corresponding frictional viscosity models. (ANSYS Fluent User's Guide, 2015; ANSYS Fluent Support, 2016). As such, Syamlal model is used for Syamlal frictional viscosity and Gidaspow model is selected for Gidaspow frictional viscosity model. For the first approach, Syamlal models are tested.

7) Turbulent dispersion

Turbulent dispersion cannot be disregarded because it has a significant impact on particle distribution profile (Ekambara, 2009; ANSYS Fluent Support, 2016). Simonin model is appropriate for turbulent multiphase models for dispersed turbulent modelling or turbulent

modelling for each phase. Due to the facts that the mixture model is used in the case under consideration, and the Burns model was tested over a wide range of applications including solid-liquid flows (Burns et al., 2004), it is selected to be the most appropriate.

8) Interfacial area

In order to get the most precise results, ia-symmetric model is usually selected. This model gives higher accuracy than the ia-particle model. The accuracy of the solution might be important at the dispersed region at the plug front, as such, the ia-symmetric model is selected for further evaluation.

III. Specularity coefficient.

It is necessary to select a specularity coefficient for particle plug propagation since the default boundary condition for particle phase is no-slip which is unfeasible in this case. Selection of the exact value of specularity coefficient for a particular case is a very challenging task. Physically the specularity coefficient represents the particle tangential momentum which is transferred to the wall by particles through collisions (Bakshi et al., 2014). The value of the specularity coefficient varies from 0 to 1, where zero represents free-slip conditions and unity represents zero tangential velocity.

It is extremely difficult to measure the specularity coefficient. Many studies have been conducted in a search of specularity coefficients for circulating fluidized beds/risers. Some of such researches are shown in the Table 4.1 with recommended values of the specularity coefficient.

Table 4.1 Previous research works on the specularity coefficient (Zhong et al., 2016)

Authors	Width or radius of the system, cm	Specularity coefficient	
		Tested	Recommended
Armstrong et al.,2010	W = 3.2	0, 0.25, 0.5, 0.75, 1	0.25
Jin, et al., 2010	W = 6	0,0.0001, 0.001, 0.01	0
Kong et al, 2014	R = 3.81	0, 0.0001, 0.0002	0.0001
Wang et al., 2010	W = 7.6	0, 0.0001, 0.001, 0.01, 0.6	0
Cloete et al., 2011	W = 7.6	0.0001, 0.01, 0.1, 1	$\geqslant$0.01

As it can be seen from the table, the variation of the specularity coefficient changes dramatically from one case to another, even though the researches were conducted basically on the same physical phenomenon - circulating fluidized beds/risers. The boundary conditions of the fluidized beds are similar to the particle plug flow, as such these estimations of the specularity coefficient are feasible for the present research work.

For the case under consideration, it is decided to use specularity coefficient of 0.01. This value is a compromise between the aforementioned studies. It could be also good to test many options for the specularity coefficient, but it is then necessary to compare the simulation results with the experiments. However, since the experimental data are available for large plugs, such sensitivity study would be computationally heavy and time demanding. Many other parameters are required to be tested which have a stronger influence on the propagating plug. If the value of 0.01 does not work well for the preliminary model and shows unrealistic results, it will be changed further in the study. As the first approach, the value of 0.01 is selected.

IV. The value of y^+_w linking to the suitable wall function.

It is important to evaluate the sensitivity of the model for different y^+_w values, or in the other words, for different first grid cells as well as for wall functions which are applicable for a particular case. Three scenarios are considered:

1) grid with $y^+_w > 30$ – standard wall function;
2) grid with $11.25 < y^+_w < 30$ – scalable wall function;
3) Enhanced Wall Treatment with different $y^+_w < 30$.

These intervals are suggested based on the fact that k-ε is used. In most literature examples of Eulerain Granular flow simulations, the standard wall function is used. In order to get reliable results with standard wall function, it is required to use the grid with $y^+_w > 30$, otherwise the results are deteriorated (ANSYS Fluent Support, 2016). At the same time, this value for y^+_w also seems reasonable in terms of granular modelling, since in this case the first cell contains higher amount of particles. As such, it is decided to test the model with these settings.

Scalable wall functions increase accuracy of the results for $y^+_w < 30$ and the best usage is when $11.25 < y^+_w < 30$ (ANSYS Fluent User's Guide, 2015). It is decided to test this option for $y^+_w = 12.5$ and $y^+_w = 25$ which gives first layer thickness of about one and two particle diameters respectively for the mixture velocity of 0.66 m/s.

The last option is Enhanced Wall Treatment which can be used for any $y^+_w <30$. However, the higher y^+_w is, the higher value the blending function has, which leads to more approximated resolution of the boundary layer. On the other hand, as it is mentioned earlier, it is better to have larger cells when one models Eulerian Granular flows. Therefore, one has to compromise between accuracy of the wall resolution and accuracy of expected granular model results. As such, it is concluded to test Enhanced Wall Treatment for $y^+_w =12.5$, $y^+_w =19$, and $y^+_w =25$. At $y^+_w =12.5$, the value of the blending function is low, so that the layer is well resolved. On the other hand, at $y^+_w =19$ and $y^+_w =25$ the boundary layer is more approximated, however, it contains more particles inside one cell, so that the solution might be more suitable for the final setup.

Based on the aforementioned observations and conclusions, many possible combinations of models are rejected. To summarize, the selected options for the preliminary model is shown in the Table 4.2. Some parameters in the table are not discussed because they do not have any other alternatives, they are constants or recommended by default in ANSYS Fluent. From the table, it is possible to see the complexity of the model and the number of parameters. This setup is run with different y^+_w and wall functions as discussed above.

Table 4.2 Preliminary model setup

Parameter	Model/Value
Particle diameter, m	0.00035
RANS model	k-ε, Realizable with mixture properties
Granular viscosity	Syamlal-O'Brien
Granular bulk viscosity	Lun et. al.
Angle of internal friction	30
Frictional viscosity	Schaeffer
Frictional modulus	Derived
Friction packing limit	0.62
Granular Temperature	Algebraic
Solids pressure	Syamlal
Radial distribution	Syamlal
Elasticity modulus	Derived
Packing limit	0.63
Drag model	Syamlal-O'Brien
Turbulent dispersion	Burns
Restitution coefficient	0.9
Interfacial area	ia-symmetric
Specularity coefficient	0.01

4.4.4 Mesh

Mesh for all the simulations is generated by ANSYS Meshing tool. For 2D simulations, Inflation method is used which allows to control first layer thickness in an easy way, so that it is possible to manipulate y^+_w appropriately. The Figures 4.4-4.7 represent the mesh for all the test cases. The mesh statistics with the most important parameters can be found in Appendix B.
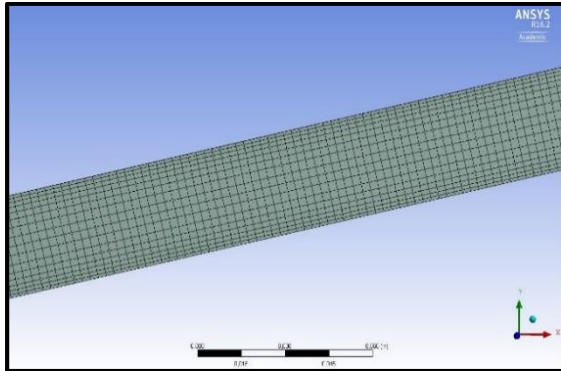

Figure 4.4 Mesh structure with y^+_w =37.5
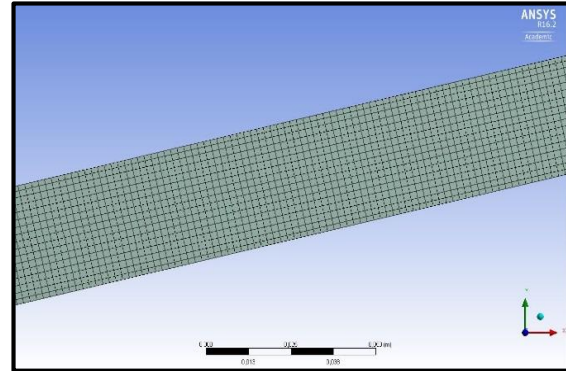

Figure 4.5 Mesh structure with y^+_w =25

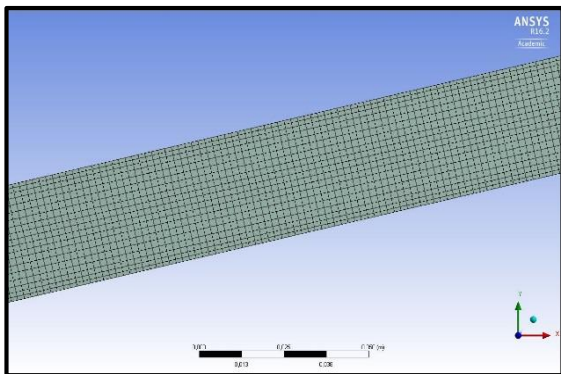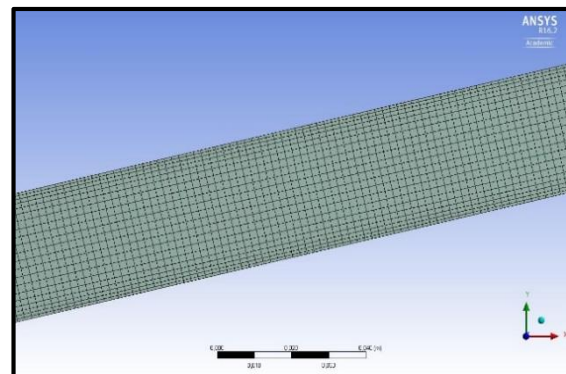
Figure 4.6 Mesh structure with y^+_w =19

Figure 4.7 Mesh structure with y^+_w =12.5

4.4.5 Boundary conditions and solver settings

The boundary conditions are shown in the Table 4.3. Phase 1 corresponds to the water phase, phase 2 corresponds to the granular (particle) phase. An initiated plug can be seen in the Figure 4.8.
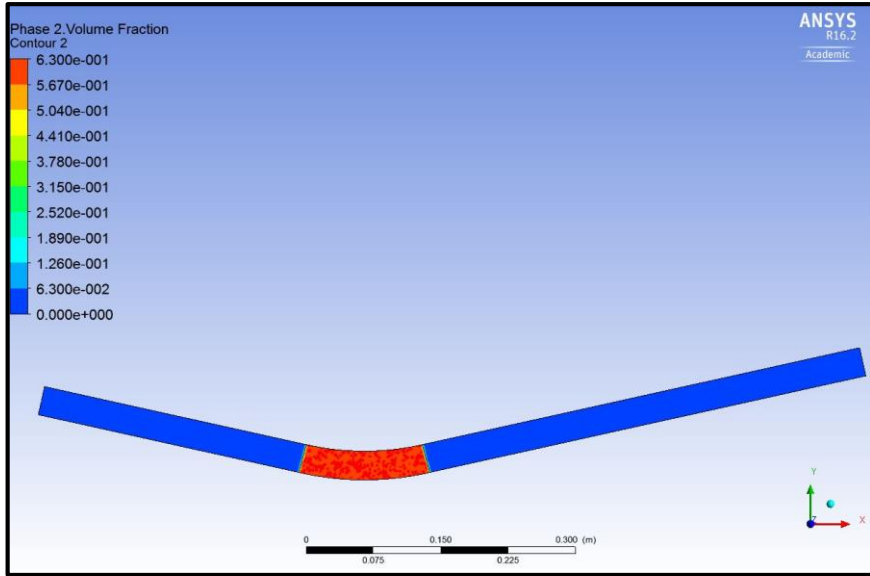
Figure 4.8 An initiated particle plug with a length of 15 cm

Table 4.3 Boundary conditions, phase properties and solver settings for 2D simulations

Phase properties	
Phase 1 Density, kg/m^3 Viscosity, kg/m.s	 998 0.001003
Phase 2 Diameter, m Density, kg/m^3	 0.00035 1070
Boundary conditions	
Inlet Turbulent intensity,% Hydraulic diameter, m Phase 1 velocity, m/s Phase 2 velocity, m/s Phase 2 fraction	 4.6 0.032 0.66 0 0
Outlet Turbulent intensity,% Hydraulic diameter, m Gauge pressure, Pa	 4.6 0.032 0
Wall Phase 1 Phase 2	 No-slip Specularity coefficient=0.01
Solver settings	
Scheme	Phase Coupled SIMPLE
Gradient	Least Squared Cell Based
Momentum	First Order Upwind
Volume fraction	First Order Upwind
Turbulent kinetic energy	First Order Upwind
Turbulent dissipation rate	First Order Upwind
Transient formulation	First Order Implicit

Turbulent intensity is calculated using the following relation:

$$I = 0.16 \cdot \mathrm{Re}_{d_h}^{-1/8}$$ (58)

The simulation is run in the transient mode with the gravity force in the negative y-direction. The time step is set to 0.001 s. Number of iterations per time step is 40. The particles are initialized in the plug region by using Patch method with the particle fraction of 0.63 which represents the packing limit. For all the residuals, the value of 10^{-3} is selected to be the convergence criteria. It is a not strong criterion for convergence, but it is selected due to difficulties of the model convergence. This is one of the main problems of this simulation. Since the flow is operated at packing limit from the beginning of the simulation and many parameters are used, the difficulties with convergence are understandable.

4.4.6 Results validation and discussion

As the first approach, it is decided to validate the results based on the visual experimental observations and physical behavior of the plug. This approach could be argued since usually validation is done based on the experimental measurements. This choice is explained by two reasons. First, there are not available experimental measurements of a plug with a length of 15 cm, but this length is selected for the simulations in order to shorten the computational time significantly. Secondly, since this model is not the final result of the whole study, visual comparison is good enough to judge the behavior of the model. If all the options look applicable and physically reasonable, all of them will be used for further evaluation and then the selection will be done based on the experimental measurements.

The Figure 4.9 shows the plug propagation in the grid with $y^+{}_w$=37.5 and standard wall function. In the figure, the dispersion region at the front of the plug can be clearly seen. In addition, the tail is well observed. However, the behavior and the shape of the propagating plug is very different from the experimental observations which can be seen in the Figures 1.4 and 1.5. The plug has the flat front, while the experiments clearly show the elongate profile. In addition, the tail should tend to propagate mostly at the bottom of the pipe, while the simulation result shows two near-symmetric regions of propagation: top and bottom. Generally, it can be said that the plug behavior is noticeably different from the experimental observations and it can be suggested that the boundary layer in the plug region has to be better resolved. As such, the option with the standard wall function obviously will not be applied in further evaluation.

The Figure 4.10 shows the particle plug behavior in the grid with y^+_w=25 and the scalable wall function. In general, behavior resembles the one with y^+_w=37.5, however, has small changes in the tail and the main body of the plug. The front of the plug becomes a little bit better resolved and less diffusive, however, it is still not satisfactory and cannot be selected for further evaluation.
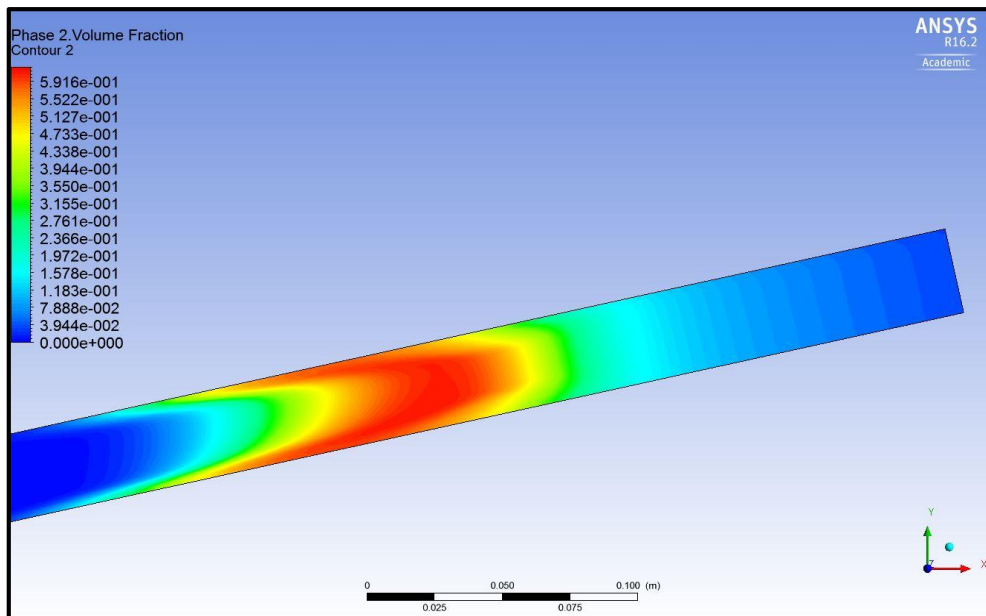

Figure 4.9 Particle volume fraction in the grid with y^+_w=37.5 and standard wall function
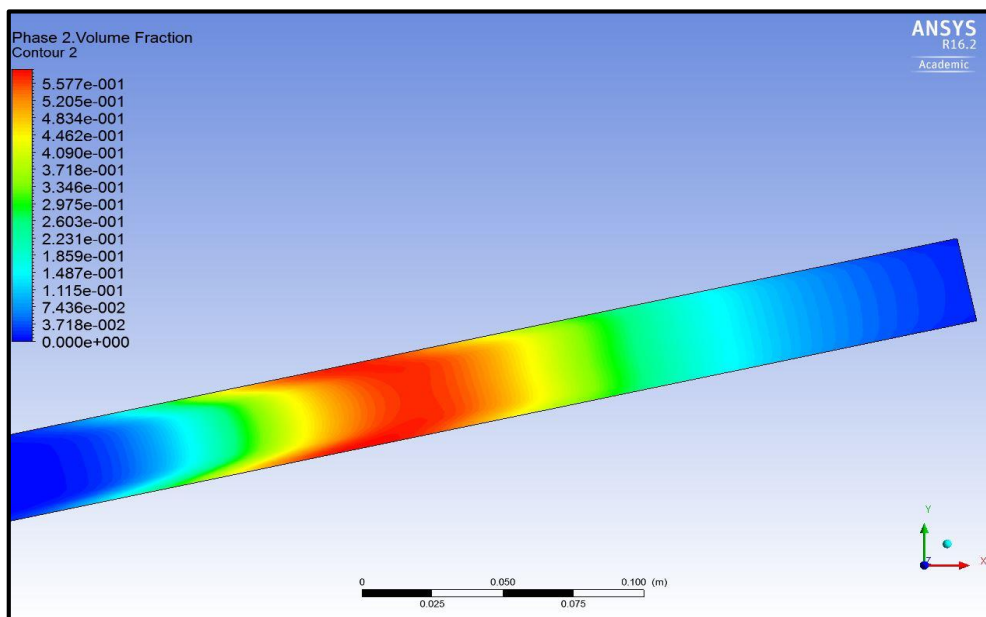

Figure 4.10 Particle volume fraction in the grid with y^+_w=25 and scalable wall function

In the Figure 4.11, the plug of the model with y^+_w=12.5 and the scalable wall function is presented. In comparison with the previous figure, the changes are very small. It can be observed that the boundary layer at the front becomes better resolved, but the plug behavior is almost the same and does not fit the experimental observations. As such, it can be concluded that much better resolution of the boundary layer is required and wall functions do not produce accurate results.
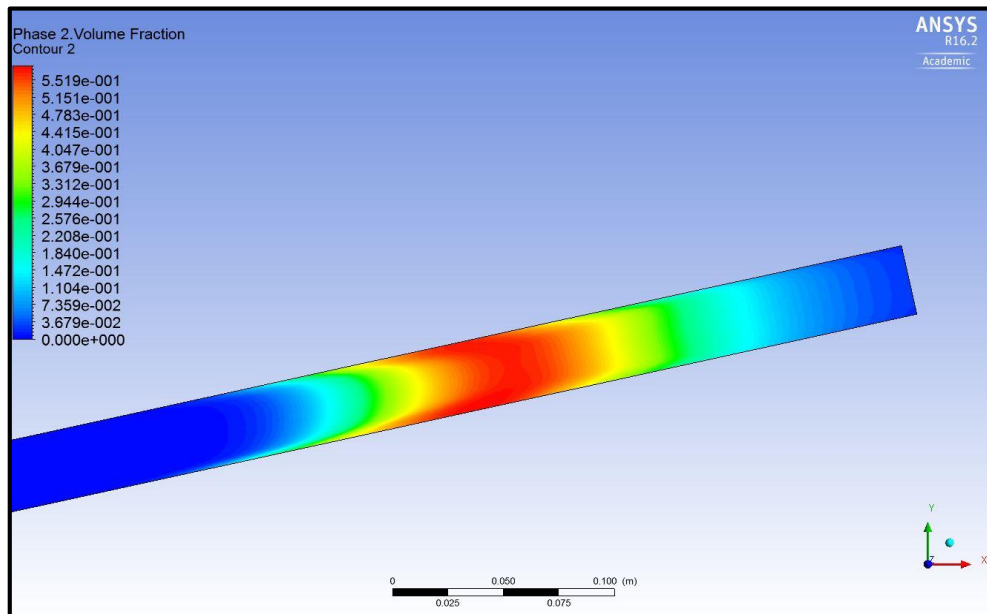

Figure 4.11 Particle volume fraction in the grid with y^+_w=12.5 and scalable wall function

The Figure 4.12 represents the model with y^+_w=25 and Enhanced Wall Treatment. It can be observed that suddenly the behavior of the plug becomes much more similar to the experimental observations. First, the tail tends to propagate mainly at the bottom of the pipe. The nose of the plug becomes elongate with the center point below the central pipe axis. This grid resolution along with EWT could be potentially used for further evaluation. However, it is first necessary to consider finer grid resolutions with y^+_w=19 and y^+_w=12.5.

In the Figure 4.13, particle volume fraction contours in the grid with y^+=19 and EWT are shown. In comparison with the previous case, very small changes can be distinguished and generally it can be said that the results are the same. However, it should be taken into account that these results are obtained using the 1st order discretization scheme for all the parameters. The 2nd order discretization might give different results between these grids. However, at this moment it can be concluded that the option with y^+_w=19 and EWT is also applicable for further evaluation.
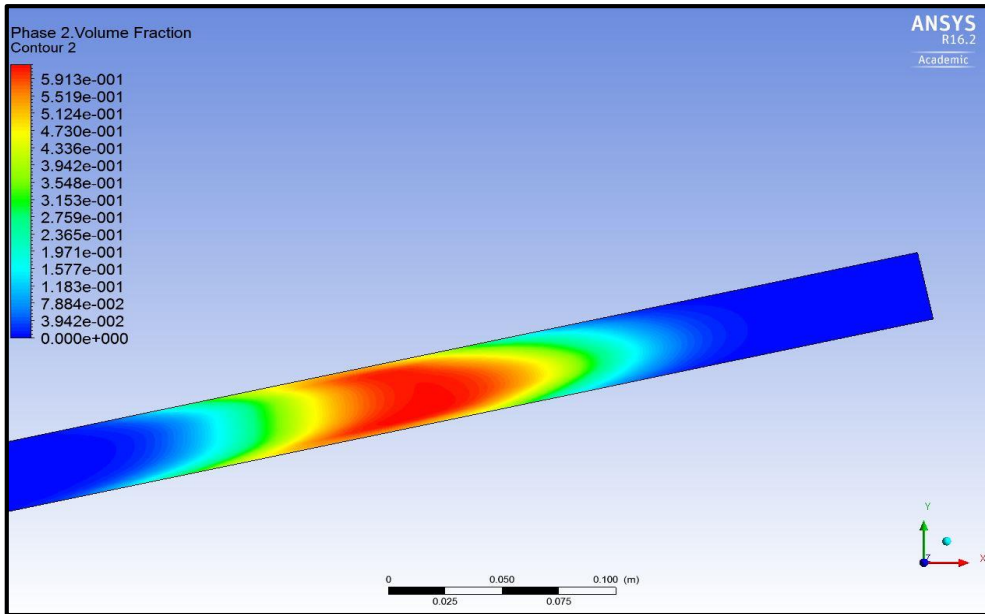
Figure 4.12 Particle volume fraction in the grid with $y^+_w=25$ and EWT
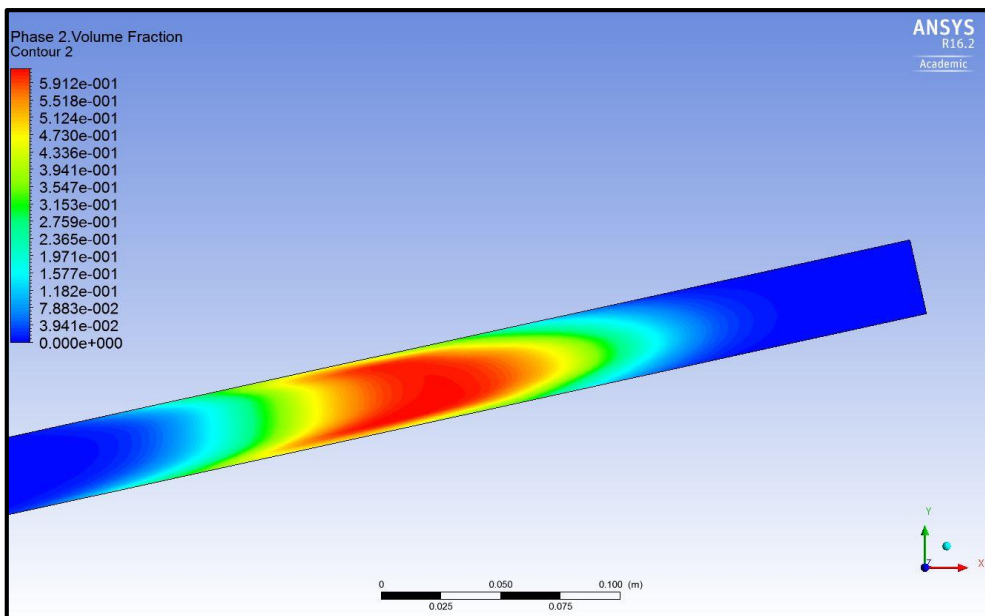
Figure 4.13 Particle volume fraction in the grid with $y^+_w=19$ and EWT

The Figure 4.14 represents the model with $y^+_w=12.5$ and EWT. In this case the boundary layer is slightly better resolved and the main body with higher particle fraction is slightly longer than in the previous cases. However, there are not any big changes if compare with the cases with $y^+_w=25$ and $y^+_w=19$. Following the logic as in the previous cases, this grid is also selected for further evaluation.

Figure 4.14 Particle volume fraction in the grid with y^+_w=12.5 and EWT

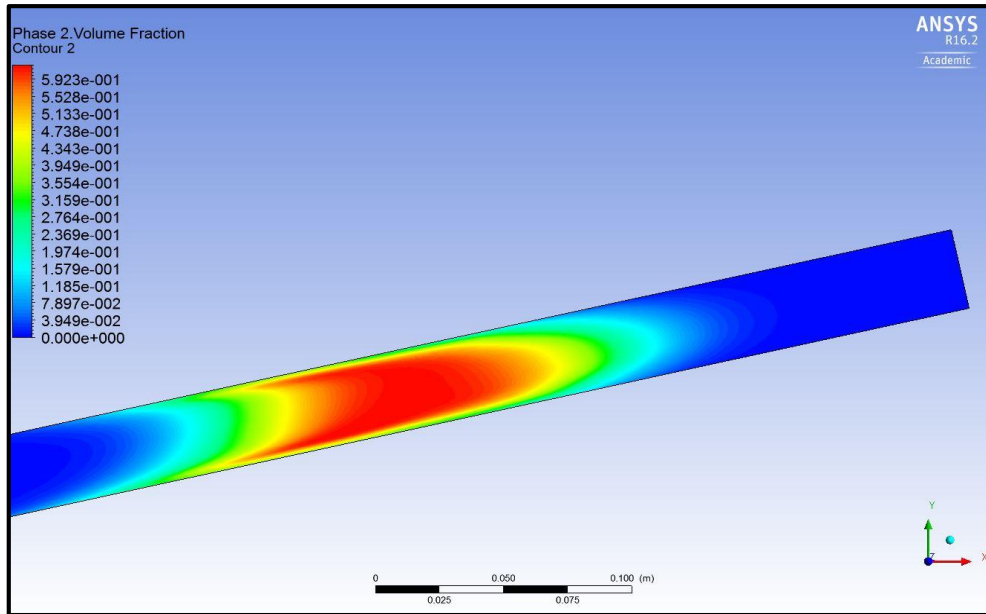As a result, three cases out of six are selected to be further tested. It is clearly shown that the standard as well as scalable wall functions do not work properly in the case with a propagating particle plug. At the same time, the Enhanced Wall Treatment option showed satisfactory results for three different grid options. Between these three options, there are very small changes in the plug behavior and generally the particle fraction contours look very similar. As mentioned, these simulations are run using the 1st order discretization scheme for all the parameters. It can be assumed that the 2nd order discretization scheme might show more different results in different grids.

Before considering an impact of the 2nd order scheme on the results, it is first necessary to see the difference between the alternative models. As concluded in the model selection discussion, the Gidaspow drag model can also be used for such type of flows instead of Syamlal model which is tested in this section. In addition, Lun et al. and Ma-Ahmadi models might be applied for the radial distribution function and solids pressure. As such, these options are tested and discussed. After that, the 2nd order discretization scheme is applied for all the appropriate models.

4.4.7 Further model evaluation

In order to check alternative models, the grid with y^+_w=12.5 and EWT is selected. All the possible models are tested in this grid and then the choice of the most appropriate models is made. The grids with y^+_w=19 and y^+_w=25 can also be used in this section, however, with the

smaller first layer thickness, it is expected to see the differences between different models in a more clear way.

As discussed, two drag and granular viscosity models together with three models for the radial distribution function and solids pressure could be tested. As such, there are 6 possibilities which could be appropriate and have to be analyzed. When all these models are compared, it could become possible to eliminate some of the models and make the final decision regarding the model before applying it to the larger scale which takes longer computational time.

The Table 4.4 summarizes the cases which will be further tested. The rest parameters are selected to be the same as it is tested in the section above since those parameters are already selected for the final model and do not have better alternatives.

Table 4.4 Possible cases of the final 2D model

Case number	Drag /Granular viscosity models	Radial Distribution	Solids Pressure
Case 1		Syamlal	Syamlal
Case 2	Syamlal	Lun et.al.	Lun et.al.
Case 3		Ma-Ahmadi	Ma-Ahmadi
Case 4		Syamlal	Syamlal
Case 5	Gidaspow	Lun et.al.	Lun et.al.
Case 6		Ma-Ahmadi	Ma-Ahmadi

It can be argued that it is possible make a mix between the models and create new cases. However, since the goal is to eliminate the number of cases and hopefully end up with a few models, it is logical to use a "consistency approach" and select the models developed based on the same theory for interdependent variables.

Each simulation takes around 2.5 hours to complete. The Figures 4.15-4.20 represent volume fraction contours for all six cases. In addition, the measurements of particle volume fraction versus time are made through the pipe outlet section in order to make the evaluation in a more clear way. As it can be seen from the figures, the propagating plugs are very similar to each other and only small differences can be observed. If compare two different drag models with the same radial distribution function and solids pressure, for example, Case 1 and Case 4, it is possible to see that there are not any differences in the form of the plug and its behavior. On the other hand, if compare the same drag model and different radial distribution functions and solids pressure functions, for example, Case 1 and Case 2, small differences can be noticed.

More specifically, the length of the high particle fraction region inside the body is slightly longer in Case 1. However, this difference is negligible since it does not add any significant change to the plug behavior.
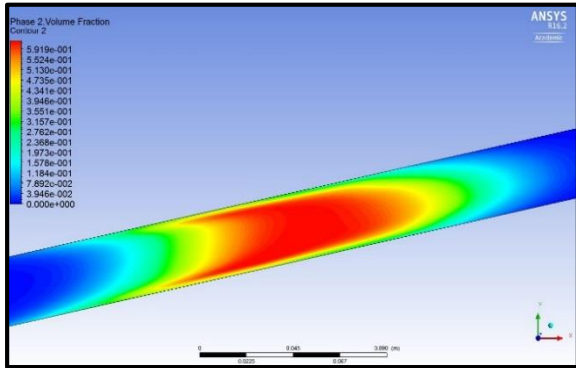
Figure 4.15 Particle volume fraction, Case 1
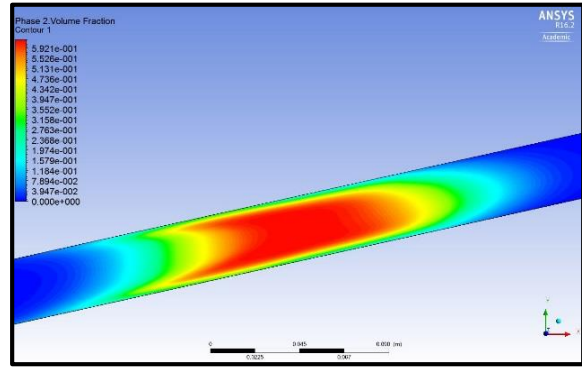
Figure 4.16 Particle volume fraction, Case 2
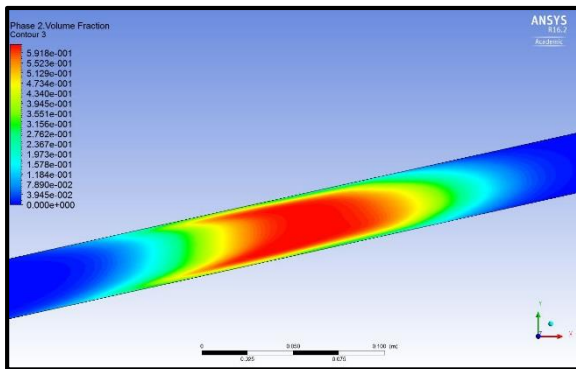
Figure 4.17 Particle volume fraction, Case 3
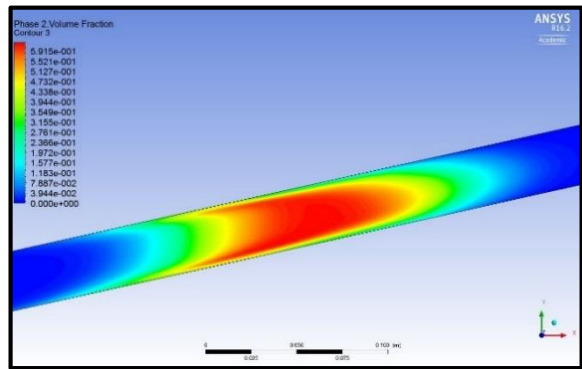
Figure 4.18 Particle volume fraction, Case 4

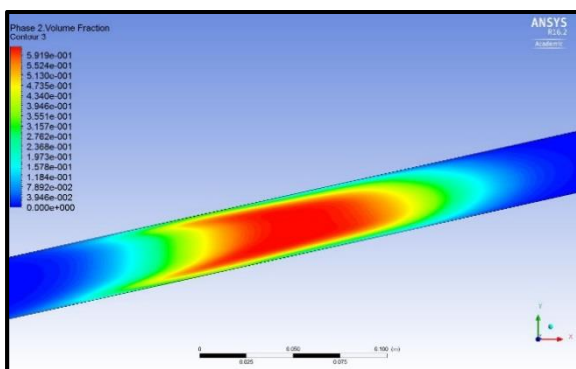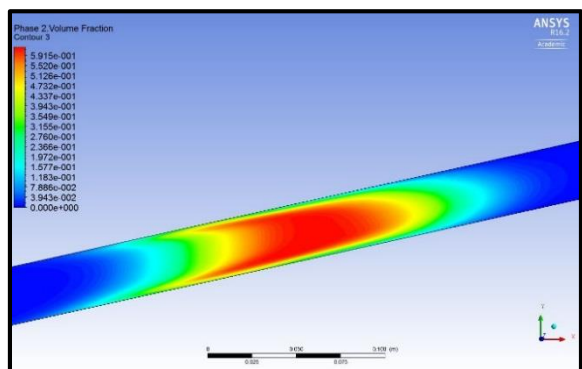Figure 4.19 Particle volume fraction, Case 5

Figure 4.20 Particle volume fraction, Case 6

In order to confirm the negligibility of the differences between the models, particle volume fraction measurements at the pipe outlet section are taken and presented in Figure 4.21. As it can be seen, the particle volume fraction is almost the same for all the cases and there is a very small difference in the peak values.

Based on these observations and measurements, it is possible to conclude that none of the models has incorrect behavior and all of them behave generally the same. As such, any of the models potentially could be used for further evaluation of the larger scale plug.
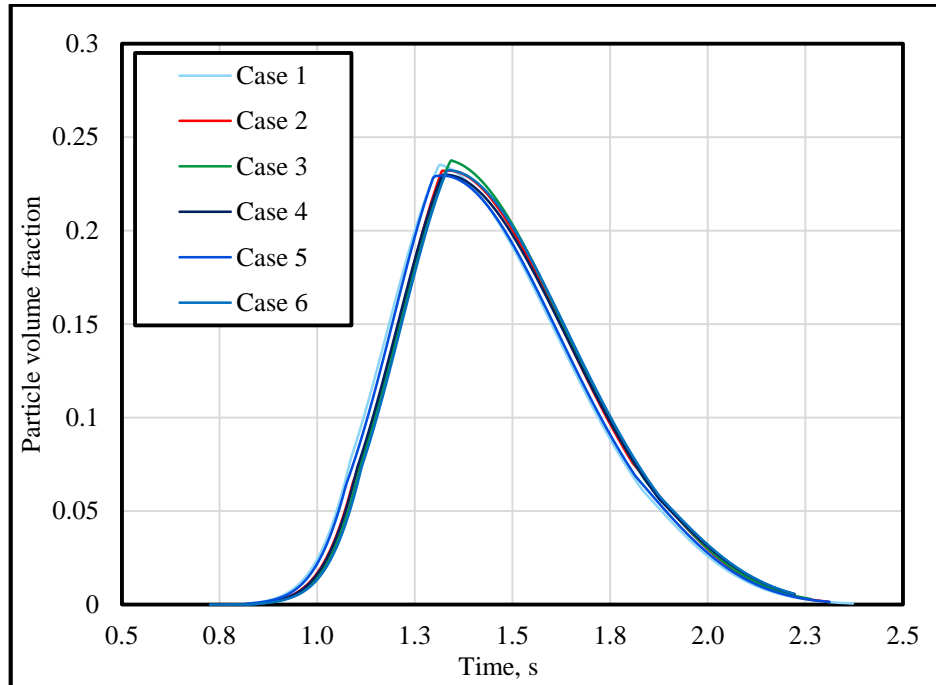
Figure 4.21 Particle volume fraction measurements at the outlet of the downstream pipe

Since it is not possible to decide which model is the most suitable due to the fact that all of them give almost the same results, the models used in the Case 1 are selected for further evaluation. The reason behind it is the fact that in most of the parameters of the Case 1 the Syamlal models are used. As such, when Syamlal models for the radial distribution, solids pressure, drag and granular viscosity are selected, all the parameters are computed based on the same assumptions and research work, so that the results are expected to be more consistent. As such, all the parameters and corresponding models used for further evaluation can be seen in the Table 4.2.

4.4.8 Second order discretization scheme

As discussed in the section 4.4.6, the grids with y^+_w=12.5, 19 and 25 are selected for further evaluation since all of them produce similar results. It is also concluded that based on the first order solution, it is not possible to see big differences between them. If such differences exist, it is assumed that the second order discretization might show the differences between these grids in a more clear way.

In addition to the comparison of the grids, analysis of the difference between the first order and the second order discretization has to be done. If the difference is small, it is then better to use the first order discretization because it saves a lot of computational time. In opposite, if the difference is not negligible, one should not rely on the first order discretization scheme as the final choice and use the second order instead. As such, the model is investigated for the different discretization methods.

In the Table 4.5, the solver settings are shown. The model setup is described in the Table 4.2.

Table 4.5 Solver settings for the second order discretization simulations

Solver settings	
Scheme	Phase Coupled SIMPLE
Gradient	Least Squared Cell Based
Momentum	Second Order Upwind
Volume fraction	QUICK
Turbulent kinetic energy	Second Order Upwind
Turbulent dissipation rate	Second Order Upwind
Transient formulation	Second Order Implicit

For the volume fraction it is not possible to select Second Order Upwind Scheme, however, there is another option – the QUICK scheme. This scheme is very accurate and gives more exact solution than the First Order Upwind Scheme (Bakker, Lecture 5 - Solutions Methods, 2002). For other parameters, except gradient, the second order schemes are available.

Each simulation takes around 4 hours to complete. The Figures 4.22-4.27 show the particle volume fraction contours with the first order and the second order discretization schemes for three grid options.

It is possible to observe many features in the figures. First, consider the difference between different numerical schemes. It can be seen that the large dispersed regions at the plug fronts in the cases with the 1st order discretization is caused by numerical diffusion and it is significantly reduced in the 2nd order simulations. The 2nd order plugs are much more dense and do not become as dilute as the 1st order plugs in the main plug body region.

Secondly, consider the differences between different grids with the 2nd order discretization. The general plug behavior is similar, however, it is possible to see small changes at the front region next to the walls. In the case with $y^{+}=12.5$, apart from the dispersed region, there is a thin green region next to the wall with lower particle fraction. This regions are not well distinguished in the other two cases since they are thicker. In all the cases, at the front there is

a zone of dispersion. Inside this zone, the particles concentrate at the pipe center while at the walls it is possible to see more dilute regions marked by the green color.

For more detailed comparison, measurements of volume fraction versus time are taken at the pipe outlet section and shown in the Figure 4.28.

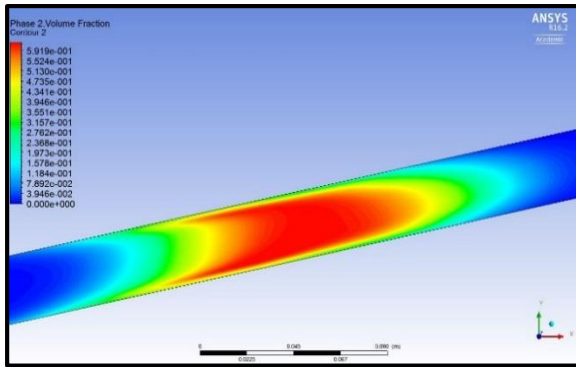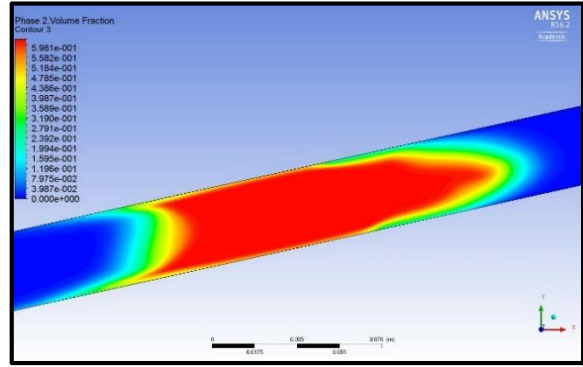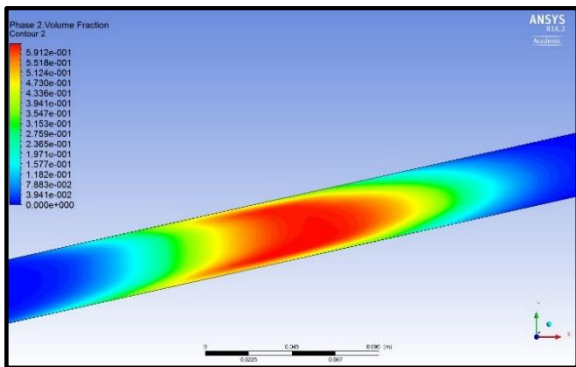Figure 4.22 y^+_w=12.5, 1st order

Figure 4.23 y^+_w=12.5, 2nd order

Figure 4.24 y^+_w=19, 1st order
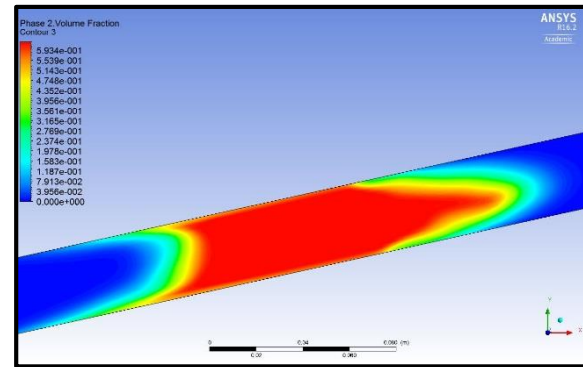
Figure 4.25 y^+_w=19, 2nd order
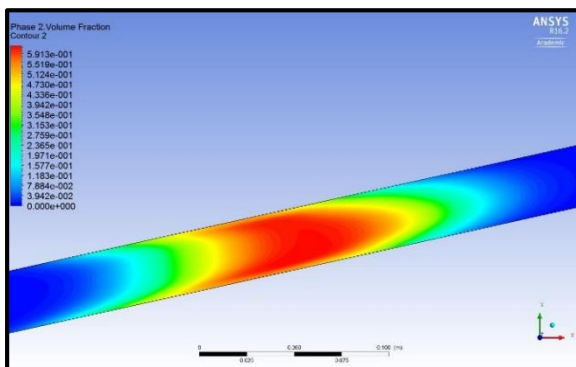
Figure 4.26 y^+_w=25, 1st order
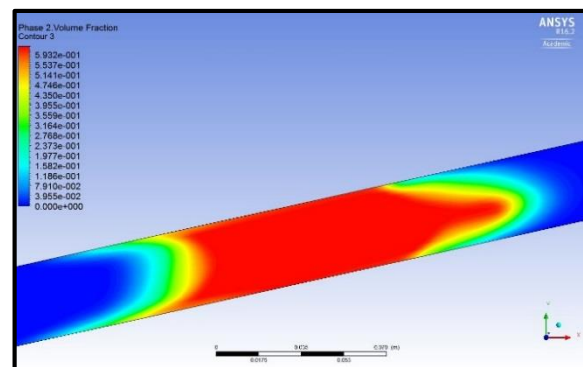
Figure 4.27 y^+_w=25, 2nd order
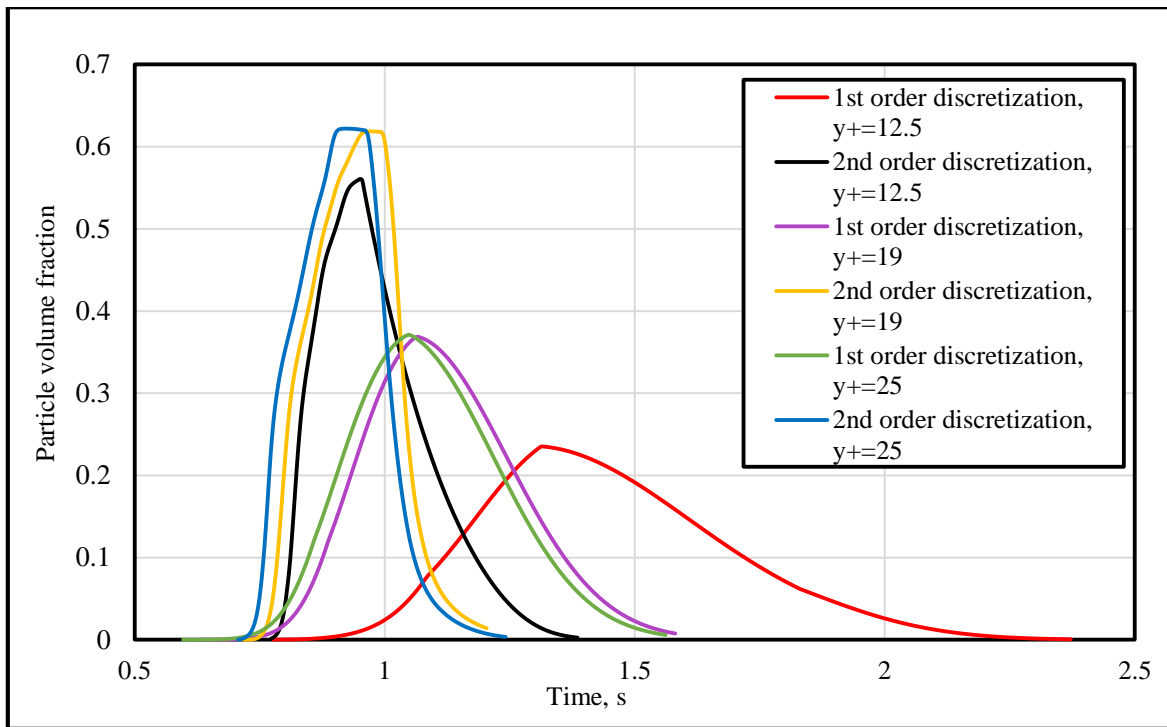
Figure 4.28 Particle fraction measurements at the pipe outlet section in the grids with y^+_w=12.5, y^+_w =19 and y^+_w =25 and the 1st and 2nd order discretization schemes

Based on the figure, it is possible to make several observations. First, it can be seen, the measurements strengthen the point about the difference between the different numerical schemes. It is clear that the 1st order plugs become much more dilute at the pipe outlet section in comparison with the 2nd order plugs. The front regions are much more dispersed and the total plug lengths is much larger in the 1st order plugs. As such, it can be said that it is smeared out numerically.

Secondly, as it can be noticed, the plugs in different grids reach the measurement point at different time for both discretization schemes. The plugs in the grid with y^+_w =25 move faster than in the rest two grids. This difference is not big, however, it should be remembered that the simulated plugs have the length of 15 cm only. It can be assumed that if the dimensions of the plugs and the entire domain are larger, the difference between the velocities can be also larger. Since there are not available experimental measurements for the plug of 15 cm, it is not possible to say which grid best corresponds to the experimental measurements. However, what is possible to conclude is that the value of y^+_w or the first layer thickness might influence the simulation results.

4.4.9 Summary of the Phase 1 section

It is worth to summarize all the conclusions and observations which have been found in the Phase 1.

- It is observed that the standard and scalable wall functions do not produce physically feasible results of the plug propagation in the pipe. The plug becomes very diffusive and the boundary layer is not well resolved in order to predict the plug behavior in an appropriate manner.

- It is obtained that the Enhanced Wall Treatment option is capable to model the particle plug behavior well in grids with different first layer thicknesses and y^+_w values.

- It is noticed that there is a small difference between different drag and granular viscosity models, radial distribution function and solids pressure. The difference might be observed in the particle layers at the wall, however it does not affect the plug behavior and the measured particle volume fraction at a specific point is almost identical for the tested models.

- It is clearly observed that there is a noticeable difference between different discretization scheme. Even though the general plug behavior is similar, the numerical diffusion in the 1st order scheme can be significant and produces unreliable results. As such, when the exact particle fraction and particle concentration profile is of interest, it is strongly recommended to use higher order discretization schemes.

- The higher order discretization scheme allows to notice some differences between three different grids, such as different thickness of the depleted particle regions at the walls or different plug velocity. However, at this moment it difficult to conclude which grid represents the plug propagation best due to lack of available experimental data on the plug of 15 cm. Further evaluation is required to make more precise conclusions.

Generally, it is shown that it is possible to reproduce the particle plug propagation in pipes using Eulerian Granular model in ANSYS Fluent. The good model setup of the particle propagation case is obtained based on the detailed discussions and analysis of the conducted simulations. The particle plug behavior looks physically reasonable and can be further tested for larger scale plugs and compared with available experimental data. All the goals of the Phase 1 is successfully achieved and all the required material for further evaluation is prepared.

4.5 Phase 2. 2D simulations of the large scale plug

4.5.1 Introduction

As a next step of the research evaluation, the 53 cm plug is simulated in grids with y^+_w=12.5, 19 and 25. This length is a compromise between the available data and the computational cost. The experimental data is available for 0.53 cm, 1 m, 1.6 m and 2m plugs. The experimental results show that in the plug of 53 cm it is possible to see the dispersed region at the first point of measurements, as such the smaller computational domain is required for the simulation. If the plug length increases, the dispersed region is mostly captured at the second measurement point. Moreover, when the plug is smaller itself, it shortens the computational time significantly. As such, the length of 53 cm is selected for the evaluation.

4.5.2 Geometry

The geometry is basically the same as in the case of the 15 cm plug but the pipe has bigger dimensions. In this case, the plug region is 53 cm and the downstream and upstream regions are increased. The downstream region is 115 cm which is exactly the same as the distance between the plug front and the first conductance ring in the experiments. The geometry is shown in the Figure 4.29
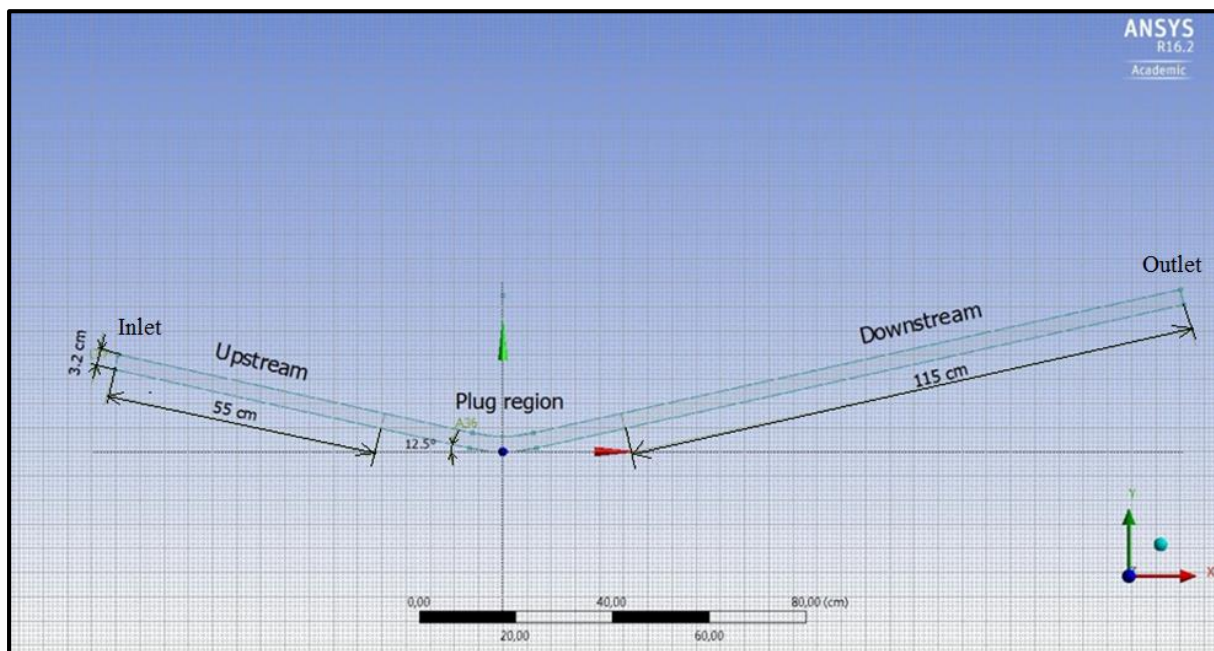

Figure 4.29 Geometry for 2D simulations of the 53 cm plug

4.5.3 Mesh

The mesh is generated with the first grid cell of 355, 530 and 710 µm which corresponds to y^+_w=12.5, 19 and 25 respectively. The mesh structure can be seen in the previous section in the Figures 4.4-4.7. The mesh statistics for the following cases can be found in the Appendix B.

4.5.4 Boundary conditions and solver settings

The boundary conditions are shown in the Table 4.6. The Phase 1 corresponds to the water phase while the Phase 2 corresponds to the granular (particle) phase. As previously, the simulations are run in the transient mode with the gravity force in the negative y-direction. The time step is set to 0.001 s. Number of iterations per time step is 40. The particles are initialized in the plug region by using Patch method with the particle volume fraction of 0.63 which corresponds to the packing limit. For all the residuals, the value of 10^{-3} is selected to be the convergence criteria. The higher order discretization schemes are used in order to obtain a more accurate solution. An initiated plug can be seen in the Figure 4.30.

Table 4.6 Boundary conditions and phase properties for 2D simulations

Phase properties	
Phase 1 Density, kg/m³ Viscosity, kg/m.s	 998 0.001003
Phase 2 Diameter, m Density, kg/m³	 0.00035 1070
Boundary conditions	
Inlet Turbulent intensity,% Hydraulic diameter, m Phase 1 velocity, m/s Phase 2 velocity, m/s Phase 2 fraction	 4.6 0.032 0.66 0 0
Outlet Turbulent intensity,% Hydraulic diameter, m Gauge pressure, Pa	 4.6 0.032 0
Wall Phase 1 Phase 2	 No-slip Specularity coefficient=0.01

Table 4.7 Solver settings for 2D simulations

Solver settings	
Scheme	Phase Coupled SIMPLE
Gradient	Least Squared Cell Based
Momentum	Second Order Upwind
Volume fraction	QUICK
Turbulent kinetic energy	Second Order Upwind
Turbulent dissipation rate	Second Order Upwind
Transient formulation	Second Order Upwind
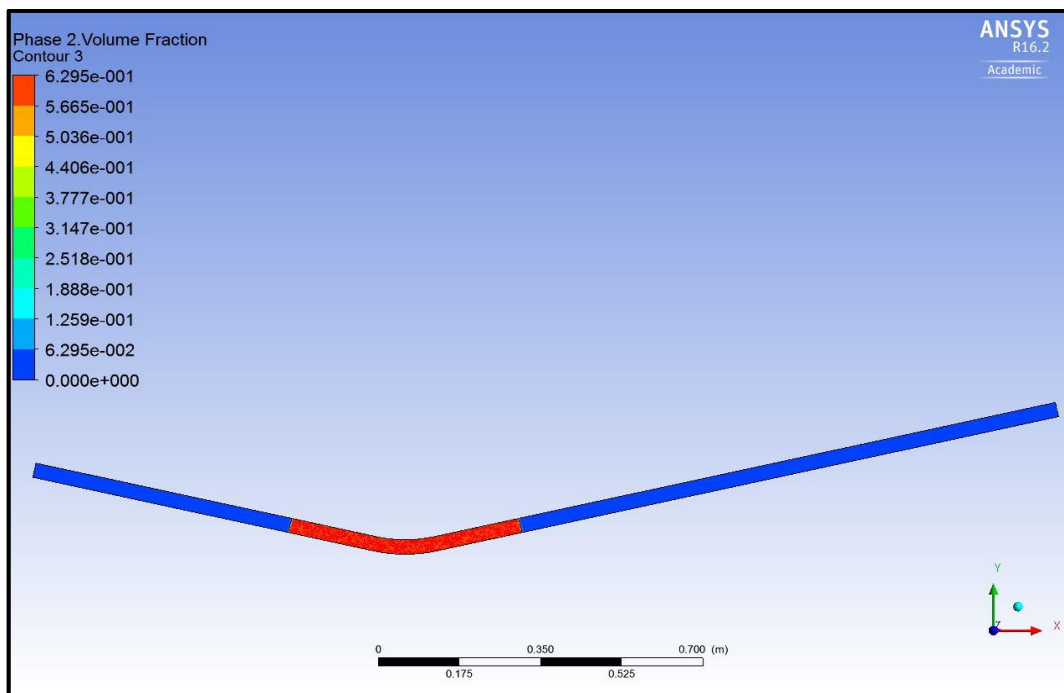
Figure 4.30 An initiated 53 cm particle plug

4.5.5 Simulation results

Since these simulations are conducted with double precision using high order discretization and the domain is relatively large, the computational time increases and every simulation takes around 12-14 hours to complete.

First, the visual observations are considered. In the Figures 4.31-4.33, the contours of volume fraction of the propagating plugs are presented. The instantaneous pictures are taken at the same pipe location – just in front of the pipe outlet.

In all the cases, the dispersion region at the front is clearly observed, however, the regions are not identical among the plugs. In the grid with the larger wall cell, i.e. with y^+_w=25, the particles are more dispersed at the front. The front becomes more dense with decreasing the first cell size.

Another very important feature is the particle depletion region at the walls in the main plug body. It is clearly seen that in the case with y^+_w=12.5, there is a long region at the walls where particle volume fraction is lower than in the center. In the case with y^+_w=19, this region becomes shorter and in the last case this region almost disappears. The existence of such a region might be caused by the fact that the shear stresses at the walls are higher than at the center of the pipe. As such, particles tend to migrate towards the center of the pipe where the shear stresses not as large as at the walls. The same particle behavior has been observed in several experiments and numerical simulations of high concentrated particle flows (Neil, 1988; Nott & Brady, 1994; Brown, 1988).

Also, as it can be remembered, the particles at the front have larger velocity due to the slip effect and axial dispersion as it has been concluded by Shabani (Shabani, 2012). This fact together with the wall depletion phenomena causes the dispersion at the front of the plug. However, as it is observed, the dispersion and wall depletion effects are affected by the y^+_w value and/or the value of the first layer thickness. The same conclusion was made at the end of the Phase 1 section, however, since the plug had a small length of 15 cm, this influence was not well observed.

Finally, it can be seen that the length of the tail is also different and the most dispersed tail is observed in the case with y^+_w=25.
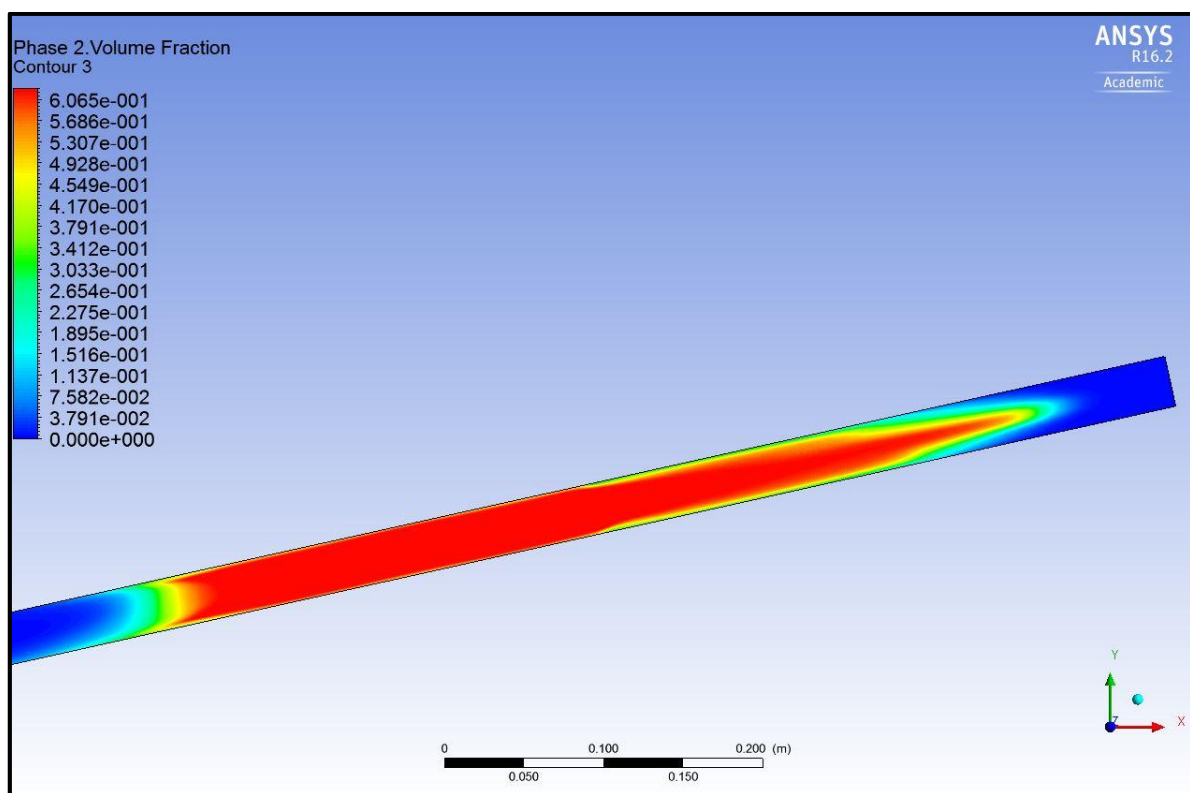

Figure 4.31 Particle volume fraction contours of the 53 cm plug in the grid with y^+_w=12.5
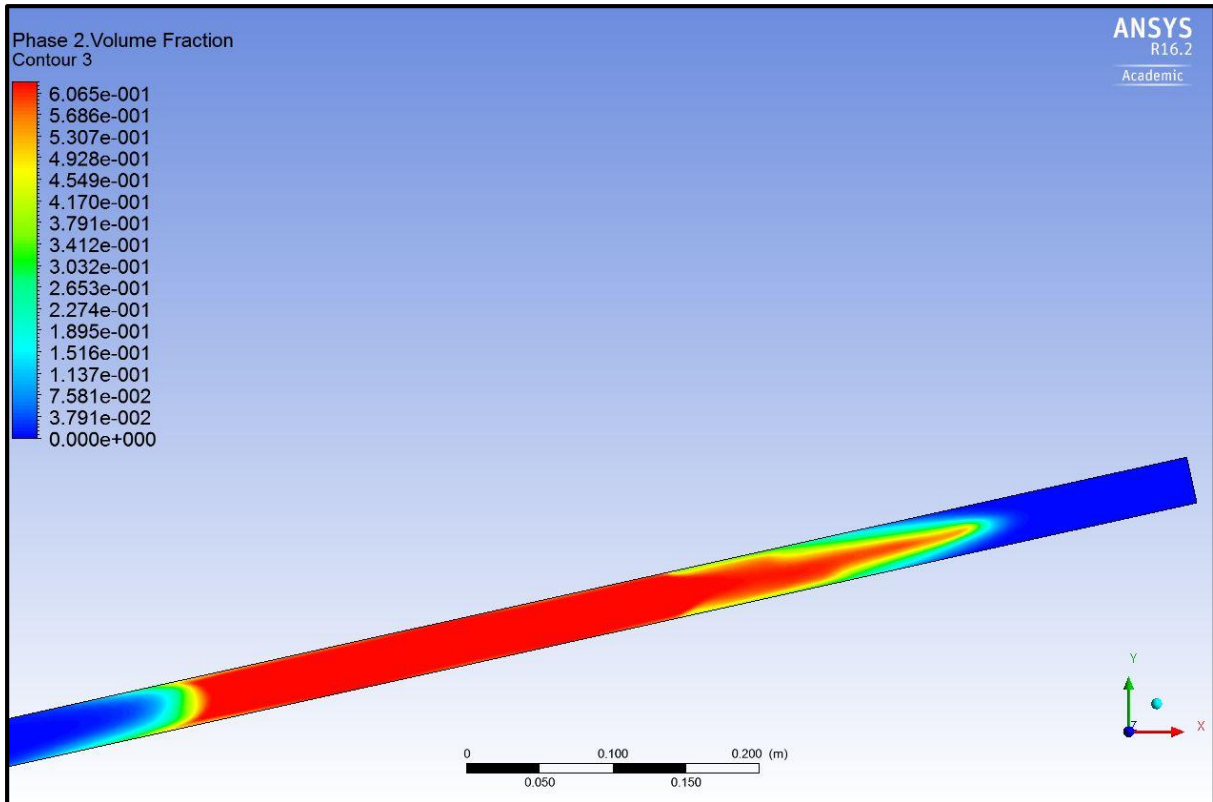
Figure 4.32 Particle volume fraction contours of the 53 cm plug in the grid with y^+_w=19
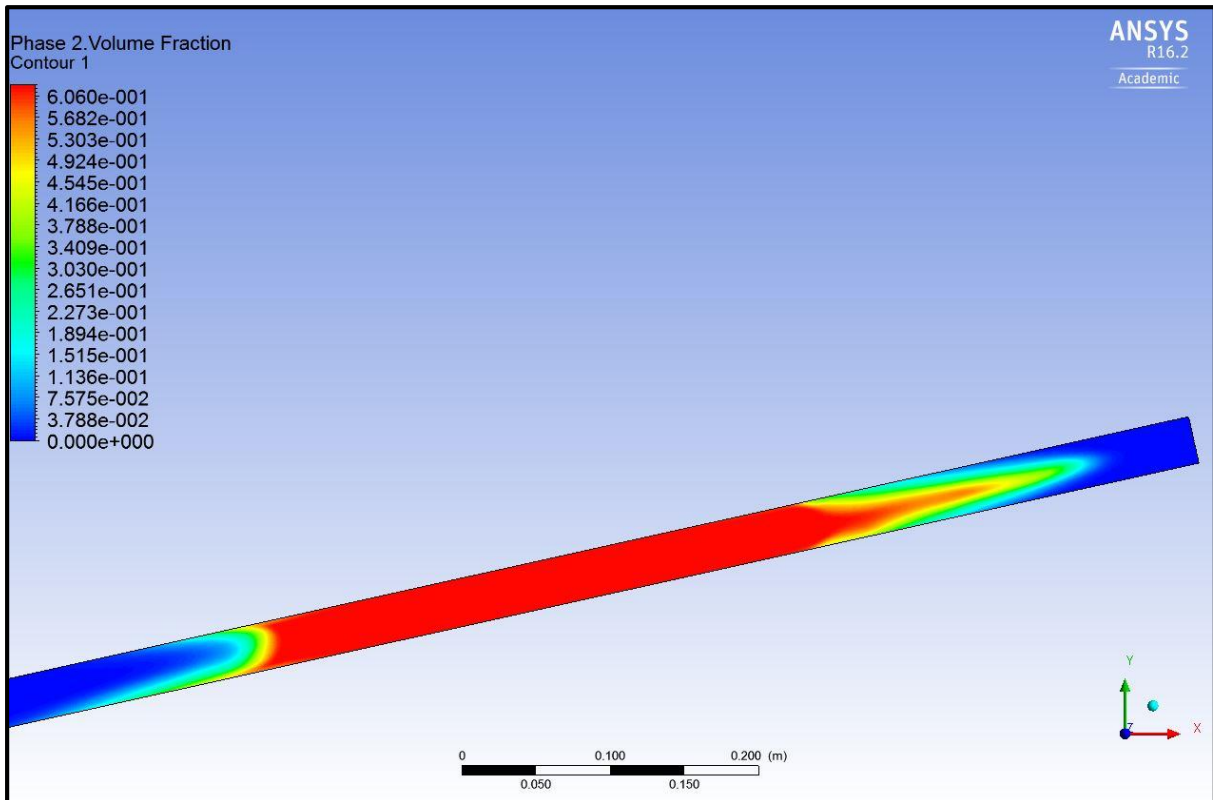

Figure 4.33 Particle volume fraction contours of the 53 cm plug in the grid with y^+_w =25

In order to estimate which case represents the real plug behavior in the most correct way, it is required to make a measurements of the particle fraction and compare it with the experimental measurements. Such measurements are taken at the pipe outlet section which has the same location as the first measuring conductance ring in the experiments. The results can be seen in the Figure 4.34.
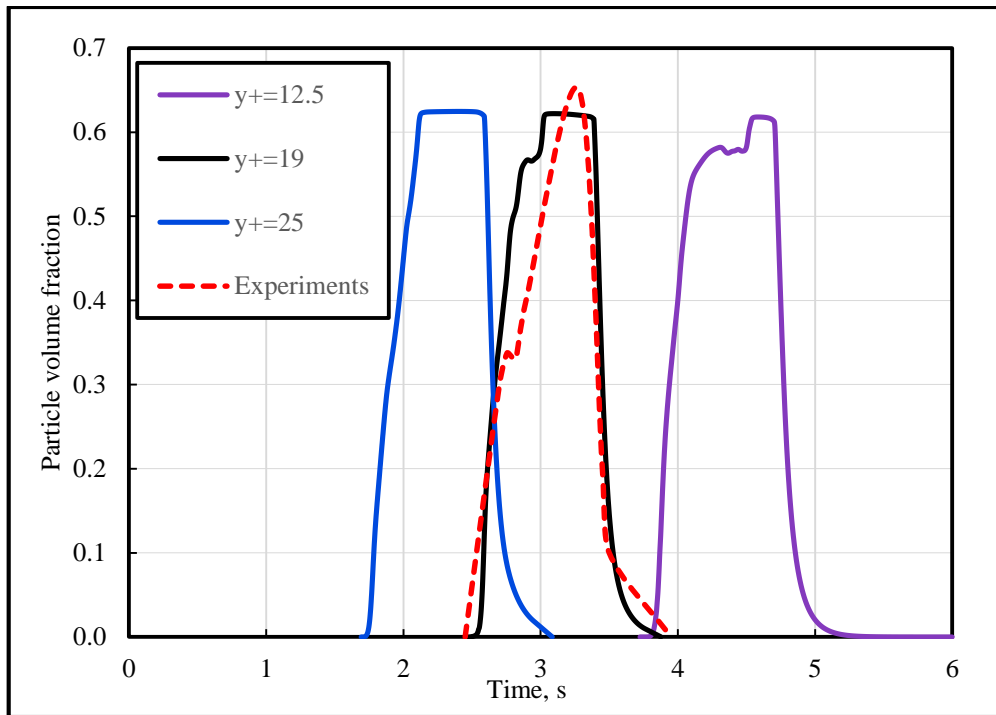
Figure 4.34 Particle volume fraction measurements at the pipe outlet section in the grids with $y^+_w=12.5$, $y^+_w=19$ and $y^+_w=25$ and experimental measurements (mixture velocity is 0.66 m/s)

Based on the comparison of the measurements, several observations can be made.

First, it can be clearly seen that the simulation results in the grid with $y^+_w=19$ have a good agreement with experimental measurements while other two cases significantly deviate from it.

Secondly, the plug velocity changes significantly between the cases. In the grids with higher y^+_w, the plugs move faster than in the grid with the smallest value of y^+_w.

In addition, the dimensions of the dispersed regions also changes between the cases and the sharp boundary between the main plug body and the dispersion is captured differently. In the case with $y^+_w=12.5$, there is a large "shoulder" region in the fraction measurements which decreases in the case with $y^+_w=19$ and almost disappears in the case with $y^+_w=25$. In the case with $y^+_w=19$, the size of this "shoulder" region fits the experimental data in the best way, but has higher volume fraction. As mentioned in the section with simulation uncertainties, the

conductance rings which measured the particle volume fraction in the experiments give approximated results for high concentrations. Therefore, the experimental particle fractions greater than 0.3-0.4 are qualitative (Shabani, 2012). As such, the difference between the "shoulder" regions in CFD and experiments might be less than it is presented. Nevertheless, the qualitative behavior of the plug has a good agreement.

In addition to these observations, it is possible to relate directly the particle fraction contours to measurements which makes the understanding of the plug behavior more clear. In the Figure 4.35, it is possible to see the parts of the plug in a correspondence to the measurements for the case with $y^+_w=19$.
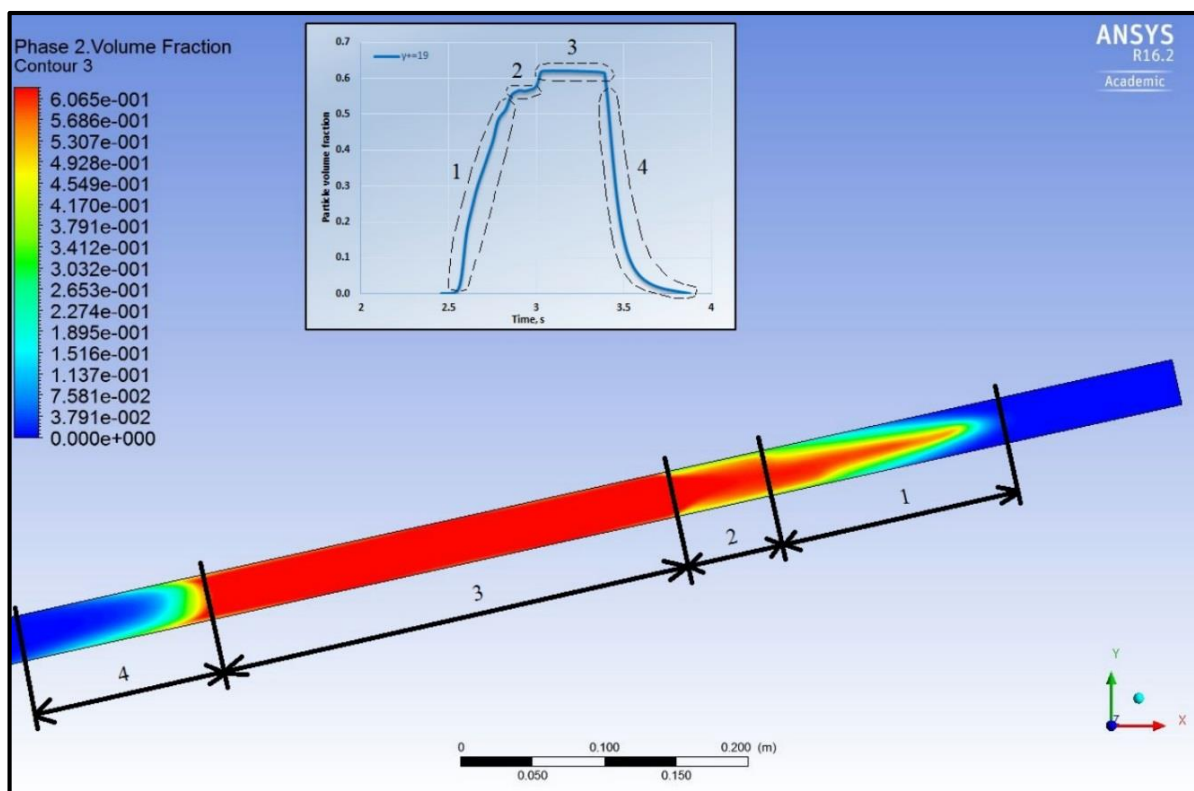
Figure 4.35 Correspondence of the particle plug regions to the measurement data

Basically, the plug can be divided by 4 parts: dispersion, "shoulder" zone (or transition zone), main body and tail. All the zones are clearly observed in the particle fraction contours as well as in the measurement line. The analogous comparison can be easily done for the rest two cases. During the experimental work, there was a trial to take an instantaneous picture of the transition zone. This picture is shown in the Figure 4.36.
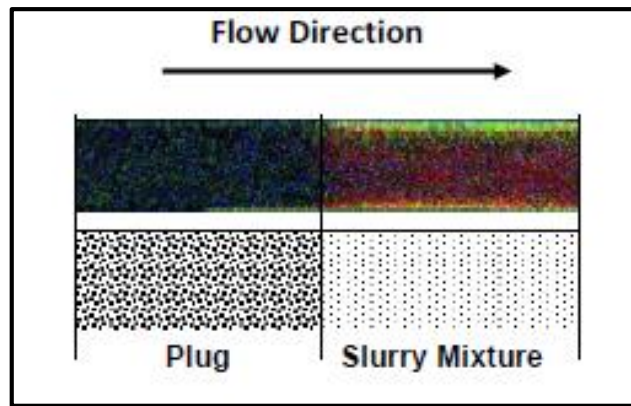
Figure 4.36 Picture of the transition zone between the main plug body
and the dispersed region (Shabani, 2012)

It can be seen that the picture taken during the experiments corresponds to the CFD results very well. At the walls, there is smaller amount of particles while in the center the plug has more dense structure. However, it can be seen that in the experimental picture, the particle fraction at the transition zone is more dilute at the pipe center than in the simulated transition zone. This fact also explains the difference between the measured values of the particle volume fraction in transitions zones in the simulations and the experiments.

Despite the small differences, it can be said that the CFD results are physically feasible and confirmed not only by experimental measurements, but also by detailed experimental visual observations. In addition, it can be said that the CFD results might help to understand the particle plug behavior better since during the experiments, it is a challenging task to make such observations within high quality while in the analysis of the CFD results these observations can be easily made.

4.6 Sensitivity study of the y^+_w value

As it is observed, the grid with y^+_w=19 has the best fit with experimental data. Such a value of y^+_w corresponds to the first layer thickness of 1.5 particle diameter at the mixture velocity of 0.66 m/s. However, at this point it is difficult to say which parameter gives a possibility to produce such good results: y^+_w or a specific first layer thickness. If it was checked, it was a useful recommendation for future studies on the topic of CFD simulations of particle plugs in pipes. As such, another sensitivity studies should be conducted to check the influence of these parameters.

In order to make such a sensitivity study, another experimental case is taken. The length of the plug is the same, but the mixture velocity is different and has a value of 0.5 m/s. First, simulation is run in the same grid as before, i.e. with the first layer thickness of 1.5 particle diameter. As such, the y^+_w value becomes 14.5. Then, the first layer thickness is changed to 685 µm, so that y^+_w=19.

All the settings and boundary conditions are the same as in the previous section, except the inlet water velocity which is changed to 0.5 m/s.

In order to compare the simulation results with the experimental data, the particle volume fraction measurements at the pipe outlet section are taken as previously. The comparison of the results can be seen in the Figure 4.37.
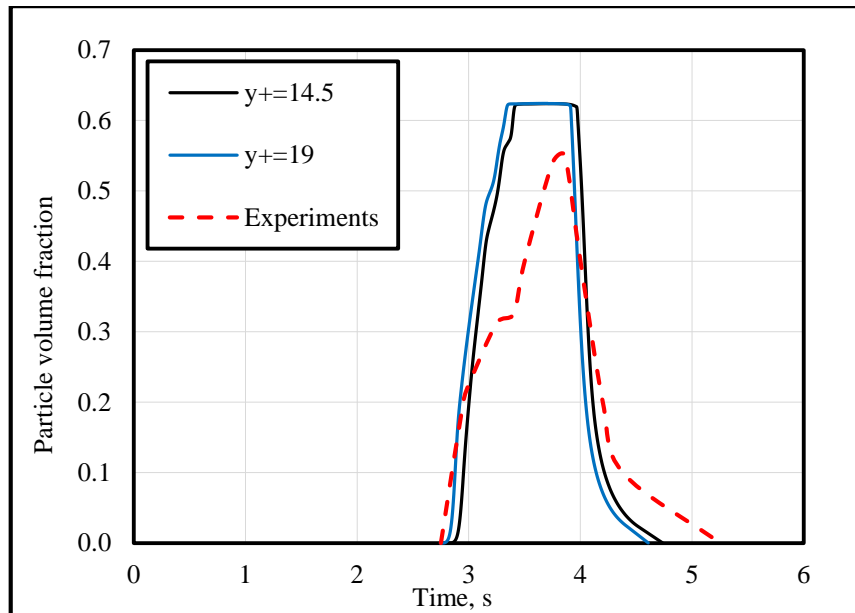
Figure 4.37 Particle volume fraction measurements in the grids with y^+_w=14.5 and y^+_w=19 and experimental measurements (mixture velocity is 0.5 m/s)

As it can be seen in the figure, the maximum value of particle volume fraction in the experiments is lower, but as mentioned, this value is qualitative and very uncertain due to inaccurate measurements by conductance rings. In reality, this value has to be around 0.6-0.65.

From the figure it can be observed that both cases have a good qualitative fit with the experimental data. The case with y^+_w=14.5 has a little bit longer "shoulder" region, while the case with y^+_w=19 has a very small "shoulder" but at lower particle fraction which is closer to the experimental results.

Generally, the plugs behave in a similar way and have a good qualitative fit with the experimental data. Based on these observations, it can be concluded that both options are good candidates for the usage in such types of flows. As such, the grid has to have the first layer thickness which corresponds to 1.5 particle diameter and/or which corresponds $y^+_w=19$. Both options show a reasonable agreement with experimental data.

Also, it is interesting to notice that in the previous section in the case with mixture velocity of 0.66 m/s, these two options are contained in one case and the results showed even better agreement with the experimental data. However, it is a coincidence and most likely it can be difficult to meet such a situation in another application. As such, the conclusions in this section are more general which make them more valuable.

4.7 Slip evaluation

As it is discussed in the Chapter 1, one of the motivations of this research work is contribution to 1D multiphase flow simulators such as OLGA. As shown, the implemented OLGA model is not capable to reproduce the axial particle dispersion in a good way when the particle plug propagates through the pipe.

As Shabani showed, the particle velocity at the front have higher velocity than the rest of the plug, as such the particles have a slip effect at the front and move faster. Based on the visual observations and particle fraction measurements, this assumption seems to be also confirmed by the CFD results, however, it has not been proved directly yet and will be checked in this section. It can be suggested that the particle slip depends on the average particle fraction and the particle velocity has the highest value where the fraction is the smallest. In this way, the dispersion region becomes more and more noticeable during the propagation time.

In order to check these assumptions and observations, the following approach is applied. Based on the already simulated plug propagation case, the particle velocity is computed using the formula below:

$$U_p = \frac{U_{sp}}{\alpha_p} \qquad (59)$$

where:

U_p – average particle velocity;

U_{sp} – superficial particle velocity;

α_p – average particle volume fraction.

The particle superficial velocity is calculated as follows:

$$U_{sp} = \frac{1}{A} \int_A \alpha_p U_p dA \qquad (60)$$

The particle average fraction is calculated as follows:

$$\alpha_p = \frac{1}{A} \int_A \alpha_p dA \qquad (61)$$

Since the simulation is two-dimensional, the averaging has to be done only in the radial direction, as such the area A has to be changed to y-coordinate. In such a way the averaging is done over the pipe diameter. As such, the formulas can be re-written as follows:

$$U_{sp} = \frac{1}{y} \int_y \alpha_p U_p dy \qquad (62)$$

$$\alpha_p = \frac{1}{y} \int_y \alpha_p dy \qquad (63)$$

The final formula for the average particle velocity can be written as follows:

$$U_p = \frac{\int_y \alpha_p U_p dy}{\int_y \alpha_p dy} \qquad (64)$$

Using this formula, it is possible to compute the average particle velocity at a particular location in the pipe. However, the goal is to find a dependency of the average particle velocity on the particle volume fraction. In order to accomplish this task, the plug needs to be discretized and the average particle velocity has to be computed at several locations along the plug. In such a way, it becomes possible to find out if there is the dependency of the average particle velocity on the average particle volume fraction. For the evaluation, the plug in the grid with $y^+_w=19$ and the mixture velocity of 0.66 m/s is taken. This case is selected since it showed the best fit with the experimental data. The discretization scheme is shown in the Figure 4.38.
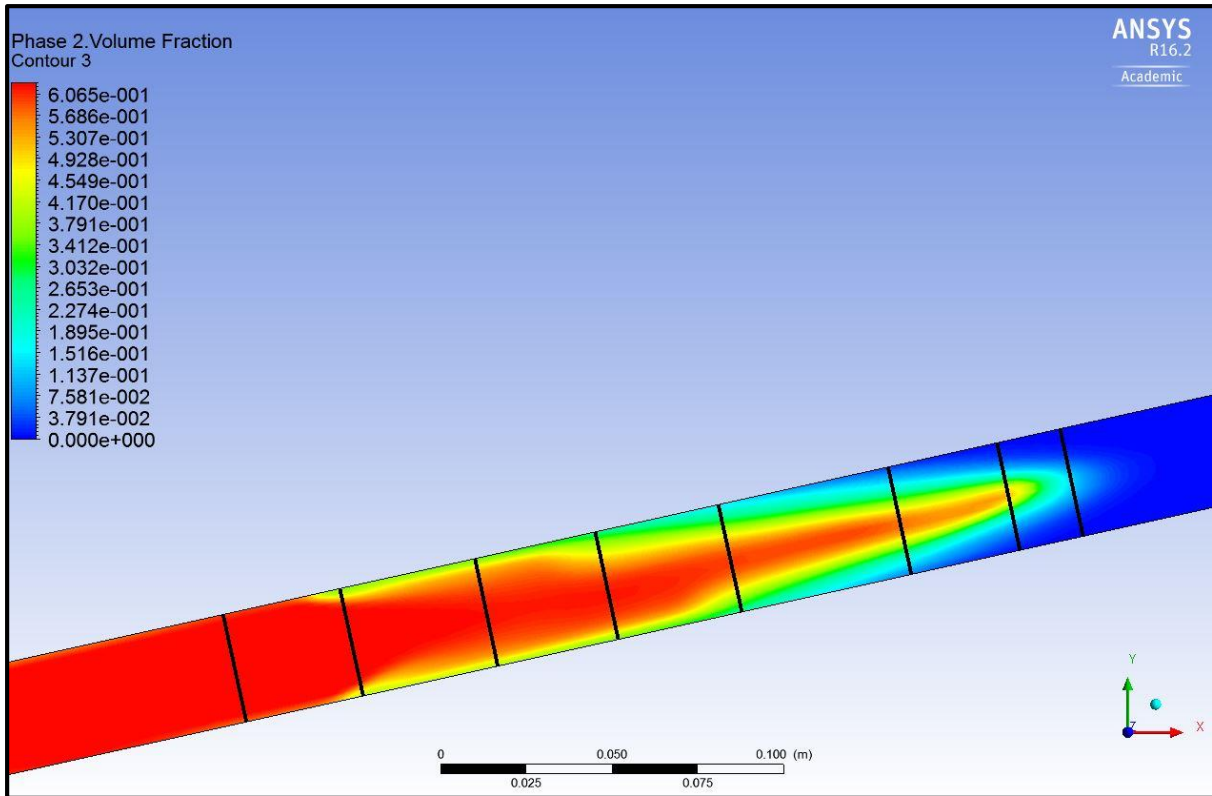
Figure 4.38 Discretized particle plug for slip evaluation

When the average particle velocity is computed at every single line marked in the figure, it is then possible to create a slip relation which would describe the particle velocity relative to the water velocity. For this purpose, the following form of the slip relation is selected:

$$U_p = C \cdot U_m \tag{65}$$

where C – dimensionless slip distribution coefficient and U_m – mixture velocity.

The mixture velocity can be computed as follows:

$$U_m = U_{sp} + U_{sw} \tag{66}$$

This formula is used for a double check purpose since the mixture velocity is equal to the boundary condition water velocity, i.e. 0.66 m/s.

Since the mixture velocity is constant and particle velocity depends on the average particle fraction, the slip distribution coefficient C also depends on the average particle fraction, so that particles move with different velocity at different fractions. Based on the data extracted from the discretized particle plug, the dependence of the coefficient C on the average particle fraction is obtained and represented in the Figure 4.39
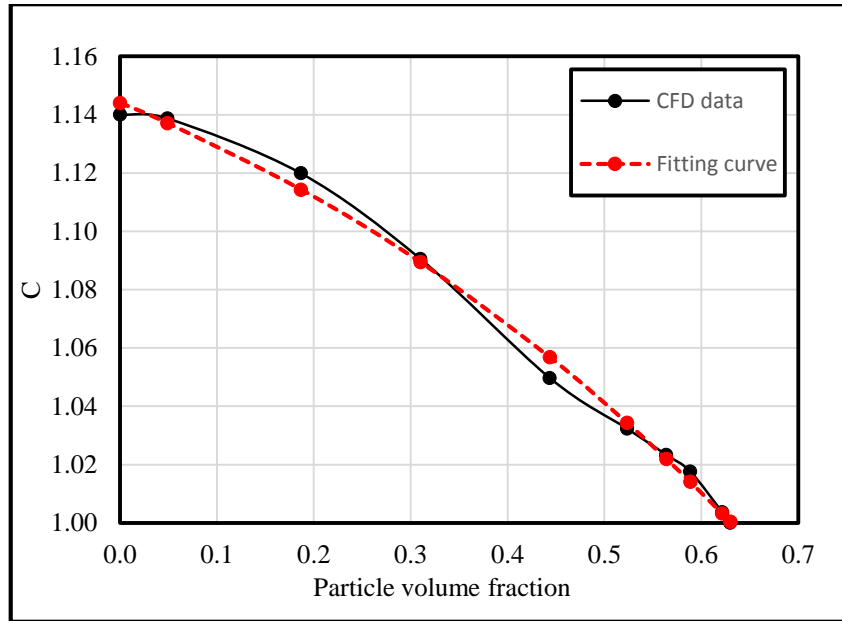
Figure 4.39 Function of the C-coefficient depending on the particle fraction

The fitting curve is developed using the Sigmoid function. There are several forms of the function but for this case one of the simples forms is taken which is written as follows:

$$C = \frac{A}{1 + B \cdot e^{D \cdot \alpha_p}}$$

(67)

where:

C – distribution slip coefficient;

A, B and D – constants;

α_p – particle volume fraction.

This function is short and easy to manipulate with if one would like to apply it for a particular 1D model. The only thing which needs to be adjusted is the values of A, B and D constants. In this particular case, the values for the constants are: A=1.22, B=0.068 and D=1.87. After that, the C-coefficient as well as the particle velocity is computed for each value of the particle volume fraction.

It is possible to find a curve which fits the simulation result better, for example, a polynomial curve. However, the order of the function has to be 5 or 6, as such, 6 or 7 constant values of the coefficients have to found which is very impractical for the usage. As such, the Sigmoid form is selected to be the most appropriate.

The function is implemented in the MATLAB code to compute the average particle fraction for the plug propagation case at every single moment. The function is linked with the mass balance which is written as follows:

$$\frac{\partial \alpha_p}{\partial t} + \frac{\partial \alpha_p U_p}{\partial x} = 0 \tag{68}$$

Based on this approach, it is possible to obtain the dispersed region at the front of the propagating particle plug shown in the Figure 4.40. The entire code can be seen in the Appendix C.
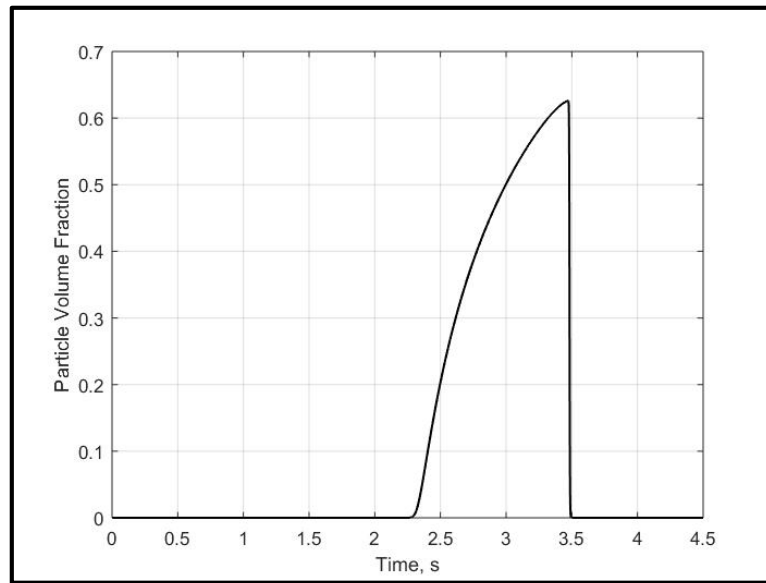
Figure 4.40 Particle volume fraction of the propagating plug developed in MATLAB

In the figure, the dispersed region at the plug front is clearly observed. The highest fraction is around 0.6 which is feasible according to the simulation and experimental results. However, it can be seen that the transition zone between the main plug body and the dispersed region is absent. As such, the developed function requires some modifications to fit the data. This modification is done in such a way that at the specified particle volume fraction the no-slip condition works. In the Figure 4.41, the no-slip condition is assigned to 0.57 as it has been obtained in the CFD simulations.

The resulting function can be written as follows:

$$C = \begin{cases} \frac{A}{1+B \cdot e^{D \cdot \alpha_p}}, \alpha_p < no-slip\ value \\ 1, \alpha_p \geq no-slip\ value \end{cases} \tag{69}$$
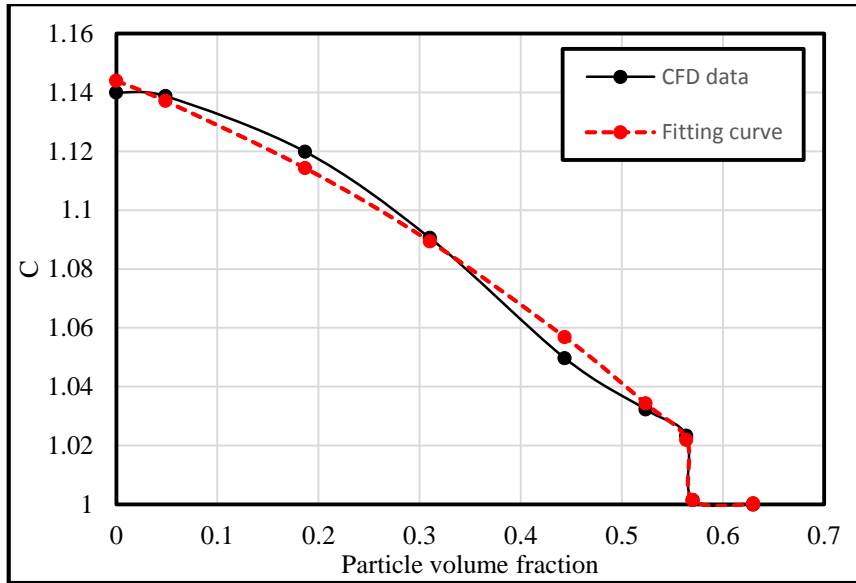
Figure 4.41 Modified function of the C-coefficient

As such, the great thing with the developed function is the fact that the no-slip condition at the transition region as well as dimensions of the dispersion region can be modified easily. The modifications depend on the goal. In this case, for example, the function can be adjusted to fit the CFD data or the experimental data. Both adjusted functions are plotted together with the experimental and CFD results in the Figure 4.42. MATLAB Case 1 represents the function adjusted for the CFD results while the Case 2 is adjusted for the experimental measurements.
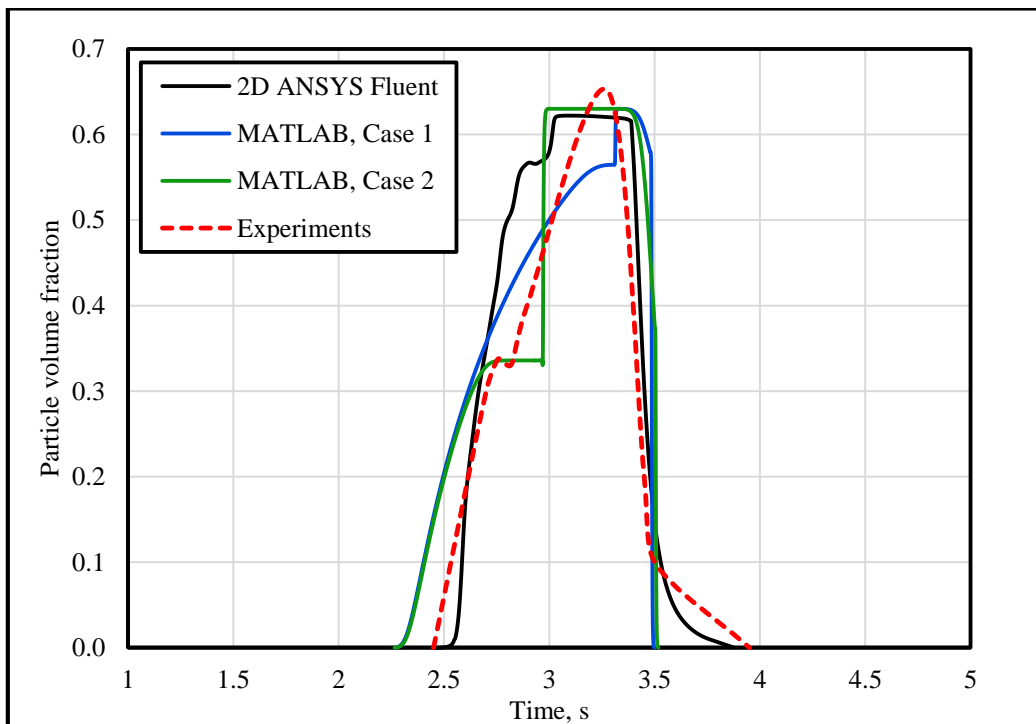
Figure 4.42 Particle fraction obtained in the experiments, MATLAB and ANSYS Fluent

As it can be seen, the MATLAB Case 1 shows a reasonable qualitative fit with the CFD results. The MATLAB Case 2 shows a very good qualitative and quantitative fit with the experimental data. As discussed earlier, the exact value of the particle fraction in the transition region as well as the peak concentration values are uncertain, since the conductance rings are not able to measure it in a perfect way. As such, the fit with the developed MATLAB code and the experimental results might be even better than it is shown in the figure.

Overall, it can be concluded that the developed 1D model with the slip relation is capable to reproduce the particle plug propagation results using extracted data from the CFD simulations. The proposed function for the distribution coefficient is easy to use and modify for a specific 1D model.

4.8 Summary of the Phase 2 section

The Phase 2 of the research work is the core of the thesis, as such, it is worth to summarize all the obtained results.

- It is obtained that the ANSYS Fluent is capable to produce the results for the large particle plugs which fit the experimental measurements and visual observations.
- The simulation results in the grid with y^+_w=19 reproduce the experimental data in a good qualitative way within a reasonable quantitative fit. All the important features of the plug are captured well, as such it is possible to understand the plug structure based on the simulation results.
- It is shown that in order to make a successful simulation of the plug propagation case, it is required to mesh the domain in such a way that the first layer thickness is 1.5 times higher than the particle diameter and/or the value of y^+_w is around 19. Using this mesh, it is possible to fit the CFD results with the experimental data in a reasonable qualitative way. In other mesh structures, the dimensions of the transition zone significantly deviate from the experimental results as well as the plug velocity does not satisfy the experimental measurements.
- The 1D model of the particle plug is created which fits the experimental data in a good way as well as reproduces the dynamic behavior. The form of the slip relation is proposed together with function of the slip distribution coefficient which depends on the average particle fraction. The function is easy to use and can be adjusted for a particle propagation case which is of interest. The developed model can be potentially

used as a basis of improvement of the 1D multiphase dynamic simulators such as OLGA.

- The simulation setup for a 3D model is obtained and can be tested in the further study.

4.9 3D model

The final step of the evaluation of the propagating particle plug is 3D modelling. The 3D model is performed based on the experience obtained in 2D modelling of the small and large scale plugs. All the best practices are used in order to perform a successful 3D plug model to complete the research work.

4.9.1 Geometry

The geometry is the same as in the previous section, but performed as a 3D pipe. Sweep operation is used in order to create a pipe. Then the pipe is rotated in such a way that upstream and downstream sections have 12.5° relative to the horizontal plane. The plug has a length of 53 cm. The geometry is shown in the Figure 4.43.
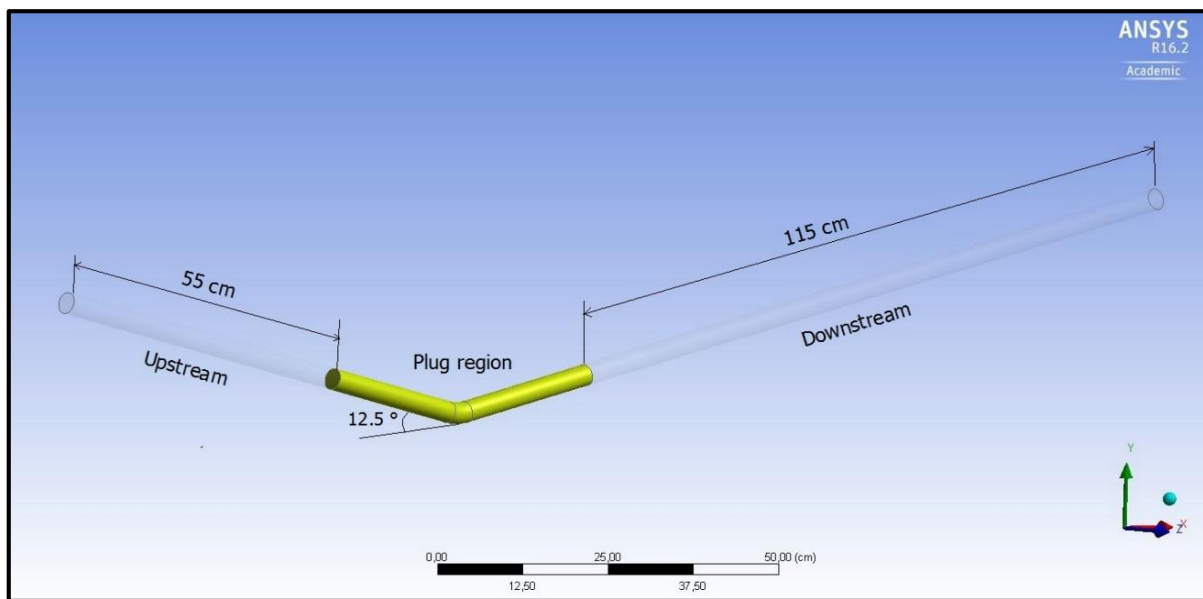
Figure 4.43 Geometry of the 3D pipe model

4.9.2 Mesh

In order to mesh the pipe, the Inflated Multizone method is used. Inflated option allows to control the first layer thickness which is very important to control y^+_w. The Multizone method

allows to avoid high aspect ratio, high skewness and low orthogonal quality. The generated mesh is shown in the Figure 4.44. In the Table 4.8, the mesh statistics is presented.
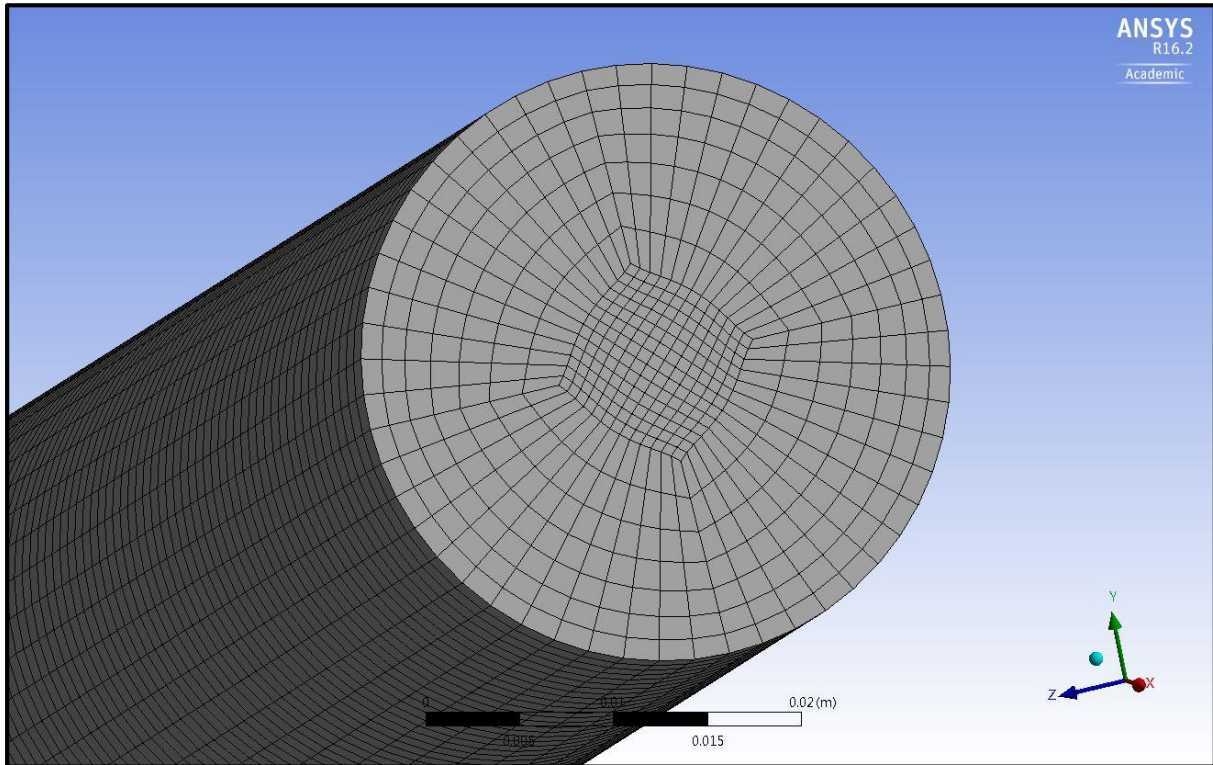
Figure 4.44 Mesh of the 3D pipe model

Table 4.8 Mesh statistics of the 3D pipe mesh

Parameter	Value
Number of elements	303831
Number of nodes	324688
Max aspect ratio	2.5
Min orthogonal quality	0.828
Max skewness	0.432

4.9.3 Boundary conditions and solver settings

The boundary conditions and solver settings are the same as in the 2D case with the plug of 53 cm and inlet velocity of 0.66 m/s. All the data can be found in the Tables 4.6 and 4.7.

4.9.4 Results and discussion

This simulation is computationally heavy and took about 110 hours to be completed. First, it is useful to make visual observations of the propagating plug. In the Figures 4.45-4.47, it is possible to see the particle volume fraction of the plug in a 3D mode as well as the cross-sectional contours along the plug.

Figure 4.45 3D representation of the particle plug
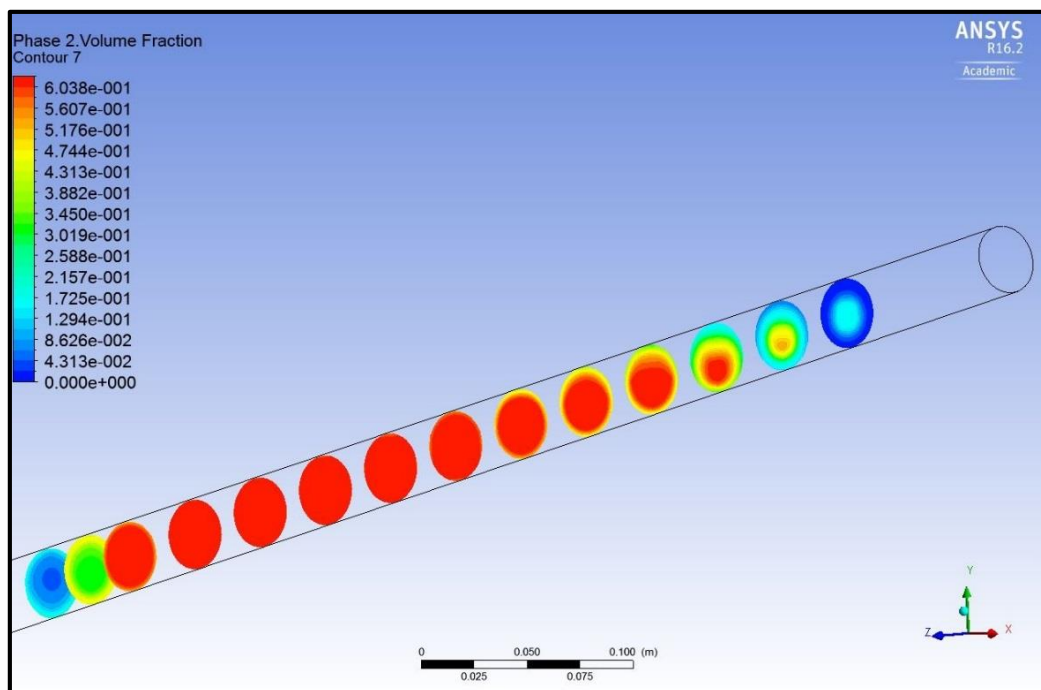
Figure 4.46 Cross-sectional contours of particle volume fraction
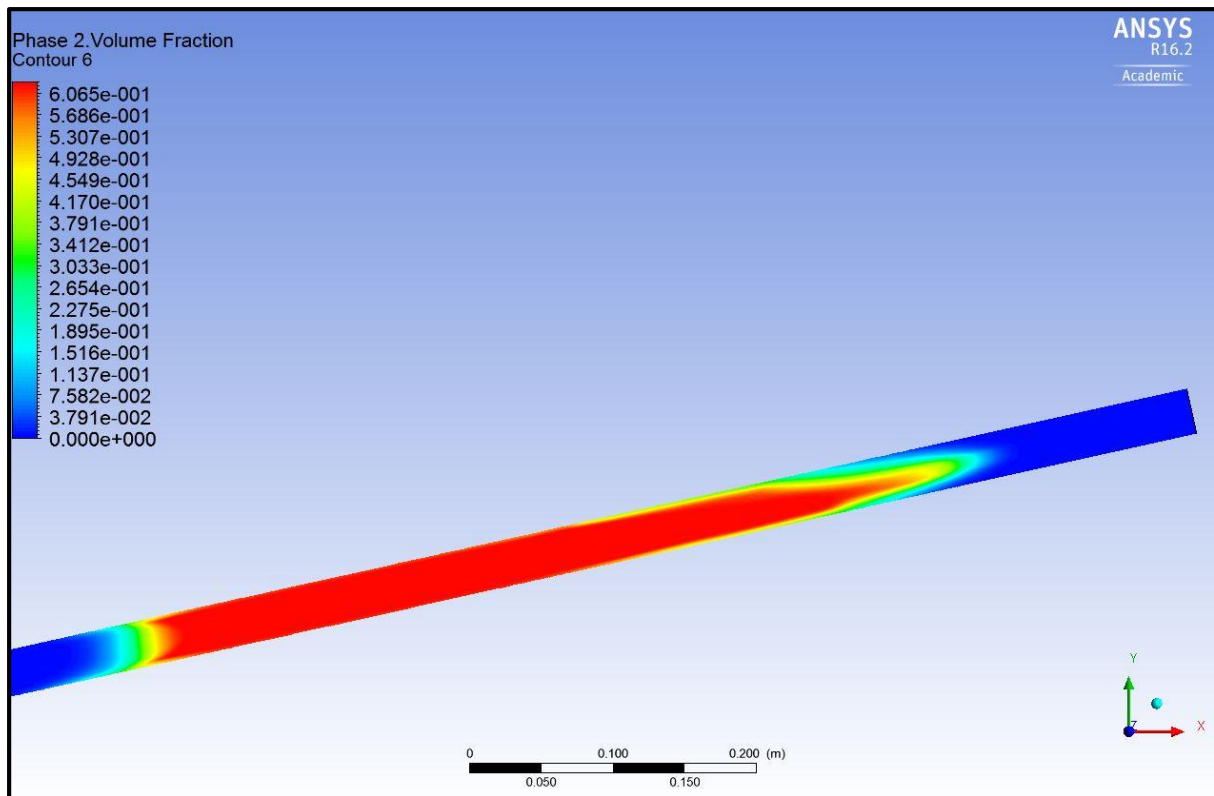
Figure 4.47 Particle volume fraction contours of the 53 cm 3D plug at the lengthwise slice

It can be clearly observed that there is the dispersion region at the front of the plug similarly to 2D simulation results. In addition, the transition zone is also clearly seen as well as the main plug body and the tail. Cross-sectional contours show that the particle migrate towards the pipe center fro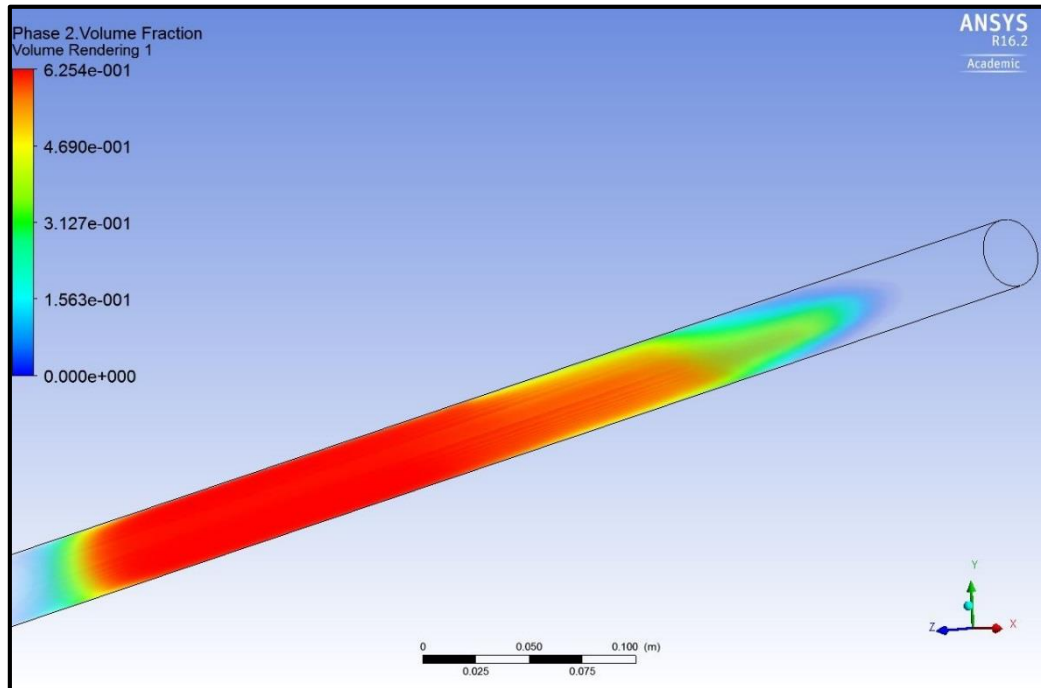m the walls in all the directions, as such the general particle behavior is similar to the 2D simulations. The dispersed particles tend to propagate at the bottom of the pipe which is exactly the same as it has been observed in the experiments. Indeed, the Figures 4.45-4.47 can be very well compared to the experimental observations shown in the Figures 1.4-1.5.

Nevertheless, some differences between 2D and 3D simulations can be observed. First, the dimensions of the transition zone is a little bit different in comparison with the 2D simulations. In addition, it can be seen that the tail form is different from the 2D simulations. These differences can be explained by the fact that the circular 3D geometry influences the particle movement and distribution, therefore, some differences between the 2D and 3D simulations are expected. Moreover, some differences in the mesh structure might exists even though a big effort is made in order to create completely the same mesh for the 3D pipe as it is used in the 2D case.

In order to compare the 3D results with the 2D simulations and the experiments, the particle volume fraction measurements are taken at the pipe outlet section. In the Figure 4.48, the comparison of the results is presented.
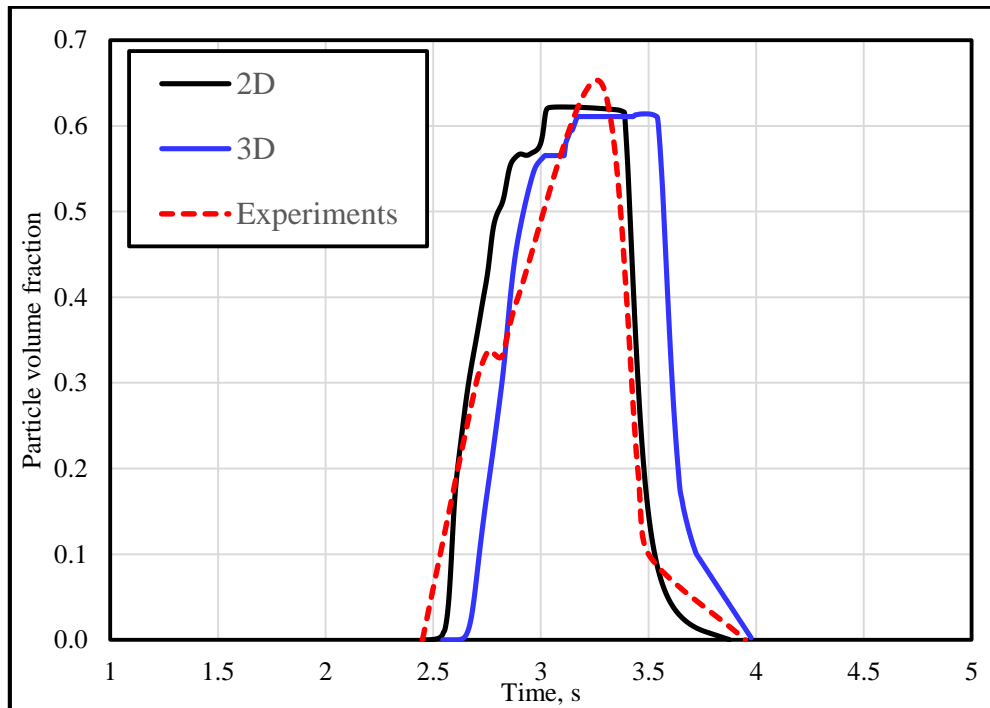
Figure 4.48 Particle volume fraction measurements at the pipe outlet section

It is clearly seen that the 3D simulation results have a reasonably good fit with the experimental results as well as the 2D simulations. In comparison with the 2D case, the small difference in the plug velocity can be observed in the 3D simulation. This fact can be explained as it is done above – the circular 3D geometry and possible small difference in the mesh structure, specifically, in the first layer height, might cause small deviation between these simulations.

As in the 2D case, in the 3D simulation the transition zone is represented by the particle volume fraction which is higher than in the experiments. Nevertheless the qualitative behavior strongly corresponds to the experimental measurements.

Based on the visual observations as well as taken measurements, it is possible to conclude that the 3D simulation of the propagating particle plug is successfully completed. ANSYS Fluent is capable to reproduce the particle plug behavior in the three dimensional pipe and the qualitative behavior of the plug is well compared with the experiments.

Chapter 5
CFD results of MTC study

5.1 Introduction

In this chapter, the CFD simulation results regarding the critical velocity of the dilute sand-water flows are discussed. This study significantly differs from the particle plug propagation case since the particle volume fraction is low. This fact gives a chance to use the DPM model of the Euler-Lagrange approach in ANSYS Fluent which is valid for particle volume fractions less than 10%. The reason for testing this model is the fact that the model might give more precise results regarding the particle position in the flow domain than the Euler-Euler approach. In addition, the model allows using particle tracking which has excellent post-processing features. These facts can be very useful for evaluation of the simulation results since the experimental results by **Yan, 2010** were evaluated based on the visual observations. Moreover, the DPM model allows using particle diameter distribution. This fact might play a crucial role in this study since the deposition velocity is significantly different for various particle diameters. In order to confirm all these advantages, the results are compared with the Eulerian Granular model.

In the DPM model, the number of parameters to be selected is less in comparison with the Eulerian Granular model, but some of the parameters require a careful consideration. As such, selection of the most important parameters is discussed in details. The Eulerian Granular model for this case is much simpler than for the plug propagation case due to the fact that the particle volume fraction is low. As such, only a short discussion on the selected parameters is provided.

5.2 Approach

Due to time limitations of the project, it is decided to conduct 3D simulations directly without evaluation of a 2D model. In the experiments, a 17 m pipe is used for the flow evaluation. It is obvious that it is not feasible to make CFD simulations of such a long pipe since it would take

a huge amount of computational time. Moreover, at least 50 simulations have to be completed (5 fractions at 10 different velocities) for the final mesh setup and some other simulations for the mesh selection process. As such, the length of the pipe has to be compromised between the expected results and computational costs.

Based on preliminary estimations, a 3 m pipe has been selected for the 3D simulations. In order to estimate such a length, first, the entrance length has been calculated for the largest flow velocity of 1 m/s as follows:

$$L_e = 4.4 \cdot \mathrm{Re}^{1/6} \cdot d \qquad (70)$$

Based on these calculations, it is possible to estimate the length which is required for the turbulent flow to be fully developed. If the numbers are put in the formula, the entrance length is computed as 1.3 m. Then this length has been increased more than two times, i.e. up to 3 m, to see if this length is enough for particles to settle and show a steady behavior in the flow. Several preliminary runs with different velocities are conducted and it is figured out that the length of 3 m is a good choice because it is sufficient for the slurry flow to be well developed and all the necessary features such as deposited and suspended particles are clearly observed. In order to confirm the assumed length, one simulation in a 10 m pipe is run for comparison at the velocity of 0.4 m/s. The results of the preliminary simulations in both pipes can be seen in the Figures 5.1 and 5.2.
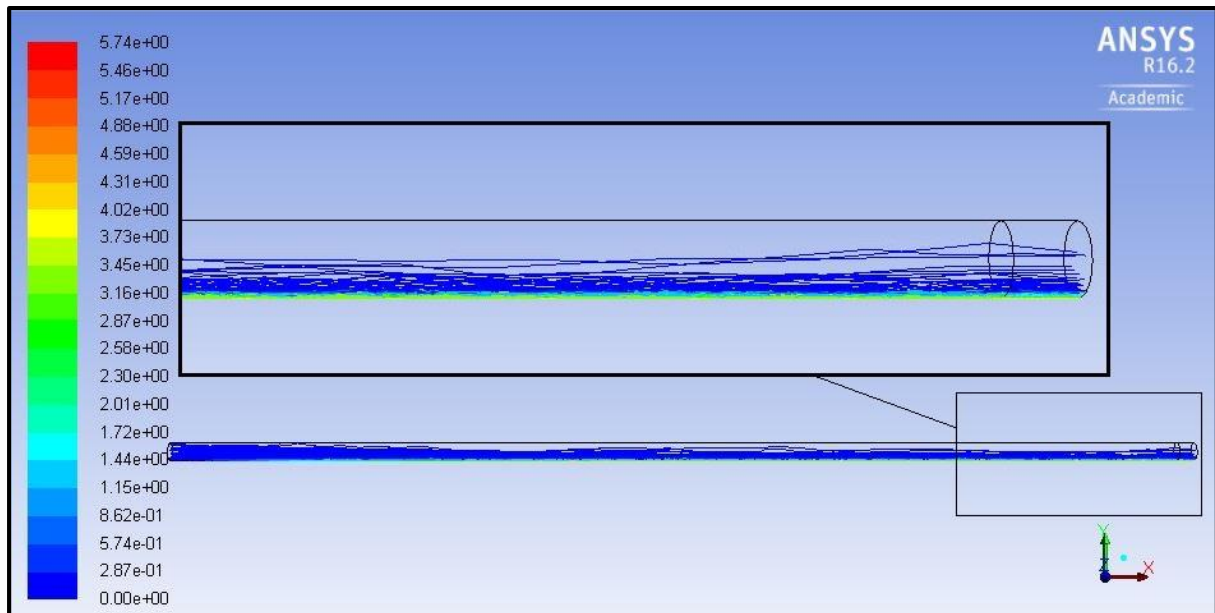

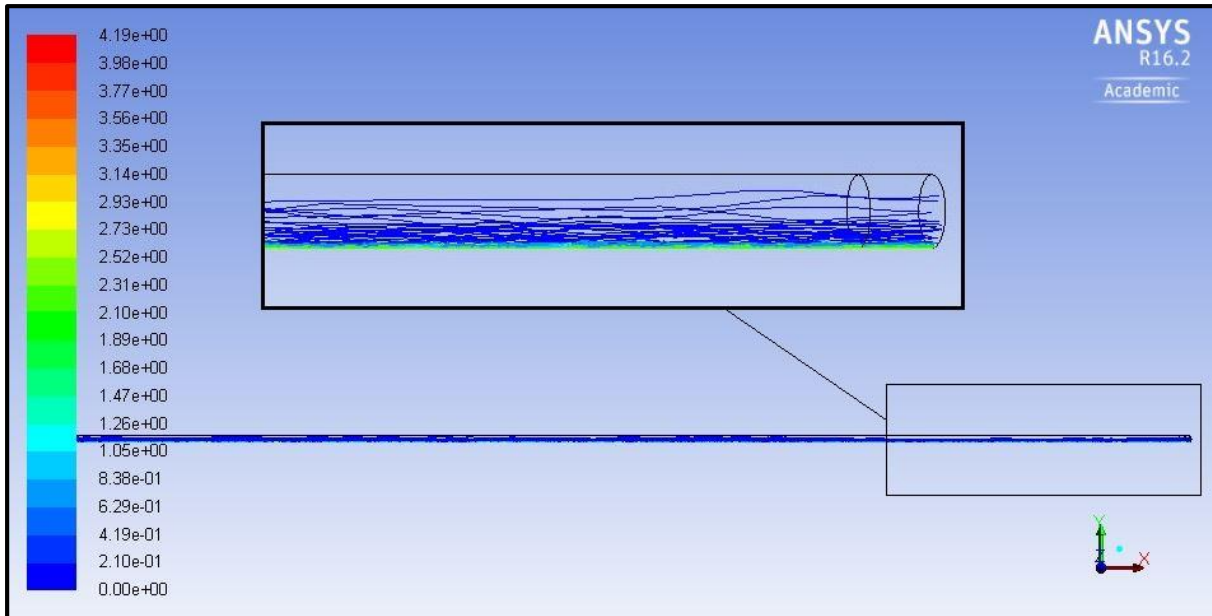Figure 5.1 Preliminary particle tracks using DPM model in a 3 m pipe

Figure 5.2 Preliminary particle tracks using DPM model in a 10 m pipe

As it can be seen, the particles show very similar behavior in both pipes. It is observed that the relative amount of the deposited and suspended particles is nearly the same in both cases, as such the 3 m pipe is selected to be the final choice.

Before running all the 50 simulations, it is first wise to select the most appropriate model (Eulerian or DPM) within the most suitable mesh. In order to select the most appropriate mesh, it has to be validated with the experimental results. In this case, the problem is the fact that no measurements were taken and only visual observations are available. As such, it is decided to select the mesh based on the experimental observations at low velocity – 0.1 m/s. The reason for this choice is the fact that at low water velocity the sand dunes were clearly observed in the experiments, while at high velocities some of the particles are suspended and the rest particles are at the bottom, but there is not any exact value of the suspended and laying fraction, as such it will be impossible to evaluate the results. In opposite, if any of the models is able to reproduce the dunes formations, it will be a clear proof for using that model in the rest of the study.

When the mesh and model are selected, the simulations are performed at all the fractions and velocities. The results are then compared with experimental and OLGA results and overall conclusions are made. The summarized approach used in the evaluation of the MTC condition in slurry flows is summarized in the Figure 5.3.
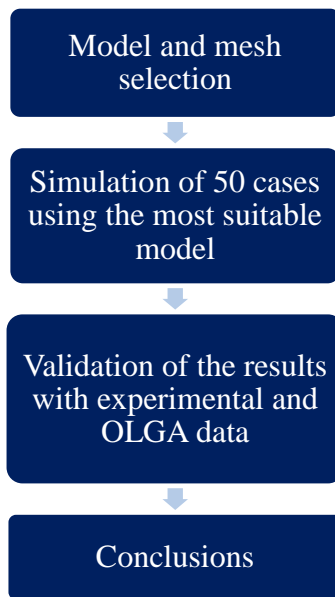
```
┌─────────────────────────┐
│   Model and mesh        │
│   selection             │
└─────────────────────────┘
            │
            ▼
┌─────────────────────────┐
│   Simulation of 50 cases│
│   using the most suitable│
│   model                 │
└─────────────────────────┘
            │
            ▼
┌─────────────────────────┐
│   Validation of the results│
│   with experimental and │
│   OLGA data             │
└─────────────────────────┘
            │
            ▼
┌─────────────────────────┐
│   Conclusions           │
└─────────────────────────┘
```

Figure 5.3 Schematic approach for evaluation of MTC in slurry flows

5.3 Assumptions and uncertainties

DPM model

Assumptions:

- all the particles are suspended in the flow when injected in the pipe domain;
- the particles are uniformly distributed along the injecting surface (pipe inlet);
- the particles have zero velocity when injected;
- the water flow is assumed to be steady;
- the particles are assumed to be spherical.

The reason behind the zero particle velocity assumption is the fact that in such a case the settling process will be faster, as such, the length of the pipe can be shortened which decreases calculation time.

Uncertainties:

1. Diameter distribution.

Even though the particle distribution is used in the simulations which increase the results accuracy, it is very hard to fit the distribution function to the experimental data in the exact way due to the fact that the experimental particle distribution has two peak values and the mean value is unclear. The particle diameters directly influence the MTC condition in slurry flow, as

such there is an uncertainty in the simulation results due to deviation of the particle distribution data between the experiments and the simulations.

2. Subjective judgment.

Since the experimental results are based the visual observations only, there is a big uncertainty between the judgment by researchers who conducted the experimental work and the judgement used in this thesis. Moreover, not for all the velocities the pictures with the observations are available which increases the uncertainty of the results evaluation. In order to decrease this uncertainty point, the researcher Wei Yan (the original experimentator) has been contacted and the results are discussed directly with him. In addition, he provided the video records of some of the experimental observations which helped to evaluate the results and reduced the uncertainty of the subjective judgement as much as possible. Otherwise, the evaluation of the results would be hardly achievable.

Eulerian Granular model

Assumptions

- all the particles have the same diameter;
- pipe walls have zero hydraulic roughness;
- water flow is assumed to be steady.

Uncertainties

1. Constant particle diameter.

The experimental data state that the particles have a wide diameter distribution. In the context of particle lifting, this fact might play a crucial role and this is the biggest uncertainty of using the Eulerian Granular model in this case.

2. Subjective judgement

This uncertainty is the same as for the DPM model.

5.4 CFD simulations of MTC in slurry flows

5.4.1 Geometry

The geometry consists of a pipe with a length of 3 m. The inlet is fed by the water-sand flow with a defined particle volume fraction. The geometry is shown in the Figure 5.4.
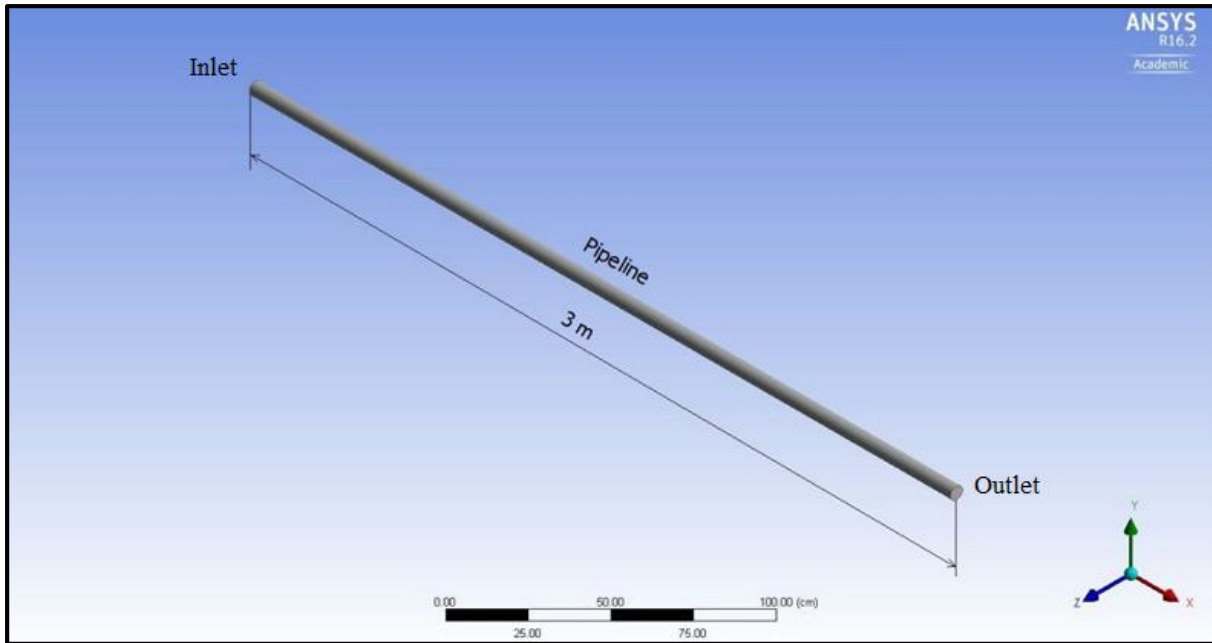
Figure 5.4 Horizontal pipe geometry

5.4.2 Mesh

As discussed, several mesh setups are studied. In all of them, the mesh is generated using the Inflated Multizone method. It allows to control the first layer thickness and avoid poor mesh quality with high skewness and low orthogonal quality. For both DPM and Eulerian models, it is very important that the mesh cell size has to be larger than the particle diameter, especially the boundary layer cells. Otherwise, the results will be unrealistic, and problems with convergence of the solution will appear. As such, the first layer thickness is selected in such a way that at least three particle diameters can be located inside the cell.

The difference in meshes is the number of nodes. More specifically, the number of nodes is changing in the axial direction while in the cross-sectional plane the mesh size is the same. The cell sizes in the axial direction are 1, 5, 10 and 15 cm. The mesh statistics can be seen in the Appendix C. The mesh structure is shown in the Figures 5.5-5.9.
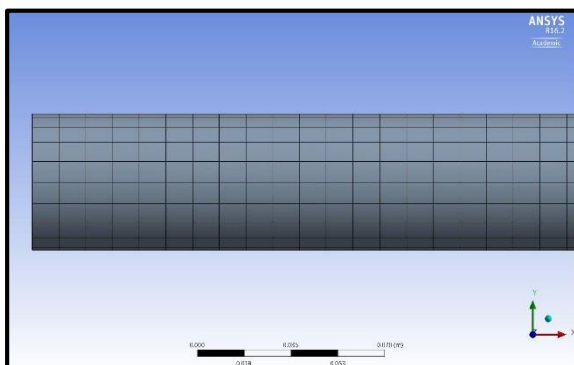

Figure 5.5 Mesh with 1 cm axial size
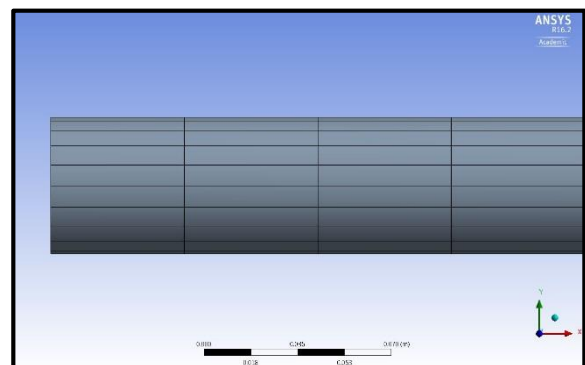
Figure 5.6 Mesh with 5 cm axial size
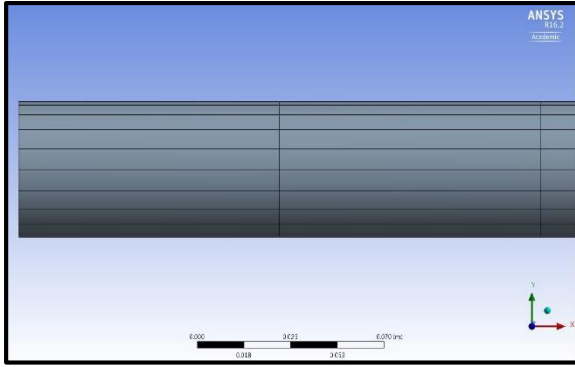
Figure 5.7 Mesh with 10 cm axial size
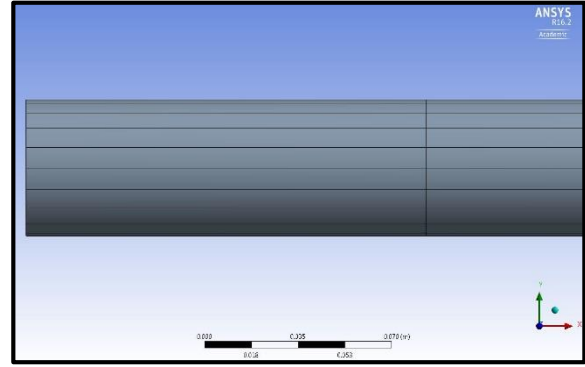
Figure 5.8 Mesh with 15 cm axial size
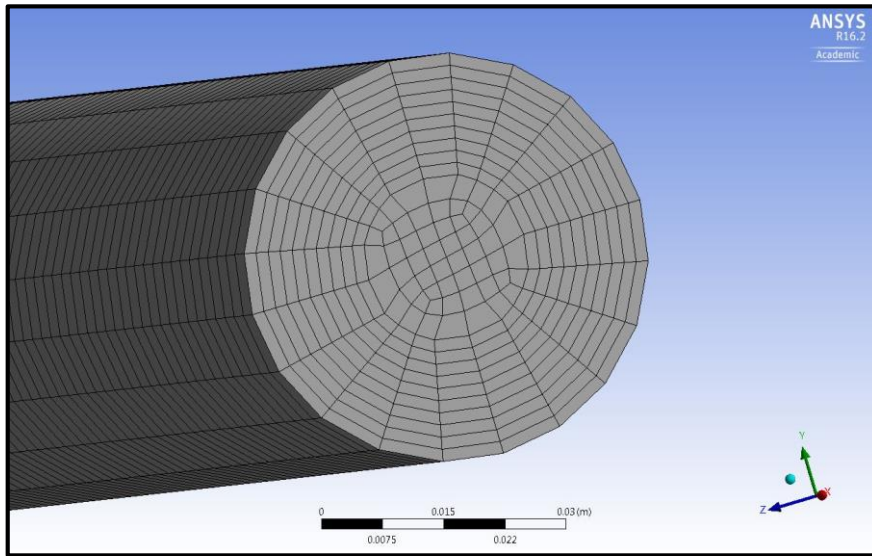
Figure 5.9 Cross-sectional mesh structure for the MTC simulations

5.4.3 Model setup

DPM model

The model setup of the DPM model requires separate settings for the continuous and discrete phases. Selection of some parameters requires a more detailed consideration while the rest parameters are more straightforward to choose. As such, the most important parameters are discussed in details and the other ones are shortly mentioned.

As for the fluid, the water flow is selected with default properties given by ANSYS Fluent. The flow is selected to be steady since the experiments are conducted at the steady conditions.

As for the DPM phase, sand material is created with the density of 2650 kg/m^3. The particle diameter has distribution over the range of 80-350 μm. In order to create such distribution, the Rosin-Rammler distribution function is used. The general calculation procedure can be found in **ANSYS Fluent User's Guide, 2015**. The resulting particle diameter distribution is shown in the Figure 5.10.
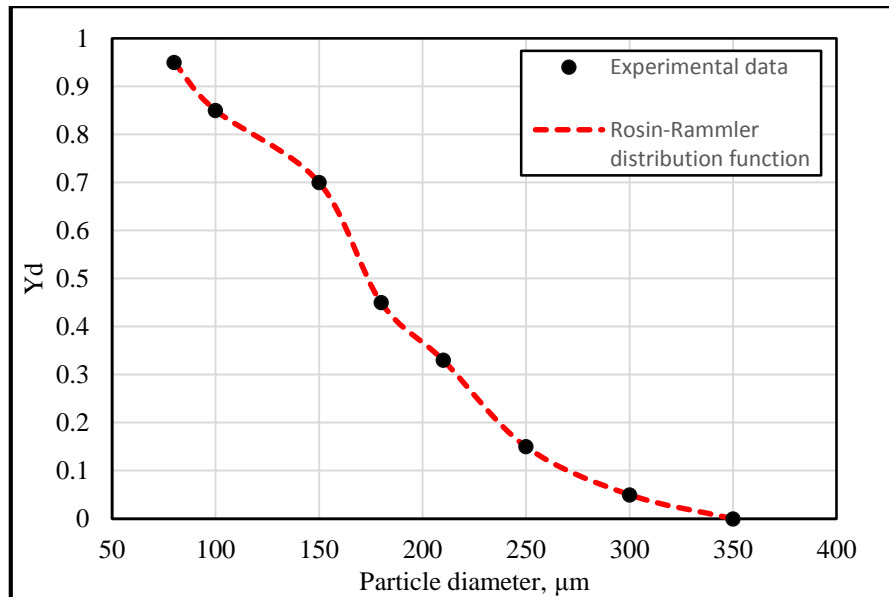
Figure 5.10 Particle diameter distribution for the DPM model

Y_d variable shows how much particles have the diameter greater than the corresponding diameter. For example, about 85% of particles by mass fraction have the diamter greater than 100 μm, 70% greater than 150 μm, etc. It can be said that the function has a very good fit with the experimental data. However, not the entire range of diameters used in the experiments is applied in the distribution function, but more than 90% (80-350 μm) is covered. In the Table 5.1, the phase properties are summarized.

Table 5.1 Phase properties for the MTC simulations

Phase properties	
Water	
Density, kg/m^3	998
Viscosity, kg/m.s	0.001003
Sand	
Density, kg/m^3	2650
Min. diameter, μm	80
Max. diameter, μm	350
Mean diameter, μm	200
Spread parameter	2.7531
Number of diameters	8

As for the DPM model settings, it is important to mention several features. First, interaction with the continuous phase is included in simulation. It is done due to the fact that it is important to capture the interaction between phases since it might have an influence on the particle suspension and deposition effects. 20 continuous phase iterations are performed for 1 DPM iteration. There is not any strict requirement for this parameter, and 20 iterations are selected as a compromise between the results accuracy and convergence behavior.

Steady tracking is used to track particles propagation through the flow domain. There is not any reason to perform unsteady particle tracking since the steady state solution is of interest in this study. As mentioned in Chapter 3, steady tracking option tracks the particles until they reach the final destination (outlet) or until the specified number of iterations are performed. In order to ensure that there are enough time steps to track the particles through the entire domain, from 25000 to 75000 time steps are specified depending on the particle velocity.

The length scale is selected to be 0.0025 m. This is one of the most important parameters because it affects the integration time step of the particle trajectory equations and the results accuracy. Such a length scale has been selected based on the rule of thumb that cell should be crossed by the particle within at least 2-3 particle steps in the finest mesh. (Bakker, Lecture 15 - Discrete Phase Modeling, 2002).

Stochastic model of turbulent dispersion is included in the particle trajectory calculations since in this case the turbulent dispersion might have a significant impact on particle lifting, especially at the boundary layer (ANSYS Fluent Support, 2016). Fifteen number of tries are used in order to capture the influence of the turbulence dispersion on the particle trajectories.

The virtual mass force is included in the simulation because at some locations, a single particle might move relatively faster than the water flow, for example, when the particle is suddenly getting suspended. To take into account such an acceleration affect, it is recommended to use the virtual mass force (ANSYS Fluent User's Guide, 2015; ANSYS Fluent Support, 2016).

Shaffman lift force which takes into account lifting effect due to shear is definitely needed to be included in the simulation because any lifting effects will impact on the critical velocity value. This force makes the model more realistic. The entire simulation setup can be seen in the Table 5.2.

Table 5.2 Model settings of the DPM model

Parameter	Model
Time integration	Steady
RANS model	k-ε, Realizable with dispersed properties
Wall treatment	Enhanced Wall Treatment
Gravity, m/s^2	9.81, negative y-direction
Interaction Interaction with continuous phase Number of continuous phase iterations per DPM iteration	ON 20
Particle tracking Mode Max. number of steps Length scale, m	Steady 25000-75000 0.0025
Physical models Shaffman lift force Virtual mass force Virtual mass factor Two-way turbulence coupling Pressure gradient force	ON ON 0.5 ON ON
Turbulent dispersion Stochastic tracking Number of tries Time scale constant	Discrete Random Walk Model 15 0.15

Eulerian model

The setup of the Eulerian model is much less complicated than in the plug case and all the models are selected based in the fact that the sand-water flow is dilute. As such, for example, the radial distribution function, solids pressure and frictional pressure are not important. The simulation setup can be seen in the Table 5.3.

The Simonin model for the turbulent dispersion is selected based on the fact that it is more suitable for dilute slurry flows (ANSYS Fluent User's Guide, 2015). Dispersed turbulent properties are selected based on the same reason. Moreover, the density ratio is 2.65 which is relatively higher than 1, as such the mixture properties are not recommended (ANSYS Fluent User's Guide, 2015). The Wen-Yu model is selected for the drag force because it is more suitable for dispersed flows than Syamlal and Gidaspow models.

In opposite to the plug case, the lift force is included. Lifting effect is important to consider in this case because of the low particle volume fraction. The Moraga model is the most suitable in case of dilute solid-liquid flows (ANSYS Fluent User's Guide, 2015).

Table 5.3 Eulerian Granular model setup for the dilute sand-water flows simulations

Parameter	Model/Value
Particle diameter, m	0.0002
RANS model	k-ε, Realizable with dispersed properties
Granular viscosity	Syamlal-O'Brien
Granular bulk viscosity	Lun et. al.
Angle of internal friction	30
Drag model	Wen-Yu
Lift force	Moraga
Turbulent dispersion	Simonin
Turbulent interaction	Simonin et al.
Restitution coefficient	0.9
Interfacial area	ia-symmetric
Specularity coefficient	0.01

5.4.4 Boundary conditions and solver settings

<u>DPM model</u>

The boundary conditions and solver settings are shown in the Table 5.4. Turbulent intensity changes according to the velocity change. Due to the limited amount of time for the project, sensitivity study between the 1st and 2nd order discretization schemes is not conducted and the simulations are run using the 2nd order discretization schemes for all the parameters with double precision to ensure high accuracy of the simulation results.

In the experiments, the mass and volume fractions at the inlet are specified. The DPM model in ANSYS Fluent allows specification of a mass flowrate only, as such, it is required to calculate the mass flowrate of the particle injections for all the cases. In order to maintain the same volume fraction for different velocities, mass flowrate must change according to the change of the velocity. The mass flowrate is calculated based on the following relation:

$$\rho_s\left[\frac{kg_s}{m_s^3}\right] \cdot C_v\left[\frac{m_s^3}{m_w^3}\right] \cdot U_w\left[\frac{m_w}{s}\right] \cdot A\left[m_w^2\right] = G_s\left[\frac{kg_s}{s}\right]$$

where:

ρ_s – sand density;

C_v – sand volume fraction given in the experiments;

U_w – water velocity;

A – pipe cross-sectional area and G_s – sand mass flowrate (discrete phase flowrate).

In the Table 5.5, calculated mass fractions for all the cases are shown.

Table 5.4 Boundary conditions, phase properties and solver settings for the DPM simulations

Boundary conditions	
Inlet Turbulent intensity,% Hydraulic diameter, m Water velocity, m/s Particle velocity, m/s	5.52 - 4-14 0.05 0.1 - 1 0
Outlet Turbulent intensity,% Hydraulic diameter, m Gauge pressure, Pa	5.52 - 4-14 0.05 0
Wall Water phase Discrete phase	No-slip Reflect
Solver settings	
Scheme	SIMPLE
Gradient	Least Squared Cell Based
Pressure	Second Order
Momentum	Second Order Upwind
Turbulent kinetic energy	Second Order Upwind
Turbulent dissipation rate	Second Order Upwind

Table 5.5 Sand mass flowrates for DPM model

Sand mass flowrate, kg/s					
	Sand volume fraction				
Water velocity, m/s	$1.61 \cdot 10^{-5}$	$5.38 \cdot 10^{-5}$	$1.08 \cdot 10^{-4}$	$2.15 \cdot 10^{-4}$	$5.38 \cdot 10^{-4}$
1	$8.37725 \cdot 10^{-5}$	$2.799 \cdot 10^{-4}$	$5.6195 \cdot 10^{-4}$	$1.119 \cdot 10^{-3}$	$2.799 \cdot 10^{-3}$
0.9	$7.53953 \cdot 10^{-5}$	$2.51942 \cdot 10^{-4}$	$5.0576 \cdot 10^{-4}$	$1.007 \cdot 10^{-3}$	$2.519 \cdot 10^{-3}$
0.8	$6.7018 \cdot 10^{-5}$	$2.23948 \cdot 10^{-4}$	$4.4956 \cdot 10^{-4}$	$8.95 \cdot 10^{-4}$	$2.239 \cdot 10^{-3}$
0.7	$5.86408 \cdot 10^{-5}$	$1.95955 \cdot 10^{-4}$	$3.9337 \cdot 10^{-4}$	$7.83 \cdot 10^{-4}$	$1.96 \cdot 10^{-3}$
0.6	$5.02635 \cdot 10^{-5}$	$1.67961 \cdot 10^{-4}$	$3.3717 \cdot 10^{-4}$	$6.71 \cdot 10^{-4}$	$1.68 \cdot 10^{-3}$
0.5	$4.18863 \cdot 10^{-5}$	$1.39968 \cdot 10^{-4}$	$2.8098 \cdot 10^{-4}$	$5.59 \cdot 10^{-4}$	$1.4 \cdot 10^{-3}$
0.4	$3.3509 \cdot 10^{-5}$	$1.11974 \cdot 10^{-4}$	$2.2478 \cdot 10^{-4}$	$4.47 \cdot 10^{-4}$	$1.12 \cdot 10^{-3}$
0.3	$2.51318 \cdot 10^{-5}$	$8.39807 \cdot 10^{-5}$	$1.6859 \cdot 10^{-4}$	$3.36 \cdot 10^{-4}$	$8.4 \cdot 10^{-4}$
0.2	$1.67545 \cdot 10^{-5}$	$5.59871 \cdot 10^{-5}$	$1.1239 \cdot 10^{-4}$	$2.24 \cdot 10^{-4}$	$5.6 \cdot 10^{-4}$
0.1	$8.37725 \cdot 10^{-6}$	$2.79936 \cdot 10^{-5}$	$5.6195 \cdot 10^{-5}$	$1.12 \cdot 10^{-4}$	$2.8 \cdot 10^{-4}$

Eulerian model

For the Eulerian model, the solver settings are identical as in the DPM model. The boundary conditions are similar except the fact that it is possible to specify the particle volume fraction at the inlet directly. The boundary conditions are shown below. Phase 1 and Phase 2 corresponds to water and sand respectively.

Table 5.6 Boundary conditions for Eulerian Granular model

Boundary conditions	
Inlet	
Turbulent intensity,%	5.52
Hydraulic diameter, m	0.05
Phase 1 velocity, m/s	0.1-1
Phase 2 velocity, m/s	0
Phase 2 fraction	0
Outlet	
Turbulent intensity,%	5.52
Hydraulic diameter, m	0.05
Gauge pressure, Pa	0
Wall	
Phase 1	No-slip
Phase 2	Specularity coefficient=0.01

5.4.5 Simulation result

Mesh and model selection

First, the results for the preliminary low velocity case are presented. In the Figures 5.11-5.18, on the left hand side the results of the DPM model are presented while the right hand side is occupied by the respective Eulerian Granular models results. The sand volume concentration in all the cases is $1.61 \cdot 10^{-5}$. The flow velocity is 0.1 m/s. The pictures are taken from the top side.
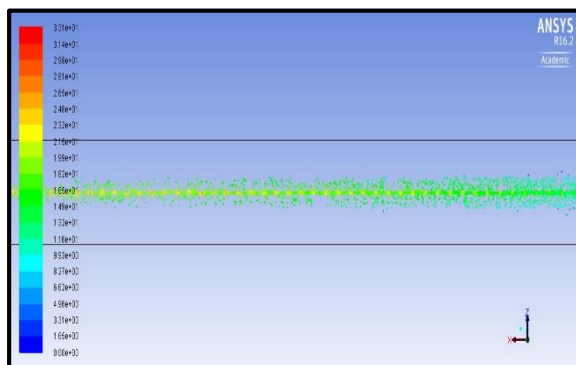

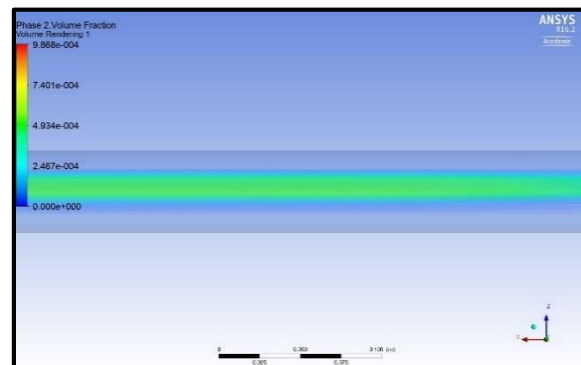Figure 5.11 DPM model, 1 cm mesh   Figure 5.12 Eulerian model, 1 cm mesh
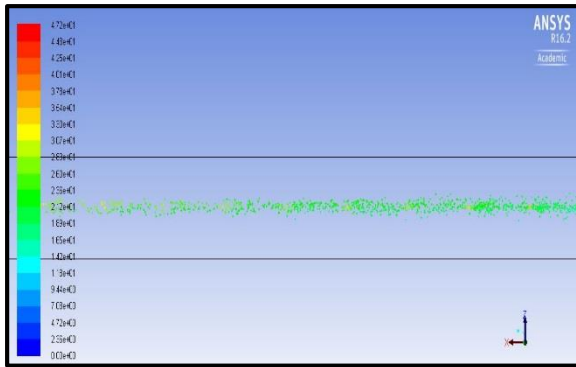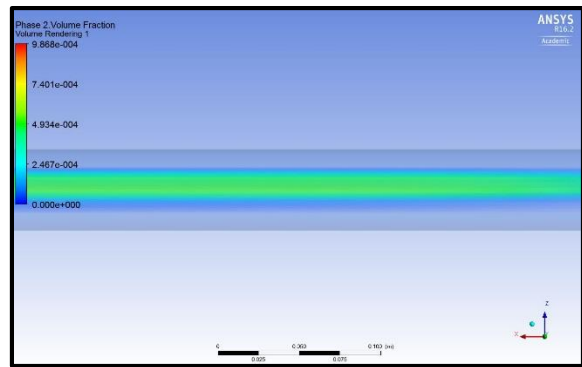
Figure 5.13 DPM model, 5 cm mesh

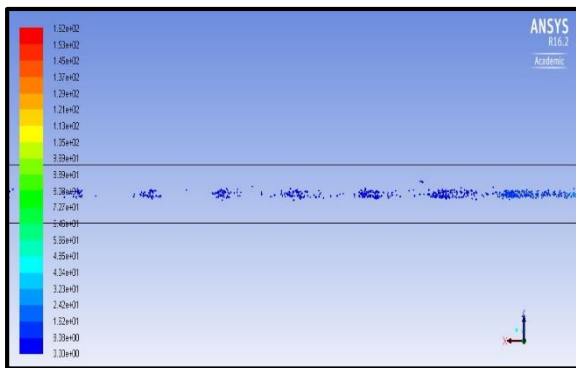Figure 5.14 Eulerian model, 5 cm mesh

Figure 5.15 DPM model, 10 cm mesh
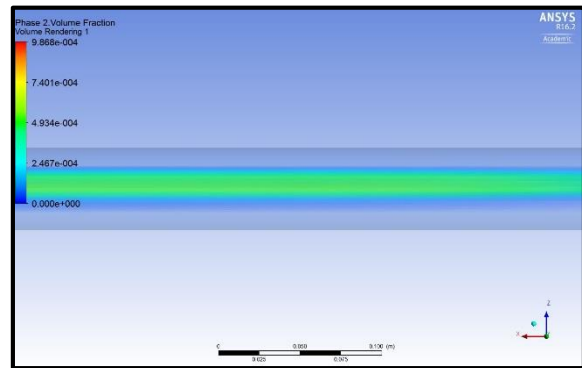
Figure 5.16 Eulerian model, 10 cm mesh
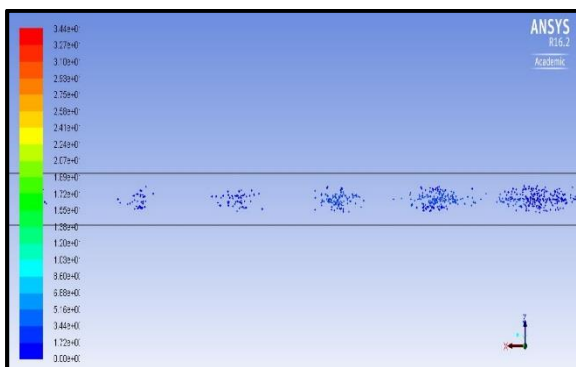
Figure 5.17 DPM model, 15 cm mesh
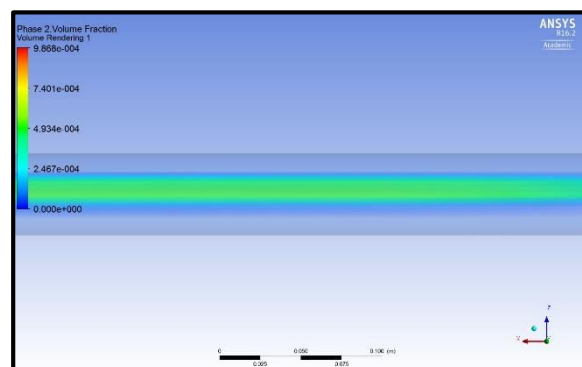
Figure 5.18 Eulerian model, 15 cm mesh

As it can be seen, there is not any difference between the different meshes of the Eulerian model. The big streak is clearly observed on the pipe bottom while the sand dunes are not reproduced. In opposite, the bed deposition in the DPM model changes with the mesh settings. In the mesh with 10 cm and 15 cm axial cell size the sand dunes are clearly observed on the pipe bottom. With the axial size decrease, the dunes disappear and represented by the streak formation.

From these results it is possible to conclude that the Eulerian model is inappropriate for this case because the dunes are not observed on the results. As such, it will be impossible to say at which velocity the MTC condition is obtained.

Another important conclusion is the fact that the simulations with larger mesh cells produce better results which is not a typical case in CFD simulations. The reason for such a behavior is difficult to explain and for a solid explanation, it is required to perform additional investigations which is hard to perform within this thesis due to time limitations. However, it cannot also be said that the results are incorrect because the visual observations are very close to the experimental results. Such results might be caused by the fact that some important physics is missing in the default DPM model. For instance, as it was shown by **Mezhericher et al., 2011**, implementation of particle-particle interaction in the DPM model might give more accurate simulation results even in dilute slurry flows. Another example of an important parameter which is not implemented in the default DPM model is the Shields parameter which plays an important role in the incipient movement of the solid particles (ANSYS Fluent Support, 2016). As such, if such parameters were included in the model, simulation results in the finer meshes were more accurate than the obtained ones.

If select between the obtained results, 10 cm case looks slightly more suitable due to the fact that the distance between the sand dunes is closer to the experimental observations. As it is observed on the video records and confirmed by the Yan Wei (the original experimentator), the distance between the dunes varies from 5 to 10 cm which is exactly the case with 10 cm axial size mesh. In addition, the dimensions of the dunes are also in the reasonable range of 3-5 cm which is also confirmed by the experimental observations. As such, the 10 cm mesh is selected for further evaluation.

Main simulation part

In this section the results of 50 simulation runs for all the particle velocities and volume fractions are presented. The simulations are performed in the 10 cm axial mesh and using the model setup described in the Table 5.2. In the Table 5.6, the summarized observations are presented as it is done on the experiments.

The observations can be validated with the instantaneous pictures of the particle concentration. The figures of two series of runs at the lowest and highest volume fractions are shown in the Appendix D. The results are also plotted for the direct comparison with other research, experimental and OLGA results and shown in the Figure 5.17.

Table 5.7 Simulation results of the MTC condition in dilute slurry flows

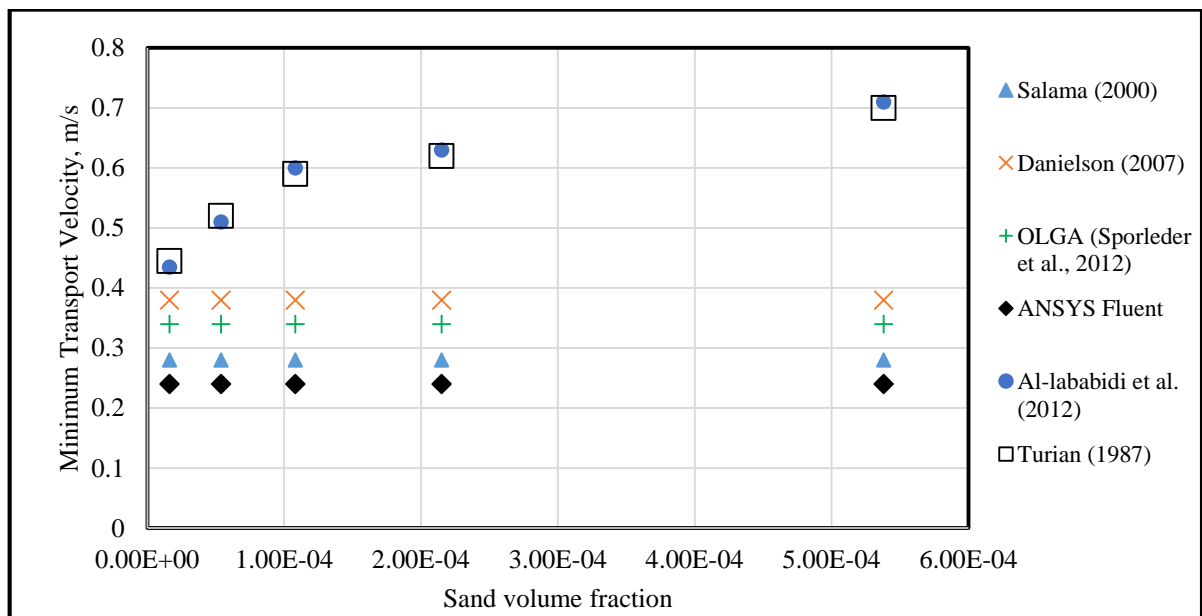| Water velocity, m/s	Sand volume fraction				
	$1.61 \cdot 10^{-5}$	$5.38 \cdot 10^{-5}$	$1.08 \cdot 10^{-4}$	$2.15 \cdot 10^{-4}$	$5.38 \cdot 10^{-4}$
1	Few sand streaks observed on the bottom	Few sand streaks observed on the bottom	Few sand streaks observed on the bottom	Few sand streaks observed on the bottom	Few sand streaks observed on the bottom
0.9	Few sand streaks observed on the bottom	Few sand streaks observed on the bottom	Few sand streaks observed on the bottom	Few sand streaks observed on the bottom	Few sand streaks observed on the bottom
0.8	More sand streaks observed on the bottom	More sand streaks observed on the bottom	More sand streaks observed on the bottom	More sand streaks observed on the bottom	More sand streaks observed on the bottom
0.7	More sand streaks observed on the bottom	More sand streaks observed on the bottom	More sand streaks observed on the bottom	More sand streaks observed on the bottom	More sand streaks observed on the bottom
0.6	More sand streaks observed on the bottom	More sand streaks observed on the bottom	More sand streaks observed on the bottom	More sand streaks observed on the bottom	More sand streaks observed on the bottom
0.5	Concentration highest in streaks	Concentration highest in streaks	Concentration highest in streaks	Concentration highest in streaks	Concentration highest in streaks
0.4	Concentration highest in streaks	Concentration highest in streaks	Concentration highest in streaks	Concentration highest in streaks	Concentration highest in streaks
0.3	Concentration highest in streaks	Concentration highest in streaks	Concentration highest in streaks	Concentration highest in streaks	Concentration highest in streaks
0.2	Scouring sand dunes formation	Scouring sand dunes formation	Scouring sand dunes formation	Scouring sand dunes formation	Scouring sand dunes formation
0.1	Developed slowly moving dunes	Developed slowly moving dunes	Developed slowly moving dunes	Developed slowly moving dunes	Developed slowly moving dunes

Figure 5.19 Comparison of the MTC in sand-water flows

As it is possible to see from the figures and the table, the critical velocity (or MTC) is independent on the particle volume fraction in ANSYS Fluent. Moreover, the value of the critical velocity is underestimated by ANSYS Fluent. For all the fractions, the critical velocity is found to be in the range of 0.2-0.3 m/s.

The reasons for the underestimation of the critical velocity value might be the same as for the difference between the fine and coarse mesh, i.e. missing of important physics in the default DPM model. There was an attempt to include DEM collision model which would simulate the particle-particle interaction, but all the attempts have been unfortunate. The model is indeed difficult to use and a few source materials are available regarding the usage of the model. As such, the DEM collision model is not included in the simulation. If the model would be included, the results might be slightly different and be closer to the experimental observations, because the model would be more realistic.

5.4.6 Conclusions of the MTC study

It can be concluded the Eulerian Granular model is not able to predict the dunes formation, as such the evaluation of minimum transport conditions in slurry flows is hardly achievable. In opposite, the DPM model in ANSYS Fluent is capable to reproduce the flow regimes of the slurry flows, specifically the dunes formations on the pipe bottom can be successfully simulated. However, the obtained results require more investigations because the better results are obtained for the cases with coarser mesh which is not typical for CFD studies. Specifically, additional models can be included in the simulation which might improve the accuracy of the results, specifically particle-particle interaction and Shields parameter.

If the default DPM model is used within the coarse mesh, the predicted critical velocity value for dilute sand-water flows are underestimated in comparison with the experimental results. Moreover, the critical velocity is obtained to be independent on the sand volume fraction which is not the same as in the experiments.

Chapter 6
Conclusions and recommendations

6.1 Conclusions

<u>Particle plug propagation</u>

ANSYS Fluent demonstrated strong capabilities in predicting of dynamic behavior of the propagating particle plug in inclined pipes. The detailed model selection has been conducted, so that it might simplify the selection process for further similar research works. ANSYS Fluent gives a possibility to analyze the structure of the particle plug in a clear way. The simulations show that it is possible to identify the dispersed front, transition zone, main plug body and the tail of the plug in an accurate way, so that it can be measured and visualized in the post-processing software.

It is demonstrated that the grid with y^+_w=19 and /or with the first layer thickness of 1.5 particle diameter predicts the flow behavior in the best way, so that all the plug regions are clearly recognizable as well as the particle volume fraction measurements fits the experimental data in a good qualitative way. Such observations are validated for 2D and 3D models.

It is shown that the 2nd order discretization scheme is essential to use for the propagating particle plug if the accuracy of the simulations is of interest. In opposite, there is a small difference between different models for radial distribution function and solids pressure, so that the minor attention might be paid for these parameters in the further research works. Enhanced Wall Treatment is another essential option which helps to reproduce accurate results while the wall functions are not applicable for the boundary layer resolution.

It is demonstrated that using the extracted CFD data, it is possible to develop a 1D model of the particle propagating plug with a reasonable accuracy of the results. The proposed function for the slip distribution coefficient is short, easy to use and adjust for a specific case of solid

particles transportation. This function can be potentially used in the further development of the 1D multiphase dynamic simulators such as OLGA.

MTC condition study

In opposite to the superior capabilities in predicting the particle plug behavior, the Eulerian Granular model does not perform well in evaluation of the minimum transport conditions of the sand-water flows. The model is not able to predict the sand dunes formation on the pipe bottom and produces the layer bed formation instead. Based on such simulation results, it is not possible to identify the minimum transport conditions of the slurry flows, at least based on the definition used in this thesis work.

The Discrete Phase Model (DPM) shows reasonable capabilities in predicting the sand dunes formation at low water velocities in horizontal slurry pipe flows which gives an opportunity to predict the minimum transport conditions. However, the obtained results require more investigations due to the fact that better results are obtained in coarser mesh which is not usual in CFD simulations. An example for an additional study can be including missing physics in the default DPM model, for example, particle-particle interaction and Shields parameter.

If the default DPM model is used, the predicted value of the critical velocity is underestimated in comparison with the experimental observations. Moreover, the value does not depend on the sand volume fraction which is not the same as in the experiments. As such, the DPM model in ANSYS Fluent produces the results which are similar to the OLGA simulations.

As one of the goals of the project was to suggest CFD techniques, specifically ANSYS Fluent software, for liquid-solid particles flow modelling. The two cases studied in this Master's thesis cover a wide range of particle volume fractions from dilute to packed particle flows. Generally, it can be said that the CFD techniques give an opportunity to study particle flows in details with a high level of accuracy. It can be said that the biggest part of the simulation results have a good fit with the experimental results even though some simulation cases require more investigations.

6.2 Recommendations

Particle plug propagation

Since the simulated case is a complex flow phenomenon, there is still a gap for improvements and further investigations. One of the evident potential investigations might be sensitivity study

regarding the exact value of the specularity coefficient. The specularity coefficient might have an influence on the results, for example, in the dimensions of the particle dispersed region, wall depletion and transition zones. Since such a sensitivity study is very time consuming, it has not been conducted in this research work, but it potentially could improve the overall simulation results and its accuracy.

The second gap for improvements is the developing a CFD model which does not depend on the first layer thickness and y^+_w value. A detailed study has been conducted in this respect in the research work, however, the independent solution has not been obtained. Even though the good match between the experimental and simulation data has been obtained and general recommendations regarding the first layer thickness have been provided, it could be a great result if one obtains the solution, which is not dependent on the first layer thickness size. It is possible that it is very hard to achieve such a result in this particular case because the independent solution might come when the first layer thickness is an order of magnitude higher than the particle diameter. However, such a solution might be worthless since the size of the first layer thickness does not allow to capture all the important features of the flow, for example, the transition zone. Keeping in mind such suggestions, it could be a worth trial to conduct such as study. Since it is also a very time consuming work, it is not done in this thesis.

The proposed model for the slip distribution coefficient can be further improved. For example, it could be very useful to have the dependency of the coefficients A, B and D on the particle properties such as average fraction, diameter and density. In such a way, it would be possible to make the function for the distribution coefficient to be more general and applicable for a various range of dynamic flow situations. In order to achieve it, one has to test different particle types in pipe flows with different pipe inclinations with a further validation of the results with the experimental data.

MTC study

The DPM simulations of the MTC study might be further improved if additional models are included in the model setup. An example of the additional model can be the Shields parameter. This parameter plays an important role in initiation of the particle movement in the flow and can be included as a User-Defined Function. Another example is including particle-particle interaction. Including such important factors, one might improve the prediction of the critical flow velocity and make it closer to the experimental observations.

References

Ahmadi, G., & Ma, D. (1990). A Thermodynamical Formulation for Dispersed Multiphase Turbulent Flows". *Multiphase Flow, 16*(2), 323-340.

Al-lababidi, S., Yan, W., & Yeung, H. (2012). Sand Transportations and Deposition Characteristics in Multiphase Flows in Pipelines. *Journal of Energy Resources Technology, 134*. doi:10.1115/1.4006433

Andersson, H. I. (2015). *Lectures of the course TEP4112 "Turbulent Flows".* Norwegian University of Science and Technology (NTNU), Energy and Process, Trondheim, Norway.

ANSYS Fluent Lectures. (2015). *Turbulence modelling.*

ANSYS Fluent Support. (2016). Retrieved from https://support.ansys.com/

ANSYS Fluent User's Guide. (2015). *Release 16.2.* ANSYS.

Arastoopour, H., & Ibdir, H. (2005). Modeling of multi-type particle flow using kinetic approach. *AICHE Journal.*

Armstrong, L. M., Luo, K. H., & Gu, S. (2010). Two-Dimensional and Three-Dimentional Computational Studies of Hydrodynamics in the Transition from Bubbling to Circulating Fludized Bed. *Chemical Engineering, 160*, 239-248.

Bakker, A. (2002). *Lecture 10 - Turbulence Models, Applied Computational Fluid Dynamics.* Dartmouth College. Retrieved from http://www.bakker.org

Bakker, A. (2002). *Lecture 11 – Boundary Layers and.* Dartmouth College. Retrieved from http://www.bakker.org

Bakker, A. (2002). *Lecture 15 - Discrete Phase Modeling.* Lectures. Retrieved May 1, 2016, from http://www.bakker.org/dartmouth06/engs150/15-dpm.pdf

Bakker, A. (2002). *Lecture 5 - Solutions Methods.* Retrieved March 10, 2016, from http://www.bakker.org

Bakshi, A., Altantzis, C., Bates, R., & Ghoniem, A. F. (2014). *Estimating the specularity coefficient for the accurate simulation of fluidized beds of different surface-to-volume ratios.* Massachusetts Institute of Technology, Mechanical Engineering. Retrieved March 15, 2016, from https://mfix.netl.doe.gov

Bikmukhametov, T. I. (2015). *Simulation of dynamic liquid-particle pipe flows.* Norwegian University of Science and Technology, Energy and Process , Trondheim.

Brennen, C. E. (2005). *Fundumentals of Multiphase Flows.* Cambridge University Press.

Brown, N. P. (1988). Three scale-up techniques for stabilized coal-water slurries. *11th International Conference on Hydraulic Transport of Sloids in Pipes*, (pp. 267-283).

Burns, A. D., Frank, T., Hamill, I., & Shi, J. M. (2004). The Favre Averaged Drag Model for Turbulent Dispersion in Eulerian Multiphase Flows. *5th International Conference on Multiphase Flow.* Yokohama, Japan. Retrieved March 12, 2016, from

http://citeseerx.ist.psu.edu/viewdoc/download?doi=10.1.1.453.2254&rep=rep1&type=pdf

Chen, L., Duan, Y., Pu, W., & Zhao, C. (2009). CFD simulation of coal-water slurry flowing in horizontal pipelines. *Korean Journal of Chemical Engineering, 26*(4), 1144-1154. doi:10.1007/s11814-009-0190-y

Cloete, S., Amini, S., & Johansen, S. T. (2011). A fine resolution parametric study on the numerical simulation of gas-solid flows in a periodic riser section. *Powder Technology, 205*, 103-111.

Danielson, T. J. (2007). Sand Transport Modeling in Multiphase Pipelines. *Offshore Technology Conference.*

Ekambara, K., Sanders, R. S., Nandakumar, K., & Masllyah, J. H. (2009). Hydrodynamic Simulation of Horizontal Slurry Pipeline Flow Using ANSYS-CFX. *Industrial & Engineering Chemistry, 48*, 8159–8171. Retrieved March 22, 2016, from http://pubs.acs.org/doi/abs/10.1021/ie801505z

Gidaspow, D., Bezburuah, R., & Ding, J. (1992). Hydrodynamics of Circulating Fluidized Beds, Kinetic Theory Approach. *7th Engineering Foundation Conference on Fluidization.*, (pp. 75–82.).

Hewitt, G. F. (2010). *Thermopedia*. doi:10.1615/AtoZ.m.multiphase_flow

Jin, B. S., Wang, X. F., Zhong, W. Q., Tao, H., Ren, B., & Xiao, R. (2010). Modeling on High-Flux Circulating Fluidized Bed with Geldart Group B Particles by Kinetic Theory of Granular Flow. *Energy Fuels, 24*, 3159−3172.

Johnson, P. C., & Jackson, R. (1987). Frictional-Collisional Constitutive Relations for Granular Materials, with Application to Plane Shearing. *Fluid Mechanics, 176*, 67-93.

Kong, L., Zhang, C., & Zhu, J. (2014). Evaluation of the Effect of Wall Boundary Conditions on Numerical Simulations of Circulating Fludized Bed. *Particuology, 13*, 114-123.

Kushal, P. (2014). *An Investigation of Solid-Liquid Flow Distribution Through Slurry Pipeline.* Master's Thesis, THAPAR UNIVERSITY, MECHANICAL ENGINEERING, Patiala, India. Retrieved February 5, 2016, from http://dspace.thapar.edu

Lahiri, S. K., & Ghanta, K. C. (2010). SLURRY FLOW MODELLING BY CFD. *Chemical Industry & Chemical Engineering, 16*(4), 295−308. doi:10.2298/CICEQ091030034L

Lun, C. K., Savage, S. B., Jeffrey, D. J., & Chepurniy, N. (1984). Kinetic Theories for Granular Flow: Inelastic Particles in Couette Flow and Slightly Inelastic Particles in a General Flow Field. *Fluid Mechanics, 140*, 223–256.

Mezhericher, M., Brosh, T., & Levy, A. (2011). Modeling of Particle Pneumatic Conveying Using DEM and DPM Methods. *Particulate Science and Technology, 29*, 197–208.

MgGlinchey, D., Cowell, A., & Crowe, R. (2012). CFD investigation of dense phase pneumatic conveying at a pipeline enlargement. *Particuology, 10*(2), 176-183. Retrieved March 5, 2016, from http://www.sciencedirect.com/science/article/pii/S1674200112000326

Nabil, T., El-Sawaf, I., & El-Nahhas, K. (2013). Computational fluid dynamics simulation of the solid-liquid slurry flow in a pipeline. *17th International Water Technology Conference.* Istanbul, Turkey. Retrieved February 7, 2016, from http://iwtc.info/wp-content/uploads/2013/11/137.pdf

Neil, R. I. (1988). *The rheology and behavior of high concentration mineral slurries.* Master's Thesis, Unversity of Cape Town, Civil Engineering Department, Cape Town, South Africa. Retrieved March 15, 2016, from http://open.uct.ac.za/handle/11427/8314

Nott, P. R., & Brady, J. F. (1994). Pressure-driven flow of suspensions : simulation and theory. *Fluid Mechanics, 275*, 157-199. Retrieved March 28, 2016, from https://core.ac.uk/download/files/200/4878925.pdf

Paterson, A. J. (1991). *The hydraulic transport of high concentration stabilized flow full plant mineral tailings.* PhD Thesis, Uni versi ty of Cape Town, Civil Engineering, Cape Town, South Africa. Retrieved March 30, 2016, from http://open.uct.ac.za/handle/11427/5011

Polanský, J. (2014). *Experimental investigation of slurry flow.* Summer internship report, University of Leeds,. Retrieved from http://home.zcu.cz/~rcermak/opvk_htt/VY_02_05.pdf,

Quek, T. Y., Wang, C., & Ray, B. (2005). Dilute Gas-Solid Flows in Horizontal and Vertical Bends. *Ind. Eng. Chem., 44*, 2301-2315.

Reynolds, O. (1895). On the Dynamical Theory of Incompressible Viscous Fluids and the Determination of the Criterion. *Philosophical Transactions of the Royal Society of London, 186*, 123-164. Retrieved May 11, 2016, from http://rsta.royalsocietypublishing.org/content/roypta/186/123.full.pdf

Salama, M. M. (2000). Sand Production Management. *Energy Resour. Technol, 122*, 29–33. Retrieved May 22, 2016, from http://energyresources.asmedigitalcollection.asme.org/article.aspx?articleid=1413890

Schaeffer, D. G. (1987). Instability in the Evolution Equations Describing Incompressible Granular Flow. *Differential Equations, 66*, 19-50.

Shabani, M. M. (2012). *Multiphase Flow with Gas Hydrate Particles.* PhD dissertation, Norwegioan University of Science and Technology (NTNU), Energy and Process, Trondheim.

Smoldyrev, A. E., & Safonov, Y. K. (1979). *Pipeline transport of concentrated slurries.*

Sporleder, F., Lutro, H., & Xu, Z. G. (2014). *Transport of Particles in Transient Multiphase Systems.* Presentation, SPT Technology Center.

Syamlal, M., Rogers, W., & O'Brien, T. J. (1993). *MFIX Documentation Theroy Guide.* Morgantown Energy Technology Center, U.S. Department of Energy , Morgantown, West Virginia. Retrieved March 15, 2016, from https://mfix.netl.doe.gov/documentation/Theory.pdf

Talmon, A. M., & van Rhee, C. (2011). Test set-up for irregular vertical hydraulic transport in deep ocean mining. *30th International Conference on Ocean, Offshore and Artic Engineering.* Rotterdam, the Netherlands.

Tebowei, R., Hossain, M., Oluyemi, G., & Islam, S. (2015). Modelling effects of particle size and pipe gradient on sand transport in multiphase pipes. *Transactions on Engineering Sciences, 89*, 323-334.

Turian, R. M., Hsu, F. L., & Ma, T. W. (1987). Estimation of Critical Velocity in Pipeline Flow of Slurries. *Powder Technology, 51*, 35-47.

Wang, X. F., Jin, B., Zhong, W. Q., & Xiao, R. (2010). Modelling on the Hydrodynamics of a High-Flux Circulating Fludized Bed with Geldart Group A Particles by Kinetic Theory of Granular Flow. *Energy Fuels, 24*, 1242−1259.

Yam, K. S. (2012). *Physical and Computation Modelling of Turbidity Currents: The Role of Turbulence-Particles Interactions and Interfacial Forces.* University of Leeds, Earth and Environment. Retrieved March 5, 2016

Yan, W. (2010). *Sand Transport in Multiphase Pipelines.* PhD Thesis, Cranfild University, Department of Process and Systems Engineering, Cranfild. Retrieved April 2016, 20, from https://dspace.lib.cranfield.ac.uk/handle/1826/8074

Zhong, Y., Ding, T., Zhu, L., & Zhao, Y. (2016). A Specularity Coefficient Model and Its Application to Dense Particle Flow Simulations. *Industrial & Engineering Chemistry, 55*, 1439−1448. Retrieved March 20, 2016, from http://pubs.acs.org/doi/abs/10.1021/acs.iecr.5b03792

Appendices

Appendix A
Experimental rigs and data

Particle plug propagation

A schematic setup of the experimental rig used for the propagating particle plug is shown in the Figure A-1. In the downstream pipe, conductance rings are installed which measure conductivity of the slurry flow. Afterwards, conductivity is converted to particle volume fraction.
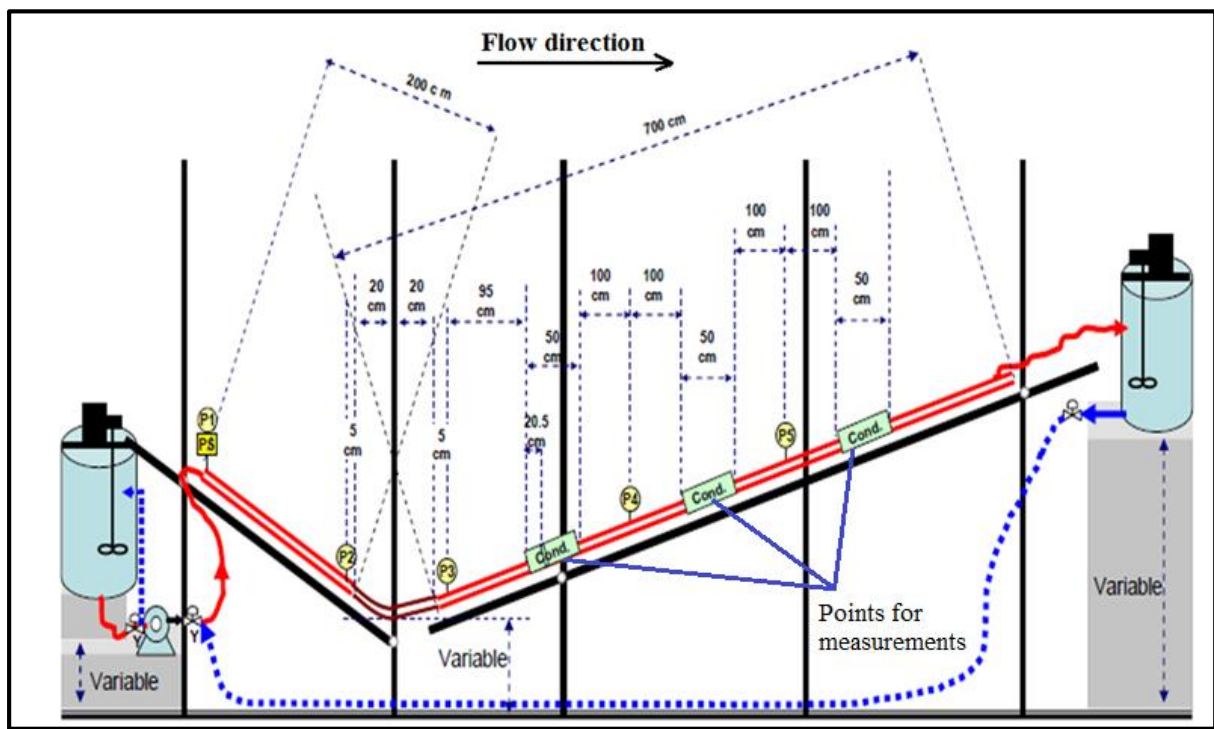

Figure A-1 A schematic drawing of the experimental setup (Shabani, 2012).

MTC condition

The experimental rig used for the MTC study is shown in the Figure A-2. Important relevant dimensions of the rig:

- length of the long horizontal pipe - 17 m;
- length of the viewing section - 1.2 m;
- pipe diameter – 0.05 m
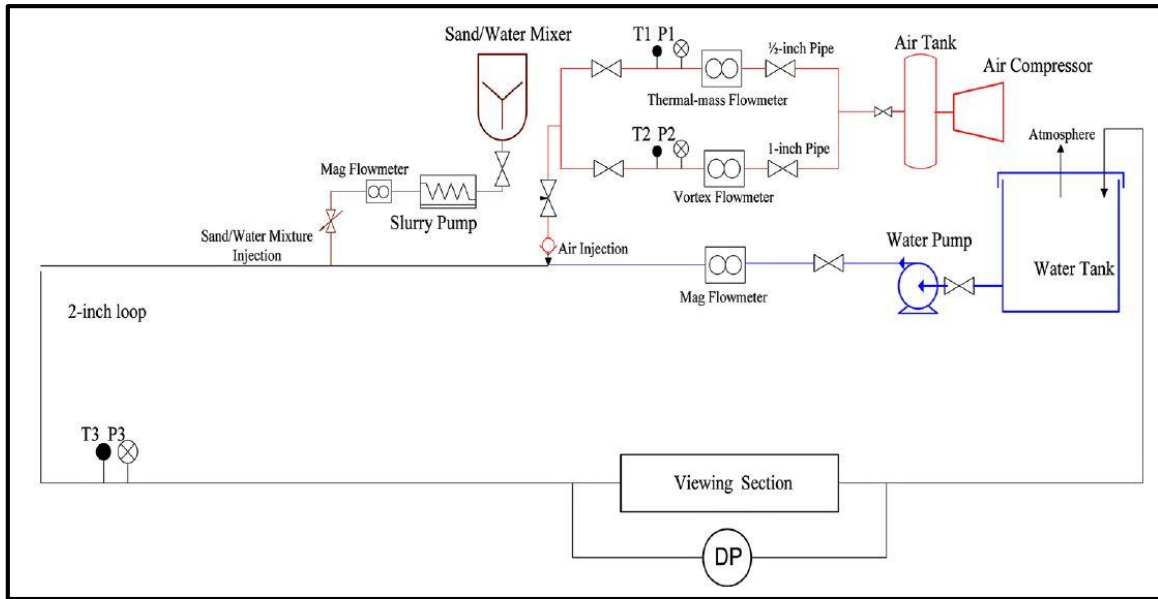
Figure A-2 Two-phase flow facility (Al-lababidi et al., 2012)

Since in this thesis only water-sand flow is considered, the air system is not described in details. As for the water system, the centrifugal pump has the maximum capacity of 40 m³/h and maximum discharge pressure of 5 bar.

The sand is fed from a cylindrical vessel which has a diameter of 0.29 m and 0.5 m of height. Inside the cylinder there is an axial flow impeller with a diameter of 0.2m which mixes sand with water. The mixed fluid is supplied to the flow loop line by a slurry centrifugal pump which has a capacity of 0.5 m³/h. (Al-lababidi et al., 2012)

Sand particles have density of 2650 kg/m³. The particle diameter varies significantly as shown in the Figure A-3.
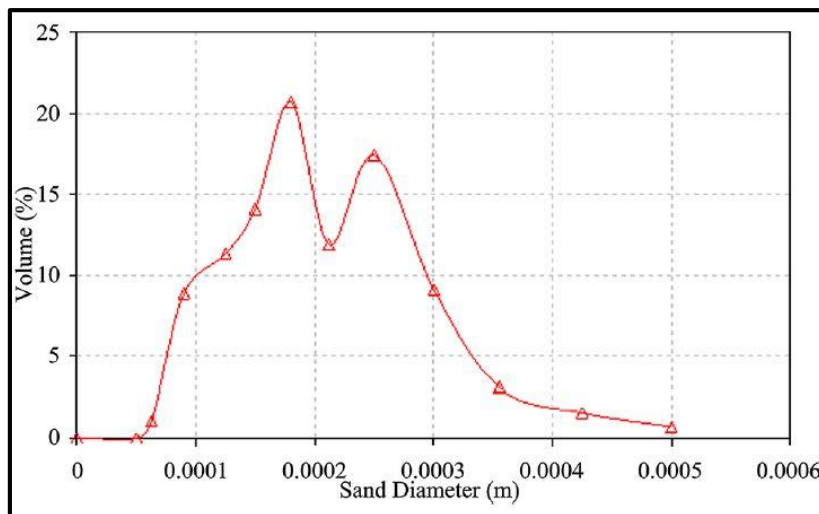
Figure A-3 Sand particle diameter distribution

Appendix B
Mesh statistics

Eulerian Granular Model

Phase 1. Preliminary model

Table B-1 Mesh statistics for the case with y^+_w =37.5.

Parameter	Value
Number of nodes	7026
Number of elements	6603
First layer thickness	0.001065 m
y^+_w	37.5
Max. aspect ratio	1.245

Table B-2 Mesh statistics of the grid with y^+_w =25.

Parameter	Value
Number of nodes	8477
Number of elements	7992
First layer thickness	0.00071 m
y^+_w	25
Max. aspect ratio	1.6393

Table B-3 Mesh statistics of the grid with y^+_w =19.

Parameter	Value
Number of nodes	9342
Number of elements	9342
First layer thickness	0.00053 m
y^+_w	19
Max. aspect ratio	1.9734

Table B-4 Mesh statistics of the grid with $y^+_w = 12.5$.

Parameter	Value
Number of nodes	10348
Number of elements	9860
First layer thickness	0.000355 m
y^+_w	12.5
Max. aspect ratio	2.8317

Phase 2. 2D simulations of the 53 cm plug

Table B-5 Mesh statistics of the grid with $y^+_w = 12.5$.

Parameter	Value
Number of nodes	34345
Number of elements	32920
First layer thickness	0.000355 m
y^+_w	12.5
Max. aspect ratio	2.4163

Table B-6 Mesh statistics for the case with EWT, $y^+_w = 19$.

Parameter	Value
Number of nodes	21589
Number of elements	20446
First layer thickness	0.00053 m
y^+_w	19
Max. aspect ratio	1.9811

Table B-7 Mesh statistics for the case with EWT, $y^+_w = 25$.

Parameter	Value
Number of nodes	20325
Number of elements	19184
First layer thickness	0.00071 m
y^+_w	25
Max. aspect ratio	1.8234

DPM Model

Table B-8 Mesh statistics for the DPM model case with axial cell size of 1 cm.

Parameter	Value
Number of nodes	77568
Number of elements	73990
First layer thickness	0.00075 m
Max. aspect ratio	7.0853

Table B-9 Mesh statistics for the DPM model case with axial cell size of 5 cm.

Parameter	Value
Number of nodes	17152
Number of elements	16170
First layer thickness	0.00075 m
Max. aspect ratio	35.591

Table B-10 Mesh statistics for the DPM model case with axial cell size of 10 cm.

Parameter	Value
Number of nodes	9728
Number of elements	9065
First layer thickness	0.00075 m
Max. aspect ratio	69.967

Table B-11 Mesh statistics for the DPM model case with axial cell size of 15 cm.

Parameter	Value
Number of nodes	7168
Number of elements	6615
First layer thickness	0.00075 m
Max. aspect ratio	104.91

Appendix C
MATLAB code for the propagating particle plug

```matlab
%------------input data------------------
NJ=2500; %Number of steps
tend=4.5;  %Simulation time
L = 2.5; %Domain length
dx=L/(NJ-1);  %Coordinate step
x=[0:dx:L];   %Coordinate vector
dt=0.001;        %time step
t=[dt:dt:tend];
k=round(tend/dt);
 %Boundary conditions
alfa = zeros(1,NJ); %b.c. for particle fraction
up = zeros(1,NJ);    %b.c. for particle velocity
alfa_ = zeros(1,NJ); %b.c for particle fraction of the following time step
up_ = zeros(1,NJ);    %b.c for particle velocity of the following time step
alfa_matrix = zeros(k,NJ); %b.c. for matrix of particle fraction
up_matrix = zeros(k,NJ);    %b.c. for matrix of particle velocity
um = 0.66;                  %Mixture velocity

%Additional boundary conditions for partilce fraction. It specifies where
%the particles are located at the beginning of the simulation
for i = 2:530
    alfa(i) = 0.63;
    up(i) = um;
    alfa_matrix(1,i) = 0.63;
    up_matrix(1,i) = um;
end
 %Calculating procedure
for j = 2:k
        up_(1) = 0;
    for i = 2:(NJ-1)
        alfa_(i+1) = alfa(i+1) + dt/dx*(alfa(i)*up(i) -
alfa(i+1)*up(i+1));% mass conservation equation

        if alfa_(i+1) == 0
            up_(i+1) = 0;
            
        elseif alfa_(i+1) <= 0.57
            C = 1.22183/(1+0.068*exp(1.873315*alfa_(i+1))); %Slip
distribution coefficient function
            up_(i+1) = C*um; %Slip relation

        else
            up_(i+1) = um;

            end;
    end

    for i = 1:NJ
        alfa_matrix (j,i) = alfa_(i);
        up_matrix (j,i) = up_(i);
        alfa(i) = alfa_(i);
        up(i) = up_(i);
    end

end;
```

Appendix D
MTC simulation results using DPM model

Some pictures show the pipe from the side view, another part from the top view depending on the velocities. At low velocities the top views are more representable because it gives an opportunity to identify the sand dunes and its transition to streaks. As the velocity increases, it is better to use the side view in order to see the difference in the amount of suspended particles. The first numbers in the figures' names are the particle volume fractions, the second numbers represent the flow velocity.
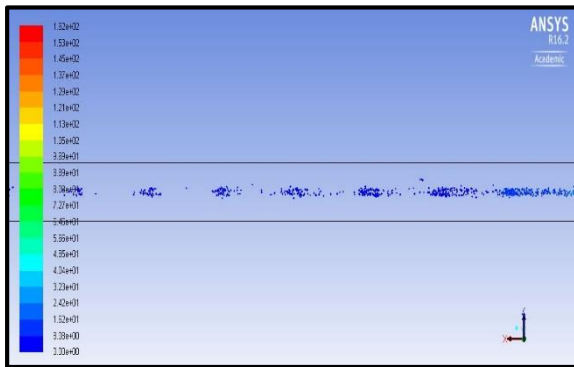
Figure D-1 $1.61 \cdot 10^{-5}$, 0.1 m/s (top view)
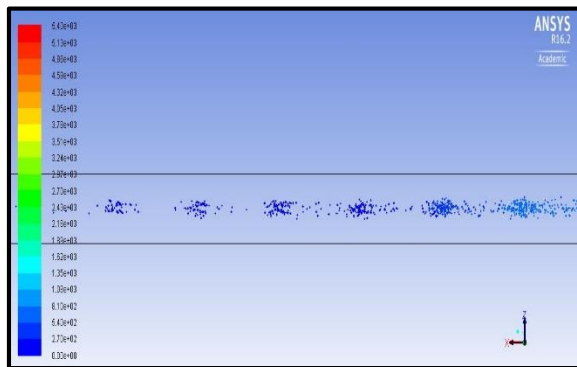
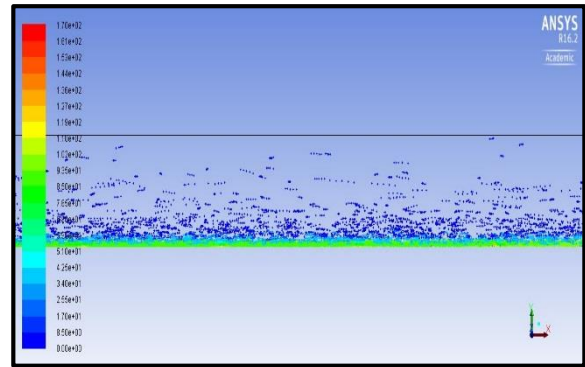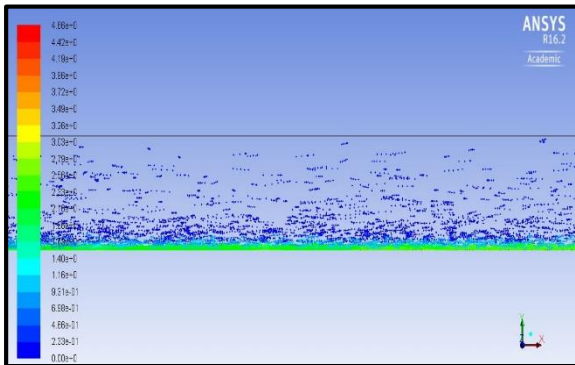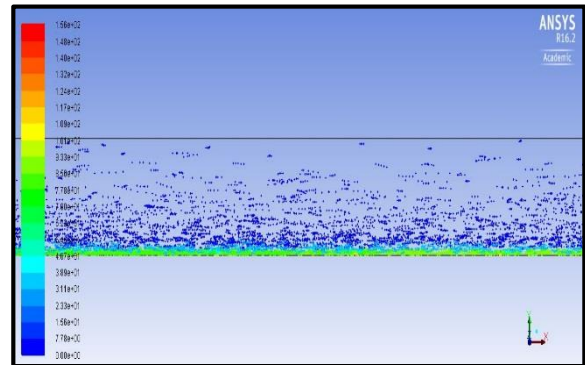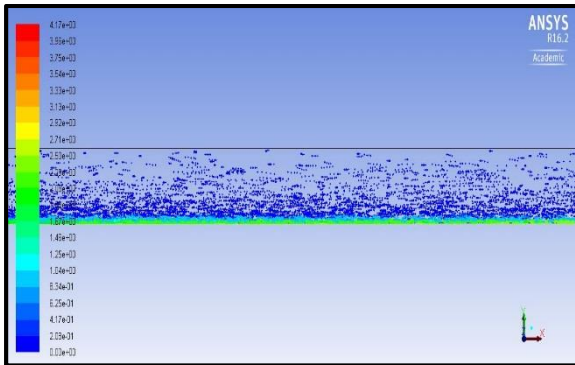Figure D-2 $5.38 \cdot 10^{-4}$, 0.1 m/s (top view)
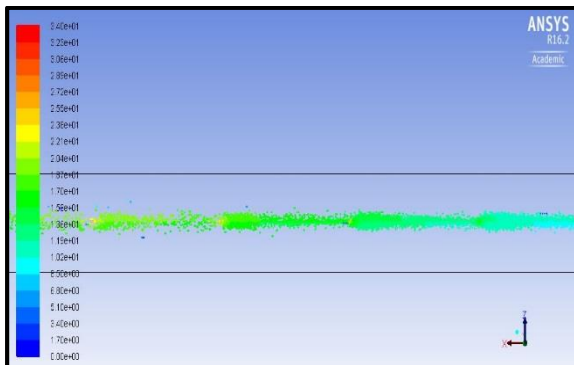
Figure D-3 $1.61 \cdot 10^{-5}$, 0.2 m/s (top view)
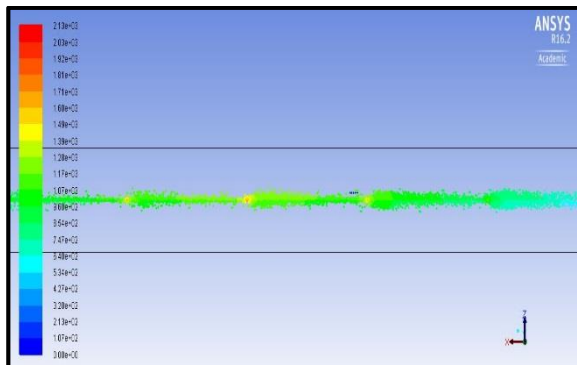
Figure D-4 $5.38 \cdot 10^{-4}$, 0.2 m/s (top view)
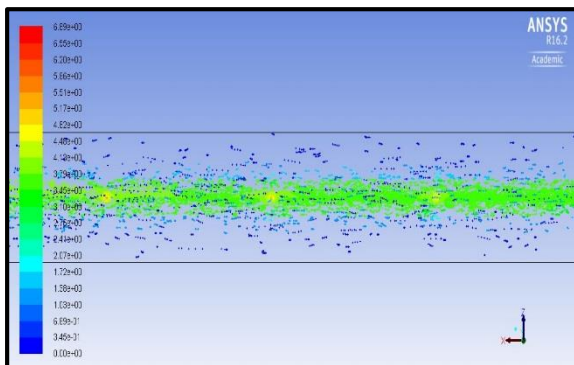
Figure D-5 $1.61 \cdot 10^{-5}$, 0.3 m/s (top view)
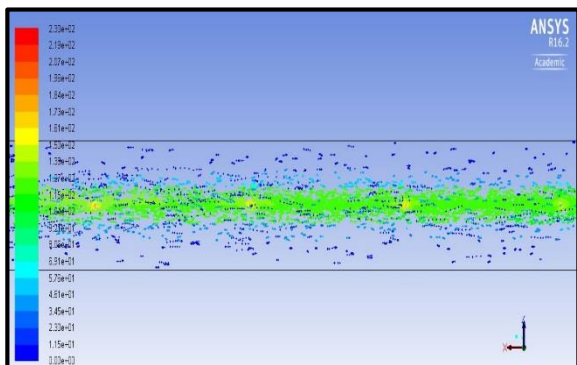
Figure D-6 $5.38 \cdot 10^{-4}$, 0.3 m/s (top view)
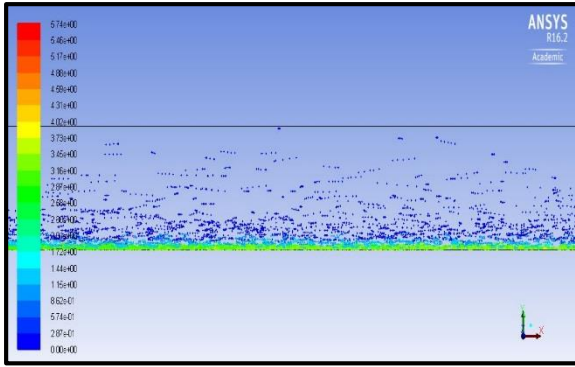
Figure D-7 1.61·10⁻⁵, 0.4 m/s (side view)
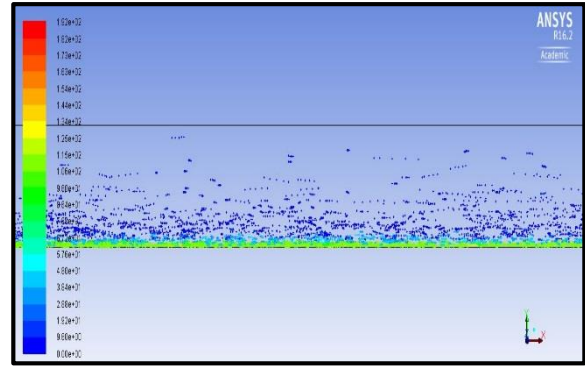
Figure D-8 5.38·10⁻⁴, 0.4 m/s (side view)
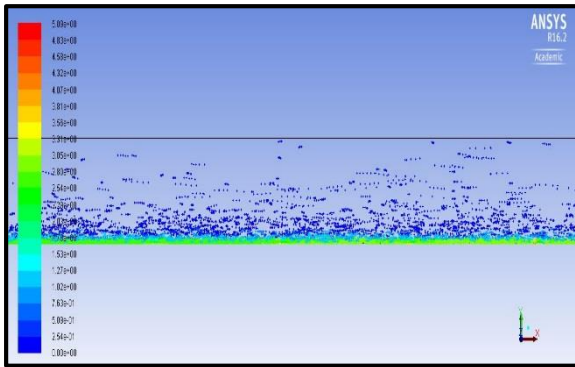
Figure D-9 1.61·10⁻⁵, 0.5 m/s (side view)

Figure D-10 5.38·10⁻⁴, 0.5 m/s (side view)

Figure D-11 1.61·10⁻⁵, 0.6 m/s (side view)

Figure D-12 5.38·10⁻⁴, 0.6 m/s (side view)

Figure D-13 1.61·10⁻⁵, 0.7 m/s (side view)

Figure D-14 5.38·10⁻⁴, 0.7 m/s (side view)

Figure D-15 $1.61 \cdot 10^{-5}$, 0.8 m/s (side view)

Figure D-16 $5.38 \cdot 10^{-4}$, 0.8 m/s (side view)
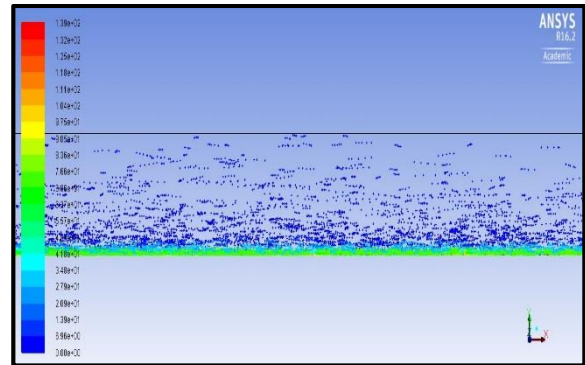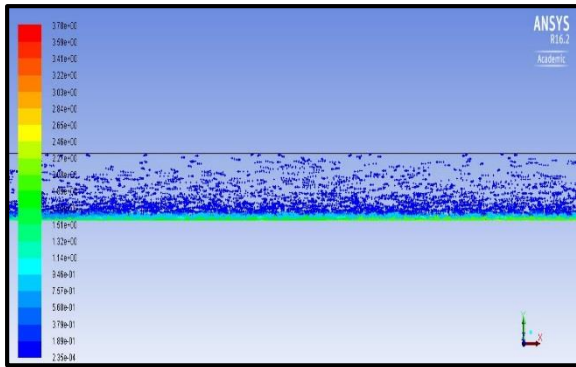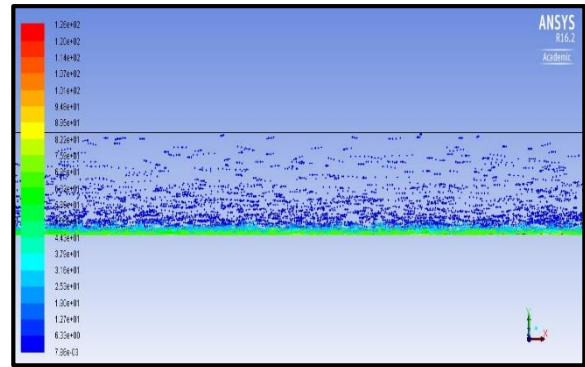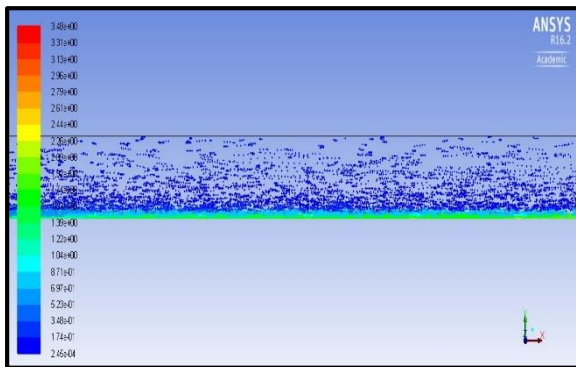

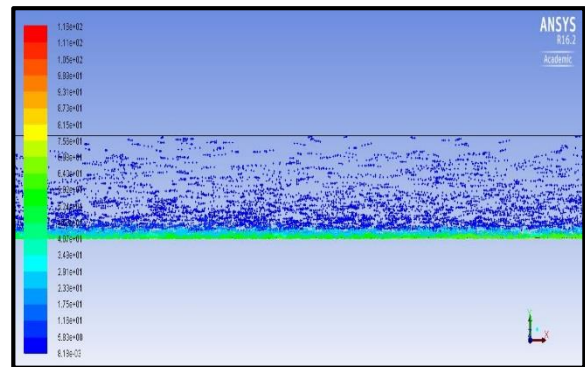Figure D-17 $1.61 \cdot 10^{-5}$, 0.9 m/s (side view)
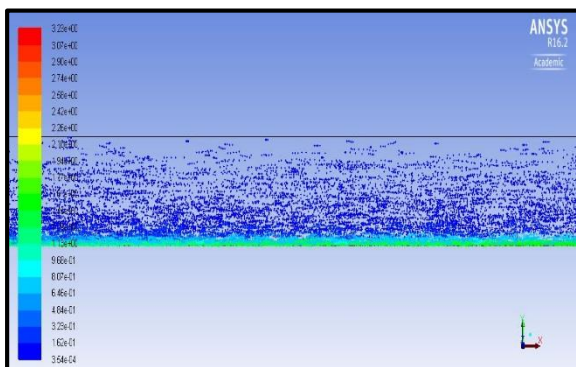

Figure D-18 $5.38 \cdot 10^{-4}$, 0.9 m/s (side view)
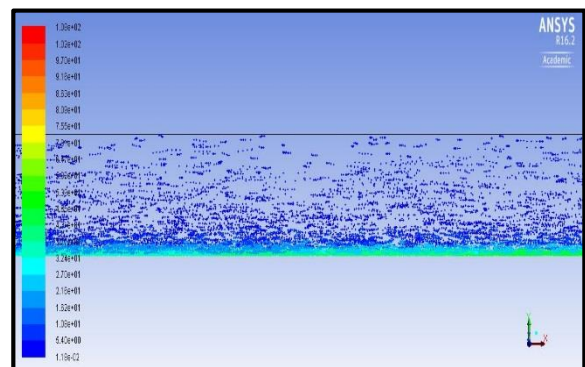

Figure D-19 $1.61 \cdot 10^{-5}$, 1 m/s (side view)

Figure D-20 $5.38 \cdot 10^{-4}$, 1 m/s (side view)

Appendix E Master's thesis development plan

In order to cover such a scope of work presented in the thesis, the Master's thesis plan has been developed. Since the author did not have any CFD experience and courses in the past, a noticeable period of time has been spent for learning purposes only.

Table E-1 Master's thesis development plan

Task	Week																				
	4	5	6	7	8	9	10	11	12	13	14	15	16	17	18	19	20	21	22	23	24
1. Plug propagation study																					
1.1 Learning the software																					
1.1.1 Design modelling	■																				
1.1.2 Meshing		■	■																		
1.1.3 Turbulent and Eulerian models			■	■	■																
1.1.4 Learning relevant CFD theory			■	■	■																
1.2 Literature review						■							■								
1.3 Approach development							■														
1.4 Approach implementation																					
1.4.1 Phase 1 implementation							■	■	■												
1.4.2 Phase 2 implementation										■	■	■									
1.4.3 3D modelling													■								
1.4.4 Slip model development													■	■							
2. MTC study																					
2.1 Learning DPM model theory															■						
2.2 Approach development															■	■					
2.3 Implementation phase															■	■	■	■			
3. Report development										■	■	■	■	■	■	■	■	■	■	■	■
4. Presentations																					
4.1 SPT Group, Schlumberger																	■				
4.2 NTNU																		■			
5. Submission																					■